NASA TECHNICAL NOTE

NASA TN D-3526

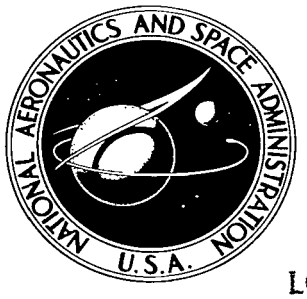

C. 1

LOAN COPY: RET
AFWL (WLI)
KIRTLAND AFB,

TECH LIBRARY KAFB, NM
0130305

NASA TN D-3526

STAGNATION AND STATIC PRESSURES ON A NOSE-MOUNTED 15° CONICAL PROBE WITH VARIOUS FOREBODY CONFIGURATIONS

by Edward M. Coates, Jr.

Langley Research Center
Langley Station, Hampton, Va.

NATIONAL AERONAUTICS AND SPACE ADMINISTRATION • WASHINGTON, D. C. • AUGUST 1966

TECH LIBRARY KAFB, NM
0130305

STAGNATION AND STATIC PRESSURES ON A NOSE-MOUNTED 15° CONICAL PROBE WITH VARIOUS FOREBODY CONFIGURATIONS

By Edward M. Coates, Jr.

Langley Research Center
Langley Station, Hampton, Va.

NATIONAL AERONAUTICS AND SPACE ADMINISTRATION

For sale by the Clearinghouse for Federal Scientific and Technical Information
Springfield, Virginia 22151 – Price $4.00

STAGNATION AND STATIC PRESSURES ON A NOSE-MOUNTED 15° CONICAL PROBE WITH VARIOUS FOREBODY CONFIGURATIONS

By Edward M. Coates, Jr.
Langley Research Center

SUMMARY

An investigation to obtain pressure-distribution data in the subsonic and transonic speed ranges for calibrating a hypersonic conical pressure probe intended for the X-15 research aircraft has been conducted in the Langley 16-foot transonic tunnel. The test vehicle consisted of a 1/3-scale model of the X-15 forebody and the data probe, which was a 15° cone with a hemispherical tip. The probe was investigated with three different lengths or portions of the X-15 forebody to determine the interference of the model body on probe pressure distributions.

Data were obtained for Mach numbers from 0.30 to 1.29, angles of attack from -4.8° to 15°, and angles of sideslip of 0° and 5°. The Reynolds number per meter varied from 5.90×10^6 to 12.76×10^6. The results indicated that the probe measured essentially free-stream stagnation pressures for Mach numbers from 0.30 to 1.00 at angles of attack from -5° to 5° and at an angle of sideslip of 0°. For Mach numbers from 1.01 to 1.29 and angles of attack from -5° to 5°, the probe measured essentially the stagnation pressure behind a normal shock to within 0.5 percent. The data indicated areas on the probe where the surface static pressures were least sensitive to changes in angle of attack. At subsonic speeds the presence of the body had a noticeable effect on surface static pressures measured by the probe. At speeds above Mach 1 the presence of the model body had no effect on probe pressure distributions. The angle of attack could be measured to an accuracy of about ±0.5° in the Mach number range from 0.30 to 1.29 by using the difference in pressure between an orifice located on the top of the probe and an orifice located on the bottom of the probe. The data indicated that for those orifices which were least sensitive to changes in angle of attack, the difference in the variation of the pressure coefficient with Mach number for angles of attack from 0.2° to 15° was less than 0.1 for Mach numbers up to 1.00.

INTRODUCTION

The results of wind-tunnel investigations on a conical pressure probe at supersonic and hypersonic speeds are presented in references 1 and 2. This probe is being considered for application to the X-15 research aircraft at hypersonic speeds. Because of the need for data in the subsonic and transonic speed ranges, the model was tested in the Langley 16-foot transonic tunnel. The probe was designed to measure stagnation pressure at the nose and static pressure at a number of axial and radial locations. This information could then be used in an onboard computer to calculate the Mach number, the altitude, the angle of attack, and the angle of sideslip. The purpose of this investigation was to determine (a) the accuracy to which the stagnation pressure could be measured; (b) the areas where the pressures would be least affected by changes in Mach number and angle of attack; and (c) whether the difference in pressure between two axially opposed orifices could be used for measurement of angle of attack and angle of sideslip. Three different lengths or portions of the X-15 forebody were investigated to determine the effect of body interference on the static pressure at subsonic and transonic speeds.

The test vehicle consisted of a 1/3-scale model of the X-15 forebody and the conical pressure probe, which was a 15° cone with a hemispherical tip. Data were obtained for Mach numbers from 0.30 to 1.29, angles of attack from -4.8° to 15°, and angles of sideslip of 0° and 5°. The Reynolds number per meter varied from 5.90×10^6 to 12.76×10^6.

SYMBOLS

C_p	pressure coefficient, $\frac{p - p_\infty}{q_\infty}$
l	length of 15° conical probe, cm
M	free-stream Mach number
p	local static pressure
p_∞	free-stream static pressure
$p_{t,\infty}$	free-stream stagnation pressure
$\frac{p_t}{p_{t,\infty}}$	ratio of local stagnation pressure measured by stagnation pressure orifice in nose of probe to free-stream stagnation pressure

p_1	local static pressure measured on top of probe
p_2	local static pressure measured on bottom of probe
$\frac{p_2 - p_1}{q_\infty}$	ratio of local static pressure on bottom of probe minus local static pressure on top of probe to free-stream dynamic pressure
q_∞	free-stream dynamic pressure
x	longitudinal distance from nose of probe to orifice location, cm
α	angle of attack referred to model center line, deg
β	angle of sideslip referred to plane of symmetry, deg
ϕ	circumferential location of probe orifice measured clockwise from top center line of probe when facing forward, deg

APPARATUS AND PROCEDURE

Model

A sketch of the model is presented in figure 1 and photographs of the three configurations tested are shown in figure 2. The model, 210.19 cm long with a maximum depth of 50.80 cm, consisted of the conical probe attached to a 1/3-scale model of the nose and canopy sections of the X-15 and a boattail fairing to smooth tunnel flow and reduce power consumption. Three different configurations were tested: Configuration 1 (figs. 1 and 2(a)) consisted of the probe and nose, the canopy, and the boattail sections; configuration 2 (figs. 1 and 2(b)) consisted of the probe and nose and the canopy sections without the boattail fairing; and configuration 3 (figs. 1 and 2(c)) consisted of the probe and nose section only.

The probe (fig. 3) was a 15° cone, 38.65 cm long with a hemispherical tip of radius 0.84 cm. The stagnation-pressure orifice was a 0.18-cm-diameter hole drilled through the hemispherical tip. The probe had 56 flush static-pressure orifices distributed axially and radially along the length of the probe at seven different stations (A to G). Stations A, C, D, F, and G each had four pressure orifices located 90° apart; station B had 12 pressure orifices located 30° apart; and station E had 24 pressure orifices located 15° apart. The model was tested with 56 static-pressure orifices in order to determine an optimum orifice configuration for air data purposes.

Wind Tunnel and Tests

The investigation was conducted in the Langley 16-foot transonic tunnel, which is a single-return atmospheric wind tunnel with a slotted octagonal test section. A test-section plenum-air-removal system was used to obtain speeds above a Mach number of 1.05.

The investigation was conducted at Mach numbers from 0.30 to 1.29 and angles of attack from -4.8° to 15°. Configuration 1 was tested at 0° and 5° angles of sideslip and configurations 2 and 3 were tested at a 0° angle of sideslip. The Reynolds number per meter varied from 5.90×10^6 to 12.76×10^6. This range was within the flight Reynolds number range for a typical flight profile for Mach numbers from 0.80 to 1.29. Model boundary-layer transition was not fixed for this investigation.

Instrumentation

The static pressures were measured on 48-channel pressure-scanning equipment with electrical pressure transducers. The outputs of the transducers were digitized and punched into data cards. Electrical pressure transducers with a capacity of 5 psi were used on all configurations except configuration 1 at Mach numbers of 0.30 and 0.50, on which 1-psi electrical transducers were used to improve the experimental accuracy. The stagnation pressure was also measured on an electrical pressure transducer.

Corrections and Accuracy

The angle of attack has been corrected for upflow of the wind-tunnel airstream, which was about 0.2° throughout the test range. The tunnel stagnation pressure for Mach numbers above 1.10 has been corrected for stagnation pressure loss due to condensation in the tunnel, the maximum loss (M = 1.29) being 0.2 percent. No other corrections have been made. The accuracies of the principal measurements are as follows:

α, deg	± 0.1
C_p	± 0.01
$p_t/p_{t,\infty}$	± 0.001
M	± 0.01

PRESENTATION OF RESULTS

The results of this investigation are presented as follows:

DISCUSSION

Stagnation Pressure

The variation of the ratio of local stagnation pressure measured by the probe to test-section stagnation pressure $p_t/p_{t,\infty}$ with model angle of attack α is shown in figure 4. The results presented in figure 4 are for configuration 1, but other data obtained but not presented herein show that the variation of $p_t/p_{t,\infty}$ with α is the same for all three configurations tested. The data of figure 4 show that the probe measured essentially free-stream stagnation pressures for Mach numbers from 0.30 to 1.00 at angles of attack from -5° to 5° and at an angle of sideslip of 0°, since $p_t/p_{t,\infty}$ is 0.999 or greater. For angles of attack greater than 5°, $p_t/p_{t,\infty}$ decreases gradually as α is further increased. For example, at a Mach number of 0.90 and an angle of attack of 15°, there is an error of about 2.9 percent in measuring $p_{t,\infty}$. (See fig. 4(a).) This deviation of the measured values from the free-stream stagnation pressure occurs gradually and increases with Mach number.

For Mach numbers from 1.01 to 1.29 at 0° angle of attack the probe measured essentially the stagnation pressure behind a normal shock. (See fig. 4(b).) In this Mach number range for angles of attack from about -5° to 5°, the probe measured the stagnation pressure behind a normal shock to within 0.5 percent. For angles of attack above 5°, the deviation of the measured values from the free-stream stagnation pressure is greater than that at subsonic speeds, with a resultant error of about 3.4 percent in measuring $p_{t,\infty}$ at a Mach number of 1.20 and an angle of attack of 15°. (See fig. 4(b).) However, at a Mach number of 1.29 and an angle of attack of 15°, the data deviate greatly from the expected result. (See fig. 4(b).) This deviation occurs for both 0° and 5° angles

of sideslip. The measured pressures were carefully checked and no reason could be found for this apparent discrepancy.

For an angle of attack of 0°, the decrease in values of $p_t/p_{t,\infty}$ between angles of sideslip of 0° and 5° increases with Mach number (fig. 4). For nonzero angles of attack, the deviation of the measured values from the free-stream stagnation pressure for an angle of sideslip of 5° is greater than that for an angle of sideslip of 0°. For Mach numbers from 0.30 to 1.20, the values of the ratio $p_t/p_{t,\infty}$ at $\alpha = 5^{\circ}$ and $\beta = 0^{\circ}$ and at $\alpha = 0^{\circ}$ and $\beta = 5^{\circ}$ are equal.

Circumferential Pressure Distributions

The circumferential pressure distributions for configuration 1 at station B, which is located at $x/l = 0.37$, are shown in figure 5. For 0° angle of sideslip, the surface static pressures are least sensitive to changes in angle of attack in the circumferential angle ranges of 130° to 140° and 220° to 230° (i.e., $\pm 40^{\circ}$ to $\pm 50^{\circ}$ from bottom of probe). These regions are symmetrical about the vertical axis. For 5° angle of sideslip, the regions of least sensitivity to changes in angle of attack shift to 115° to 125° and 215° to 225°. (See fig. 5.) It should be noted that these regions are not symmetrical about the vertical axis for a 5° angle of sideslip. The same information for configuration 1 at station E, which is located at $x/l = 0.63$, is shown in figure 6. The pressure distributions at these two locations are in general agreement.

Longitudinal Pressure Distributions

The pressure distributions for four radial locations ($\phi = 0^{\circ}$, 90°, 180°, and 270°) at seven longitudinal stations are shown in figures 7 to 22. Figures 7 to 14 show data for the three model configurations at 0° angle of sideslip, and figures 15 to 22 show the same information for model configuration 1 at 0° and 5° angles of sideslip. The subsonic data in figures 7 to 10 indicate that there is generally no appreciable difference in the pressure coefficients of configurations 1 and 2. However, there is a definite drop in the pressure coefficient between configurations 1 and 2 and configuration 3. The increase in measured pressure on configurations 1 and 2 is due to interference of the canopy and body. The drop in pressure coefficient between configurations 1 and 2 and configuration 3, which appears to be independent of circumferential location of the orifice and angle of attack, is greatest at Mach number 0.30 and decreases as the Mach number increases. (See figs. 7 to 10.) The supersonic data (figs. 11 to 14) show that there is no appreciable difference in pressure coefficient for the three configurations, and that the canopy thus has no effect on the supersonic pressure distributions. The pressure coefficient is essentially constant between values of x/l of 0.45 and 0.65.

Sensitivity of Pressure Ratio to Changes in Angle of Attack

The calibration lines which are drawn through the mean of the pressure data at each angle of attack in figures 23 and 24 show that the ratio of the pressure on the bottom of the probe minus the pressure on the top of the probe to dynamic pressure $\left(\frac{p_2 - p_1}{q_\infty}\right)$ varies uniformly with angle of attack. Thus, the ratio $\frac{p_2 - p_1}{q_\infty}$ can be used to determine angle of attack. The variation of $\frac{p_2 - p_1}{q_\infty}$ with angle of attack for 0° angle of sideslip at stations B and E is shown in figures 23(a) and 24(a). Using the mean of the data at each angle of attack allows a calibration accuracy within about $\pm 0.5^\circ$ for the Mach number range investigated. Data in the same form for 5° angle of sideslip are shown in figures 23(b) and 24(b), and the calibration accuracy is the same as for 0° angle of sideslip. In addition, for angles of attack from -5° to 10°, the values of the ratio $\frac{p_2 - p_1}{q_\infty}$ for both 0° and 5° angles of sideslip at any one angle of attack are equal. Thus, in this angle-of-attack region, this method for determining angle of attack is independent of angle of sideslip when the sideslip angle is between -5° and 5°. However, the values of the ratio $\frac{p_2 - p_1}{q_\infty}$ vary for 0° and 5° angles of sideslip as the angle of attack increases above 10°.

Mach Number

The variation of the pressure coefficient with Mach number at several circumferential locations for configuration 1 at station E ($x/l = 0.63$) is shown in figure 25. Included in these families of curves are those for circumferential locations which exhibited minimum sensitivity of the pressure coefficient to changes in angle of attack. (See figs. 5 and 6.) These curves show faired data with data points plotted on them where available. The slopes of these curves indicate the usefulness of the various orifices for determining Mach number. Although the slopes of the curves which exhibited minimum sensitivity to changes in angle of attack (orifices $\pm 45^\circ$ from bottom of probe for $\beta = 0^\circ$ and -60° and 40° from bottom of probe for $\beta = 5^\circ$) are not constant, their shapes are such that they could easily be programed for a computer. For those orifices which were least sensitive to angle of attack, the difference in the variation of the pressure coefficient with Mach number for angles of attack from 0.2° to 15° is less than 0.1 for Mach numbers up to 1.00.

CONCLUSIONS

A wind-tunnel investigation has been conducted at subsonic and transonic speeds to measure the stagnation and static pressures on a nose-mounted 15° conical probe

intended for the X-15 aircraft at hypersonic speeds. Also investigated was the interference of the aircraft fuselage on the static pressure. Data were obtained for Mach numbers from 0.30 to 1.29, angles of attack from -4.8° to 15°, and angles of sideslip of 0° and 5°. The Reynolds number per meter varied from 5.90×10^6 to 12.76×10^6. The results of this investigation lead to the following general conclusions:

1. The probe measured essentially free-stream stagnation pressures for Mach numbers from 0.30 to 1.00 at angles of attack from -5° to 5° and at an angle of sideslip of 0°. For Mach numbers from 1.01 to 1.29 and angles of attack from -5° to 5°, the probe measured essentially the stagnation pressure behind a normal shock to within 0.5 percent.

2. The data indicated areas on the probe where the surface static pressures were least sensitive to changes in angle of attack. For 0° angle of sideslip these areas were at circumferential locations of $\pm 40^{\circ}$ to $\pm 50^{\circ}$ from the bottom of the probe.

3. At subsonic speeds the presence of the body had a noticeable effect on surface static pressures measured by the probe. There was no aerodynamic interference of the model forebody on probe static pressure distributions at speeds above Mach 1.

4. The angle of attack could be measured to an accuracy of about $\pm 0.5^{\circ}$ in the Mach number range from 0.30 to 1.29 by using the difference in pressure between an orifice located on the top of the probe and an orifice located on the bottom of the probe.

5. The data indicated that for those orifices which were least sensitive to changes in angle of attack, the difference in the variation of the pressure coefficient with Mach number for angles of attack from 0.2° to 15° was less than 0.1 for Mach numbers up to 1.00.

Langley Research Center,
National Aeronautics and Space Administration,
Langley Station, Hampton, Va., March 29, 1966.

REFERENCES

1. Mallard, Scott R.: Calibration Tests of a Litton Conical Air Data Probe at Mach Numbers of 2 to 8. AEDC-TDR-62-186, U.S. Air Force, Oct. 1962.

2. Mallard, Scott R.: Calibration Tests of a Litton Hades Air Data Probe Configuration at Mach Numbers of 1.5 to 10. AEDC-TDR-64-156, U.S. Air Force, Aug. 1964.

Configuration

1	Nose with canopy and boattail sections
2	Nose with canopy section
3	Nose section only

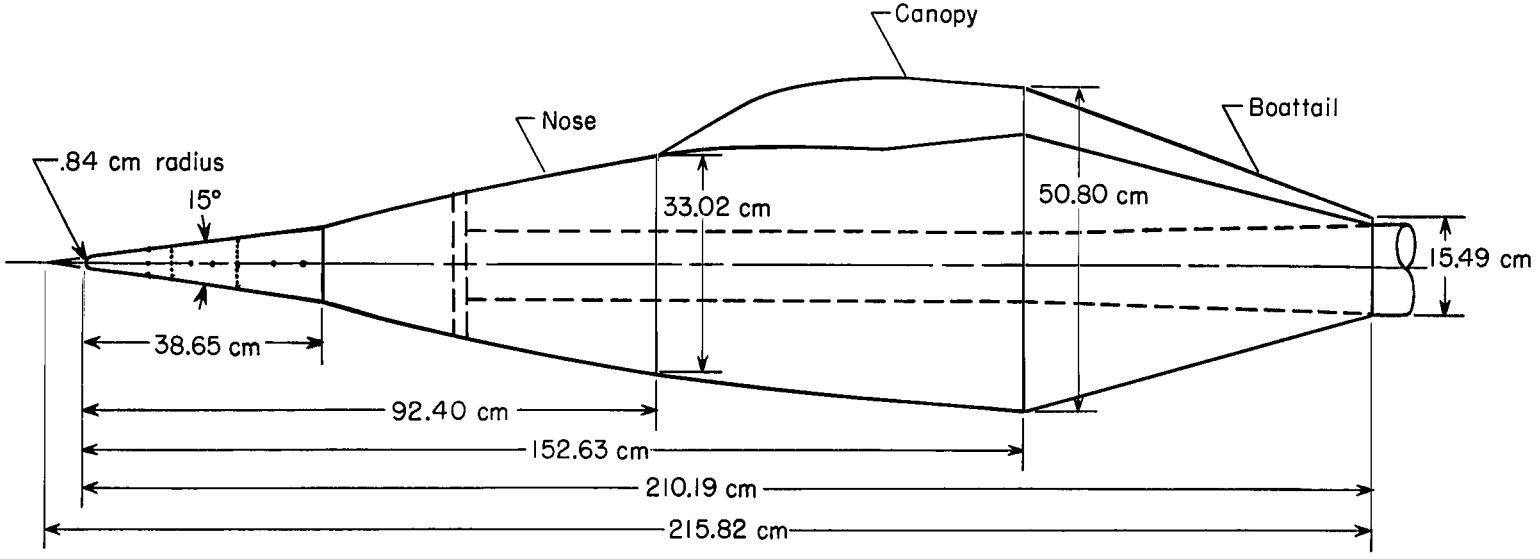

Figure 1.- Sketch of model.

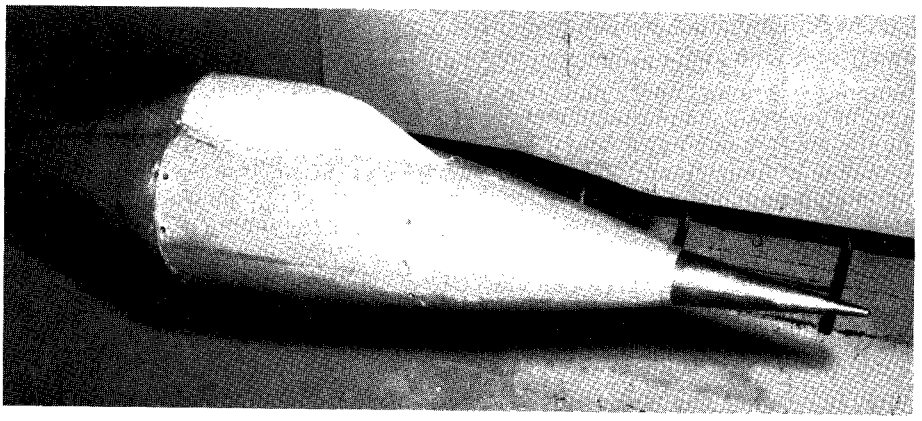

(a) Configuration 1. L-64-5665

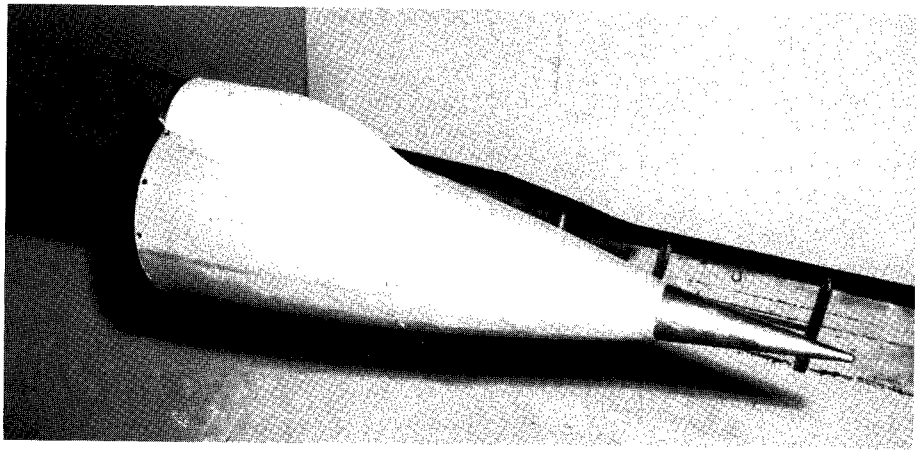

(b) Configuration 2. L-64-5663

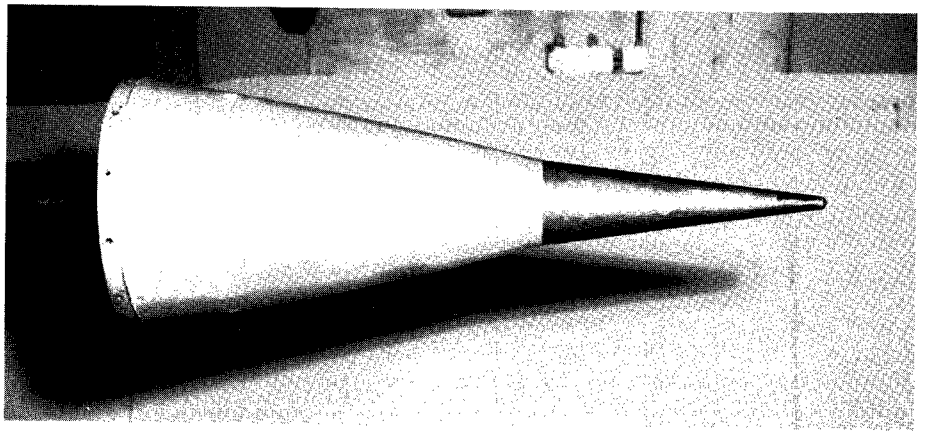

(c) Configuration 3. L-64-5664

Figure 2.- Photographs of model configurations.

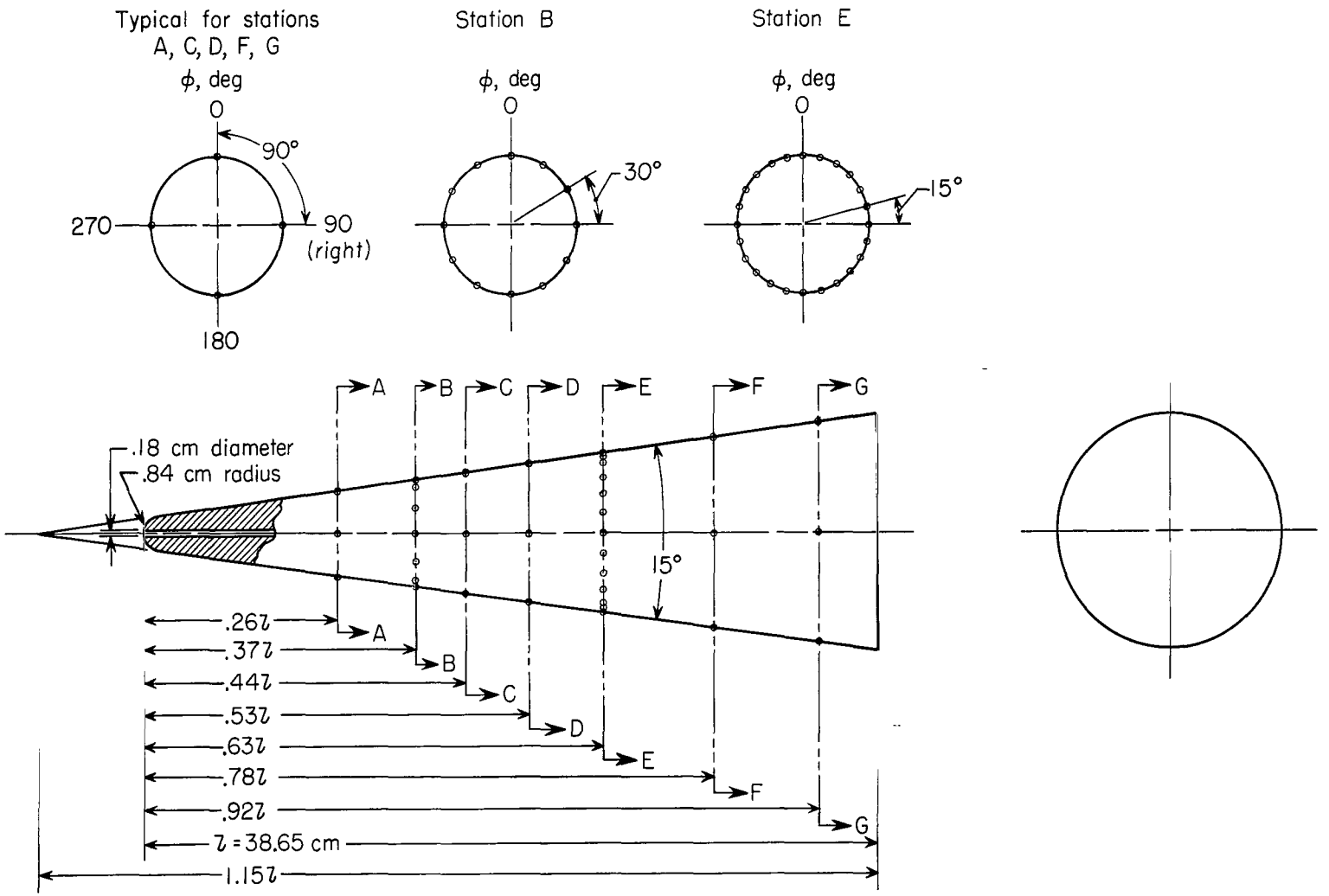

Figure 3.- Details of 15^0-conical probe.

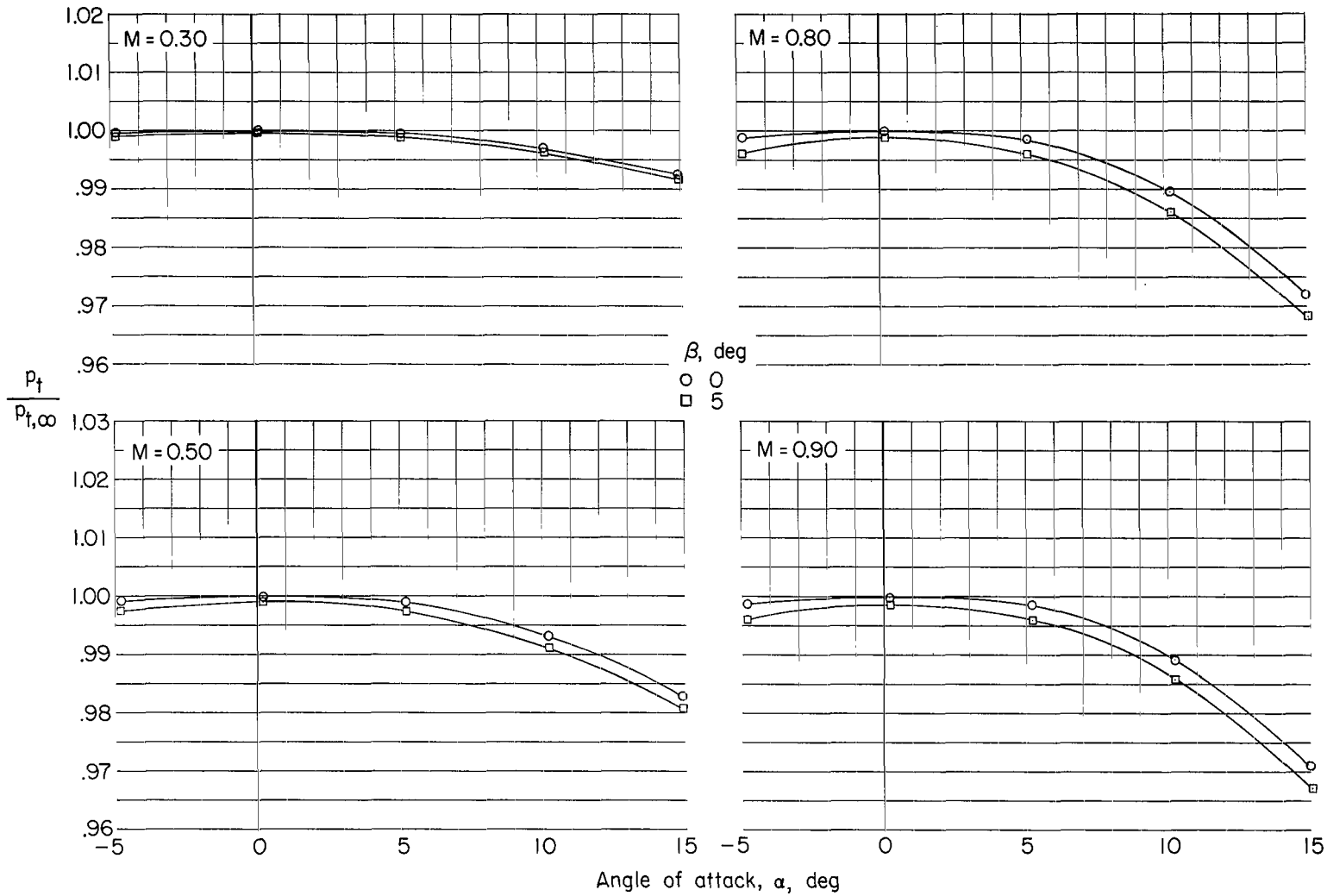

(a) M = 0.30 to M = 0.90.

Figure 4.- Variation of $p_t/p_{t,\infty}$ with α for $\beta = 0^0$ and $\beta = 5^0$.

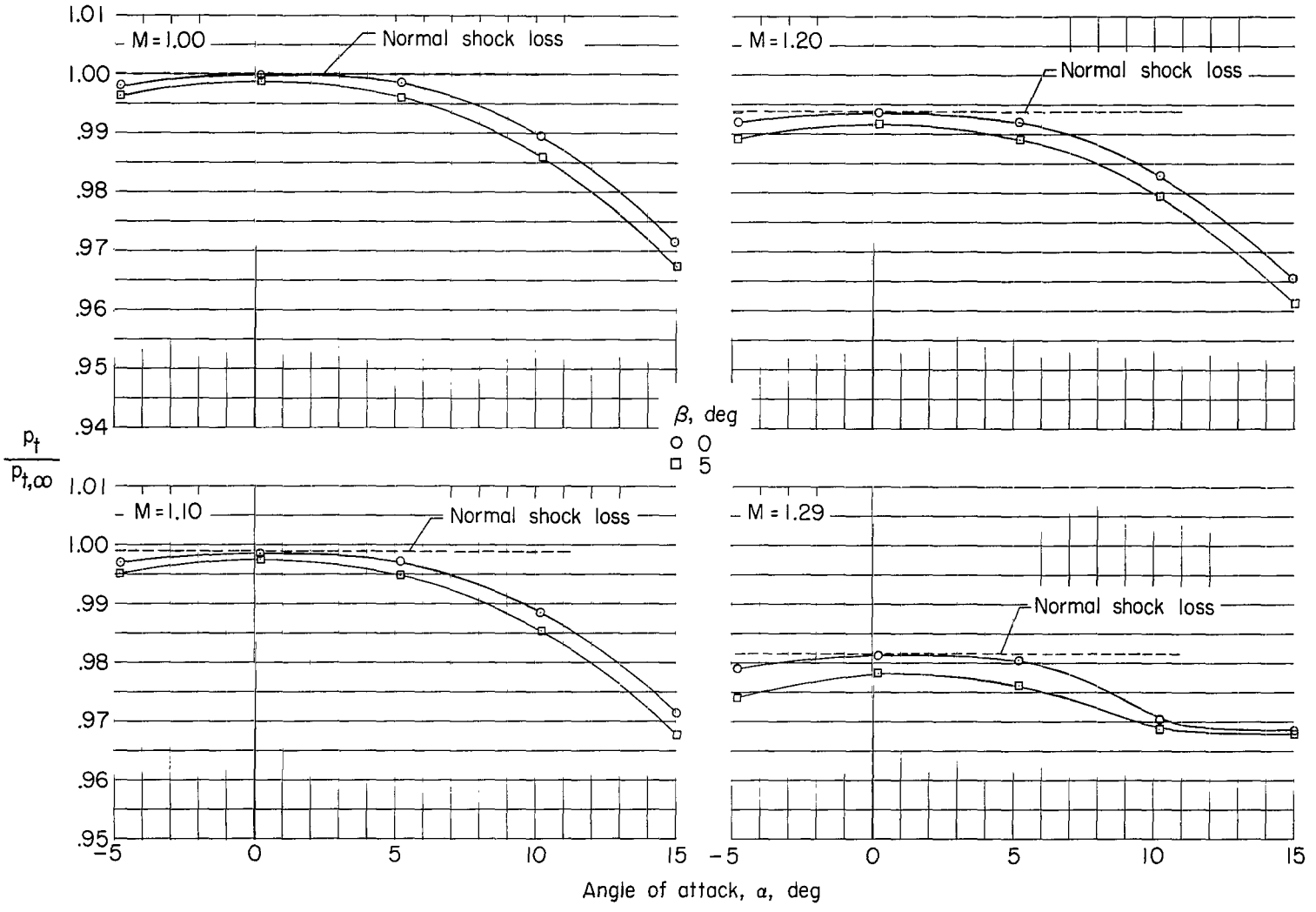

(b) M = 1.00 to M = 1.29.

Figure 4.- Concluded.

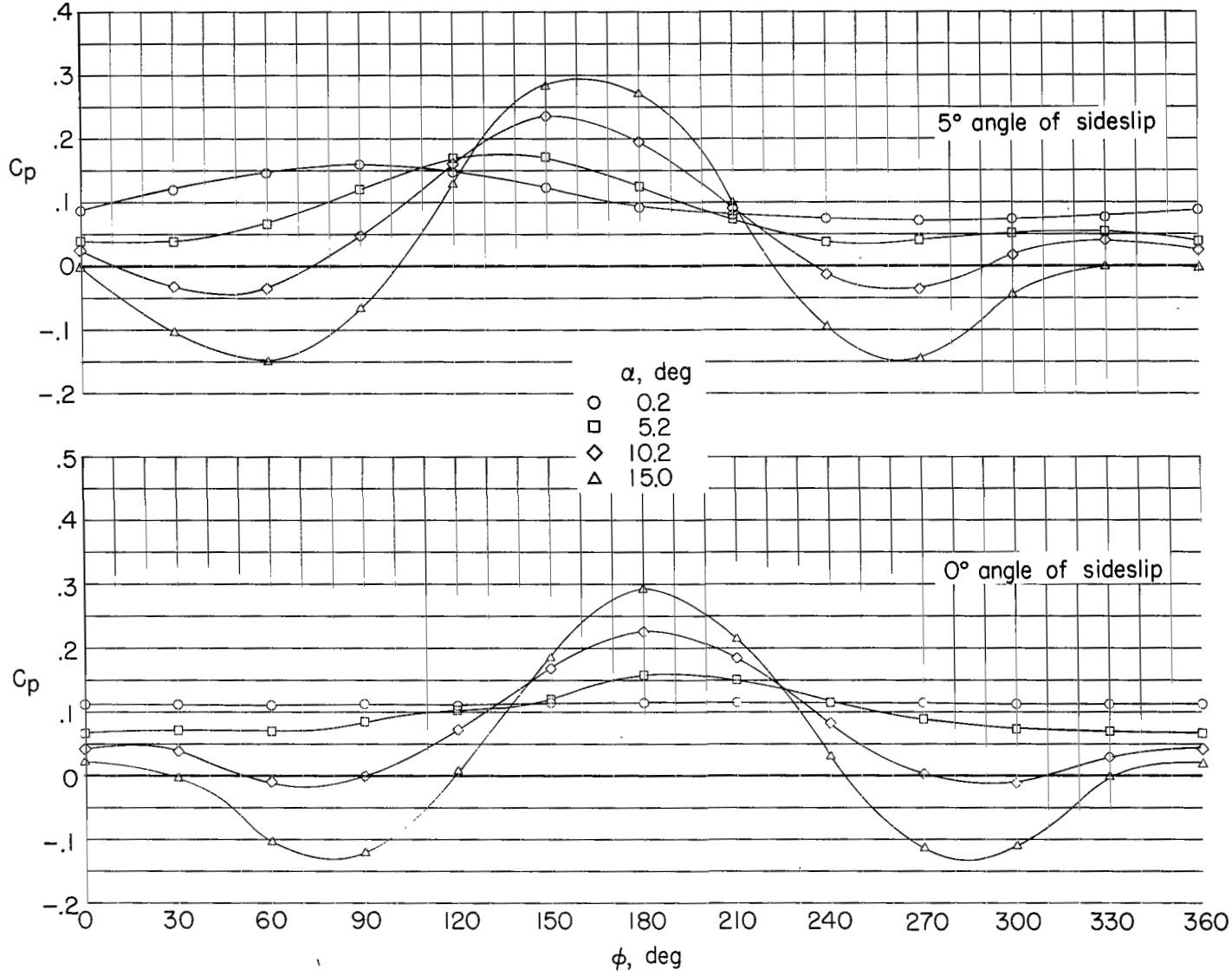

(a) M = 0.30.

Figure 5.- Circumferential pressure distributions at station B.

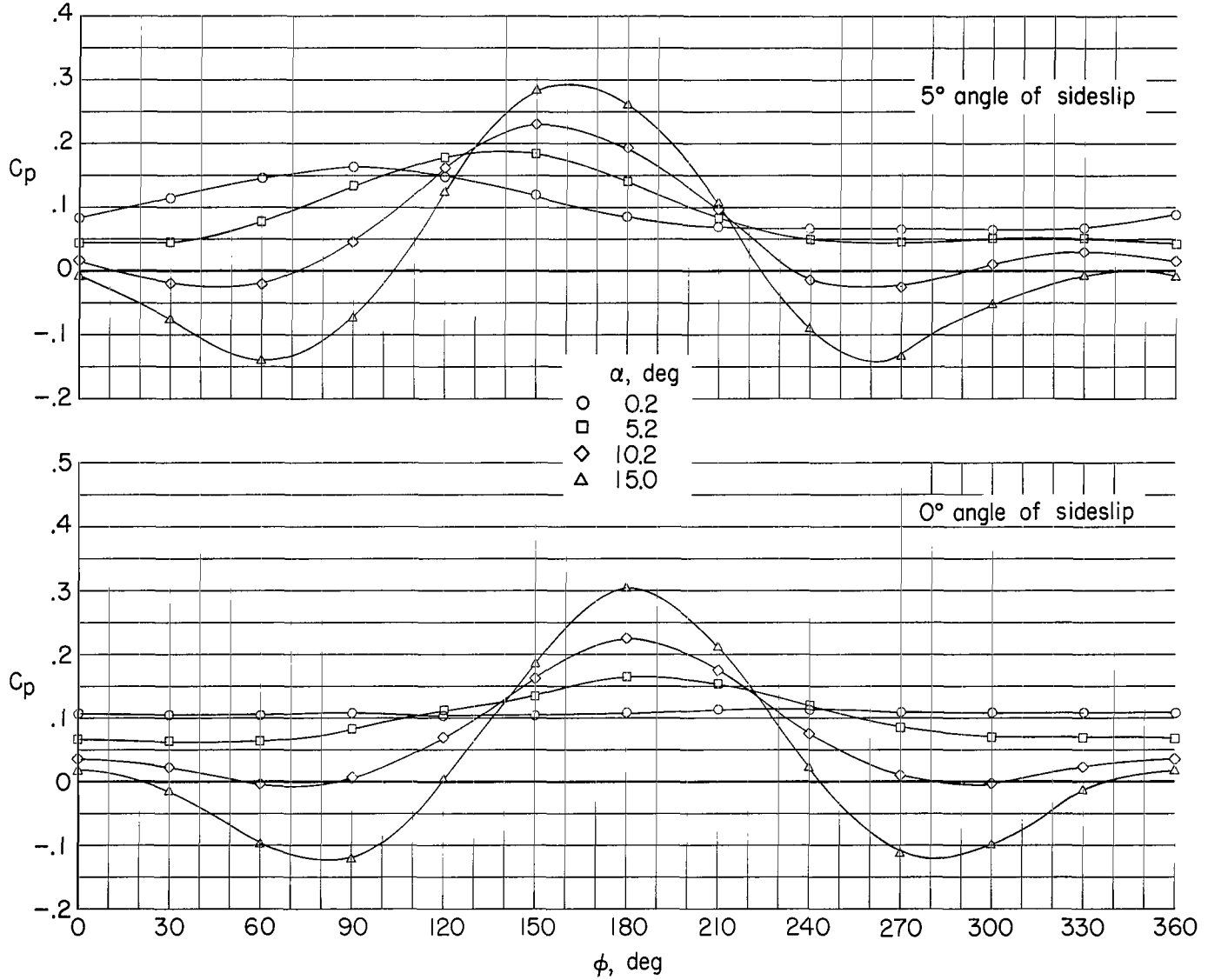

(b) M = 0.50.

Figure 5.- Continued.

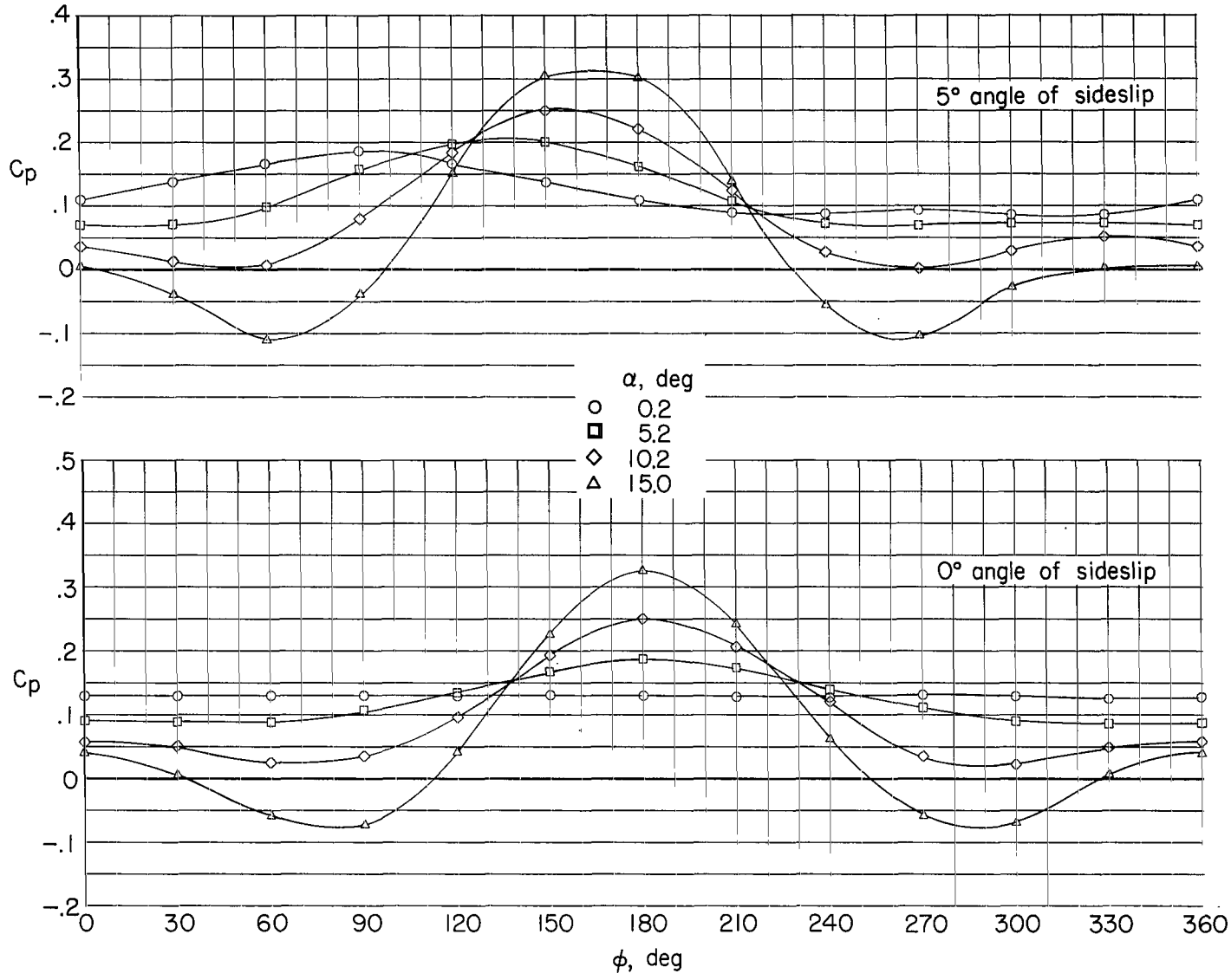

(c) M = 0.80.

Figure 5.- Continued.

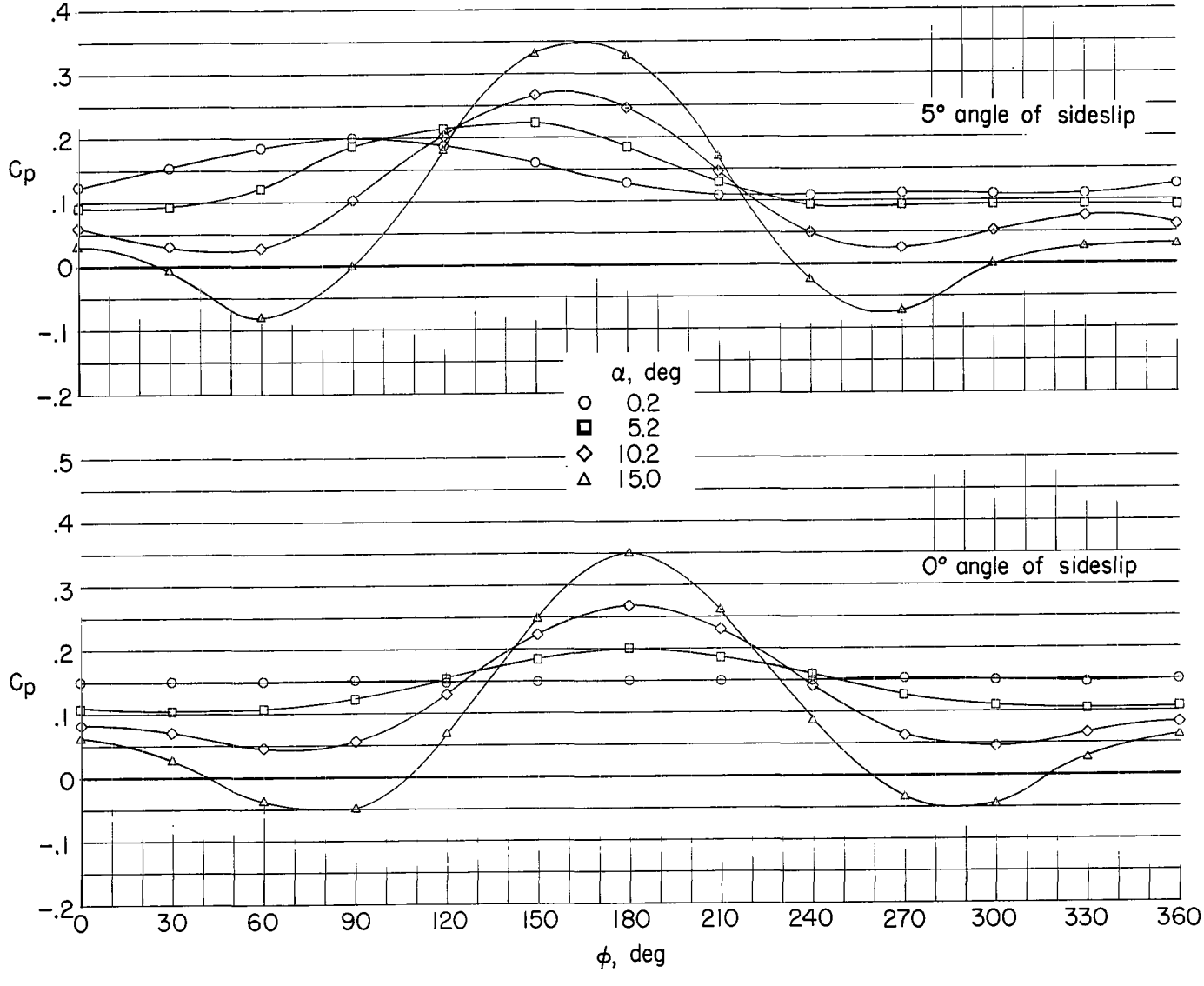

(d) M = 0.90.

Figure 5.- Continued.

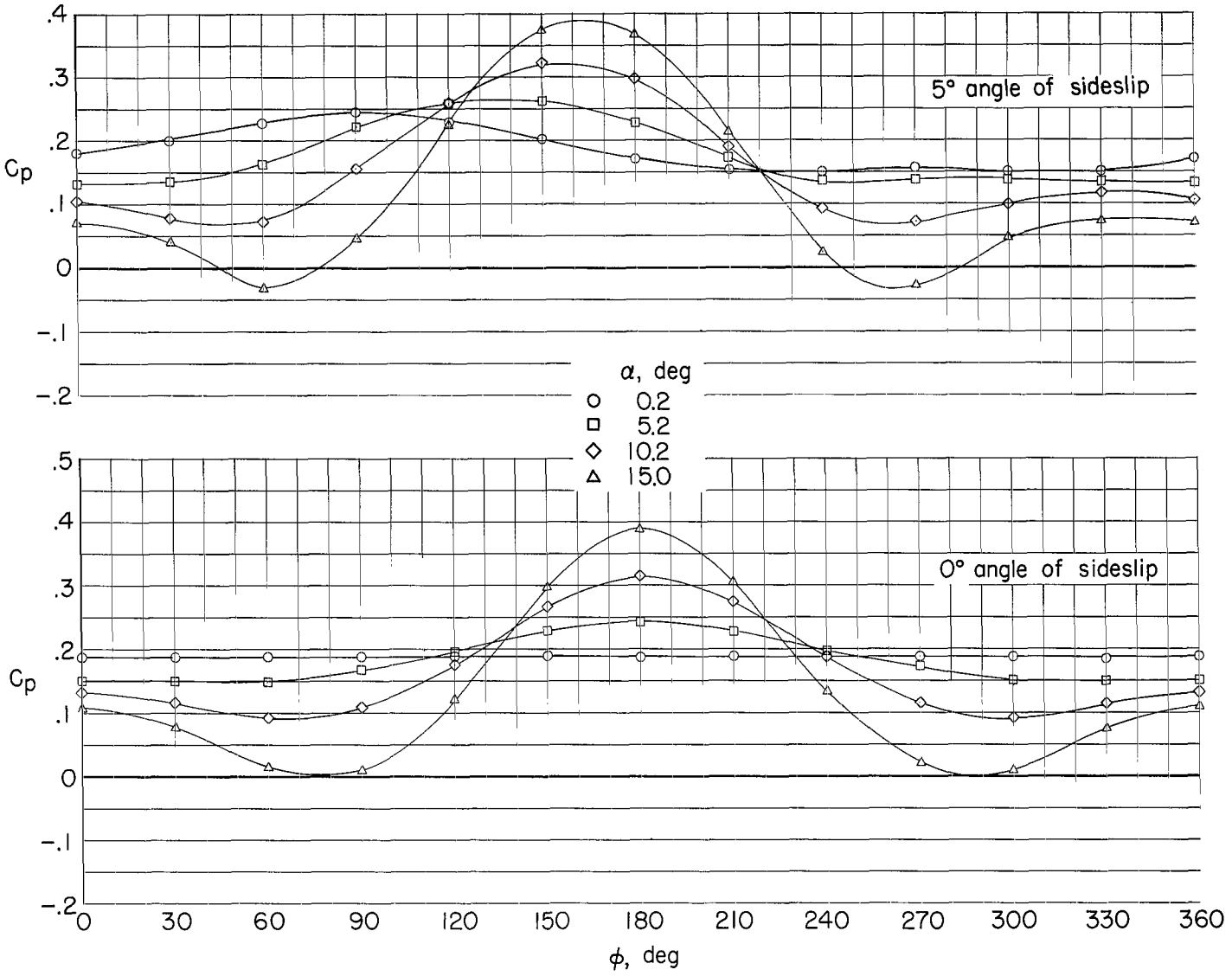

(e) M = 1.00.

Figure 5.- Continued.

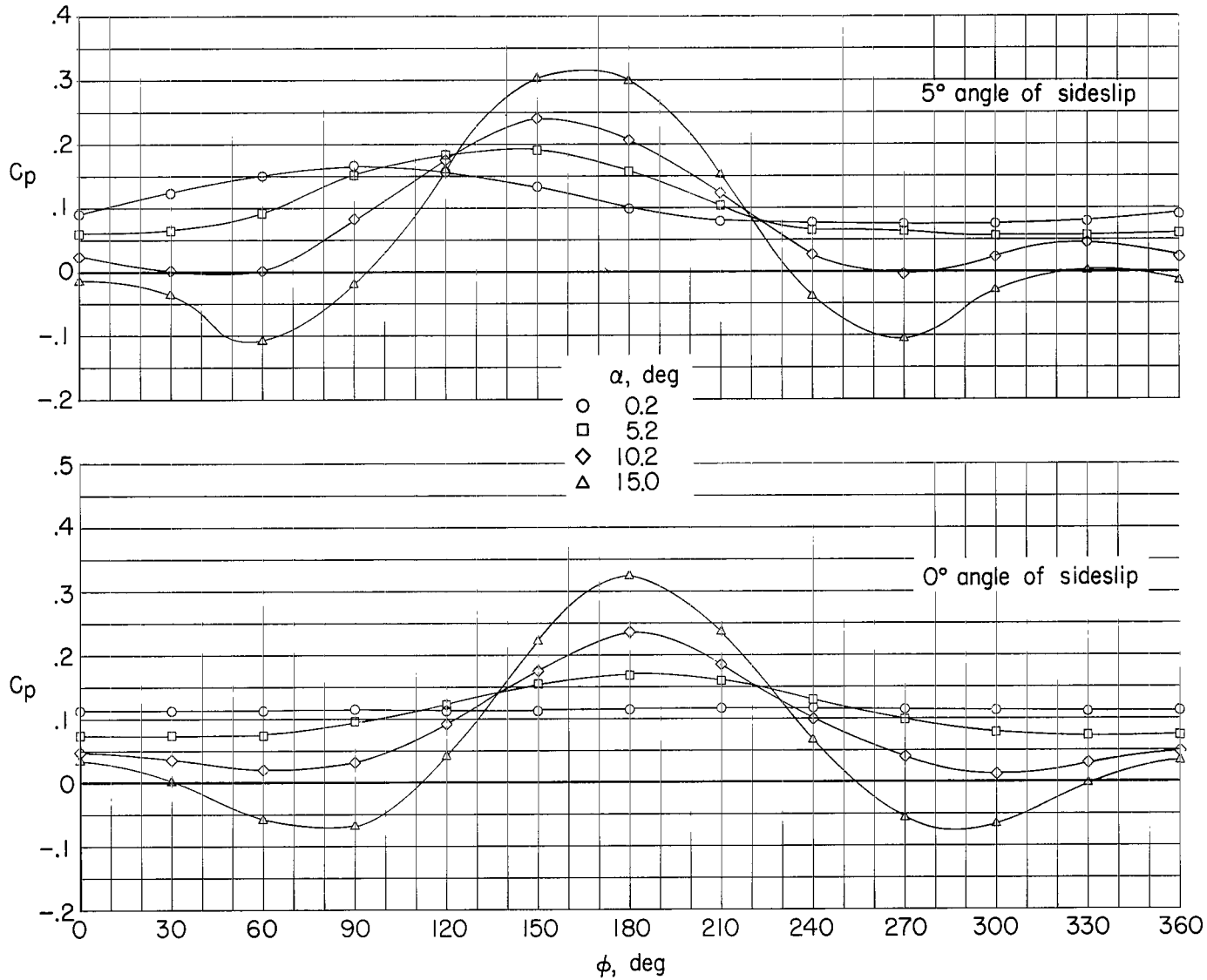

(f) M = 1.10.

Figure 5.- Continued.

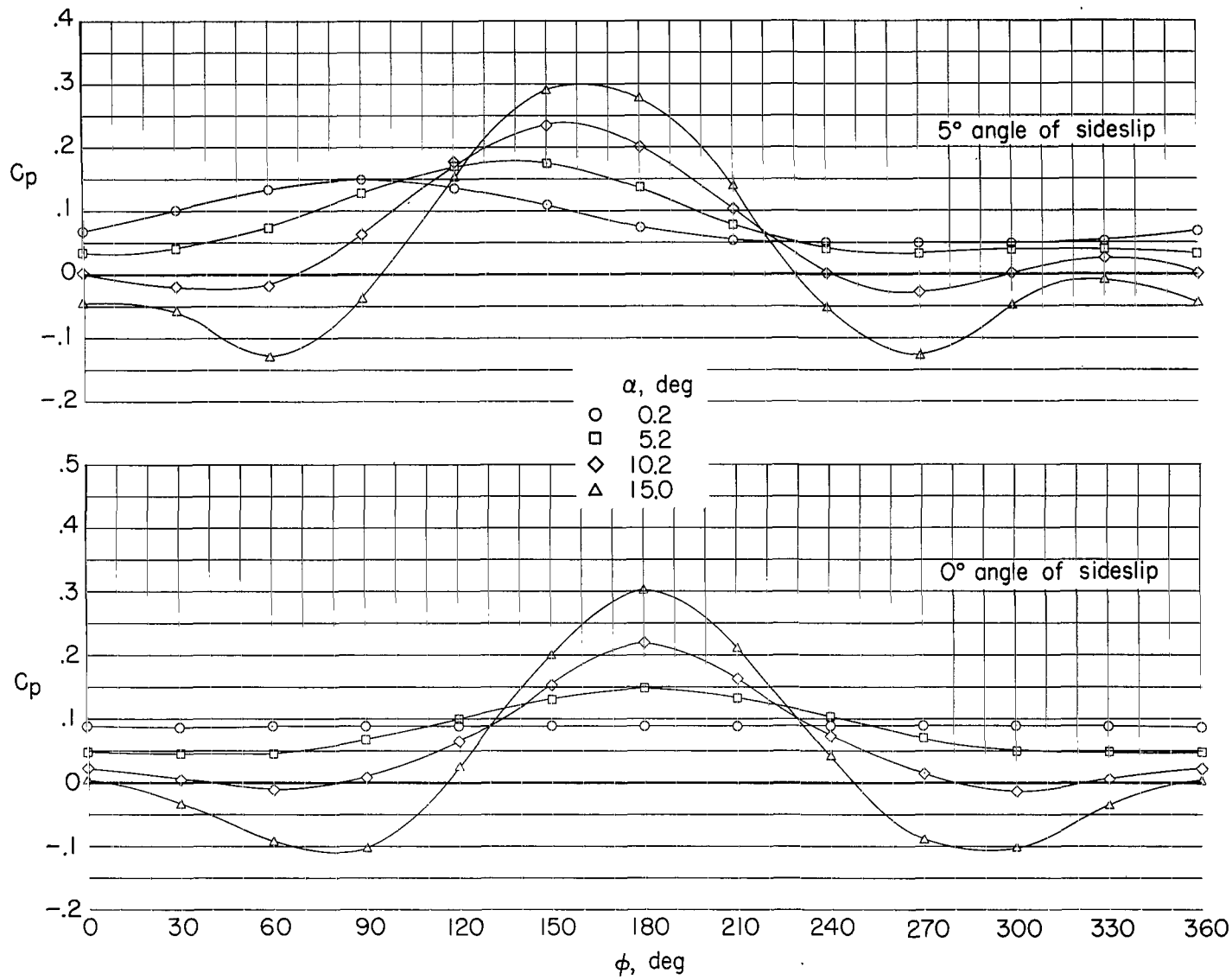

(g) M = 1.20.

Figure 5.- Continued.

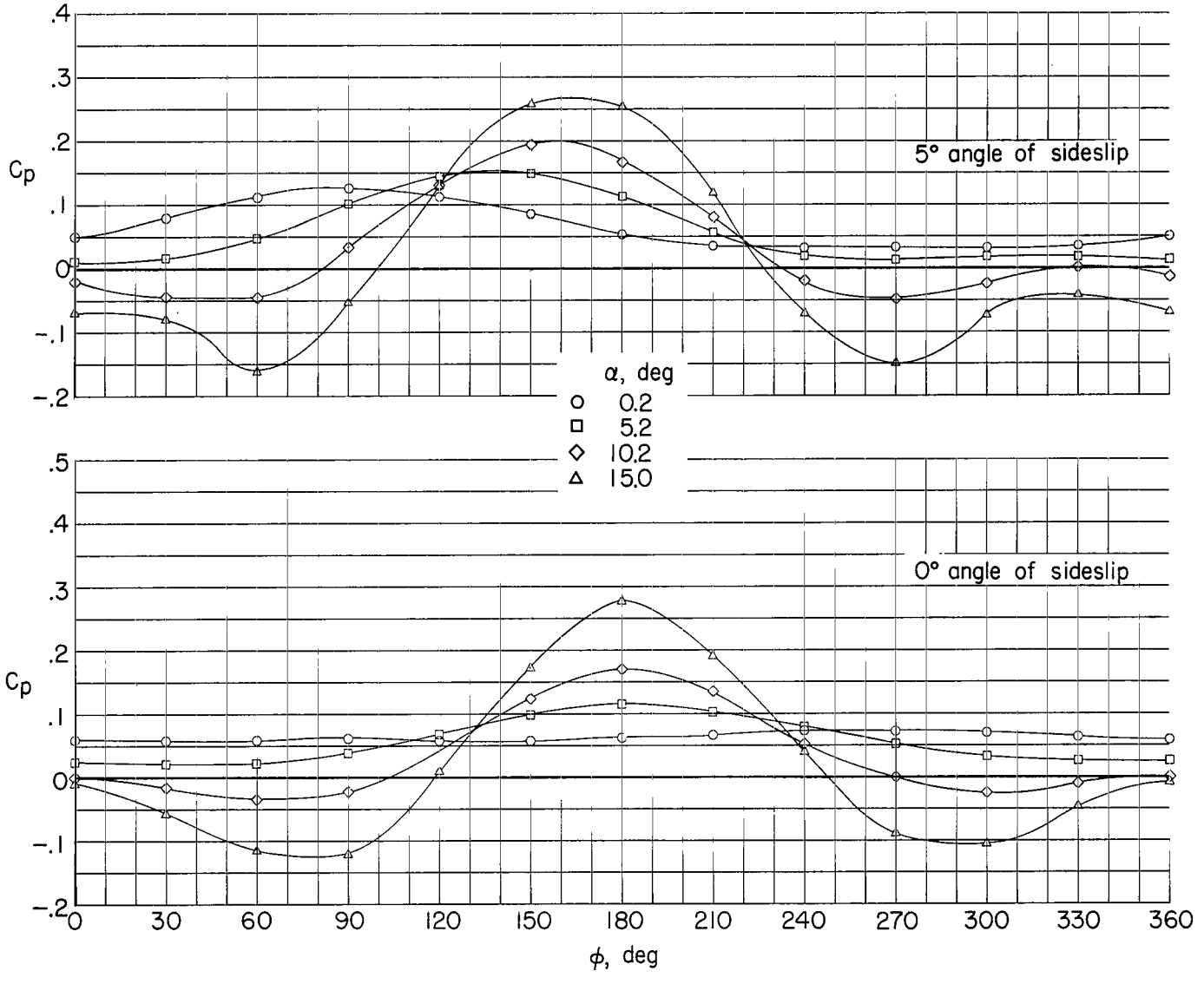

(h) M = 1.29.

Figure 5.- Concluded.

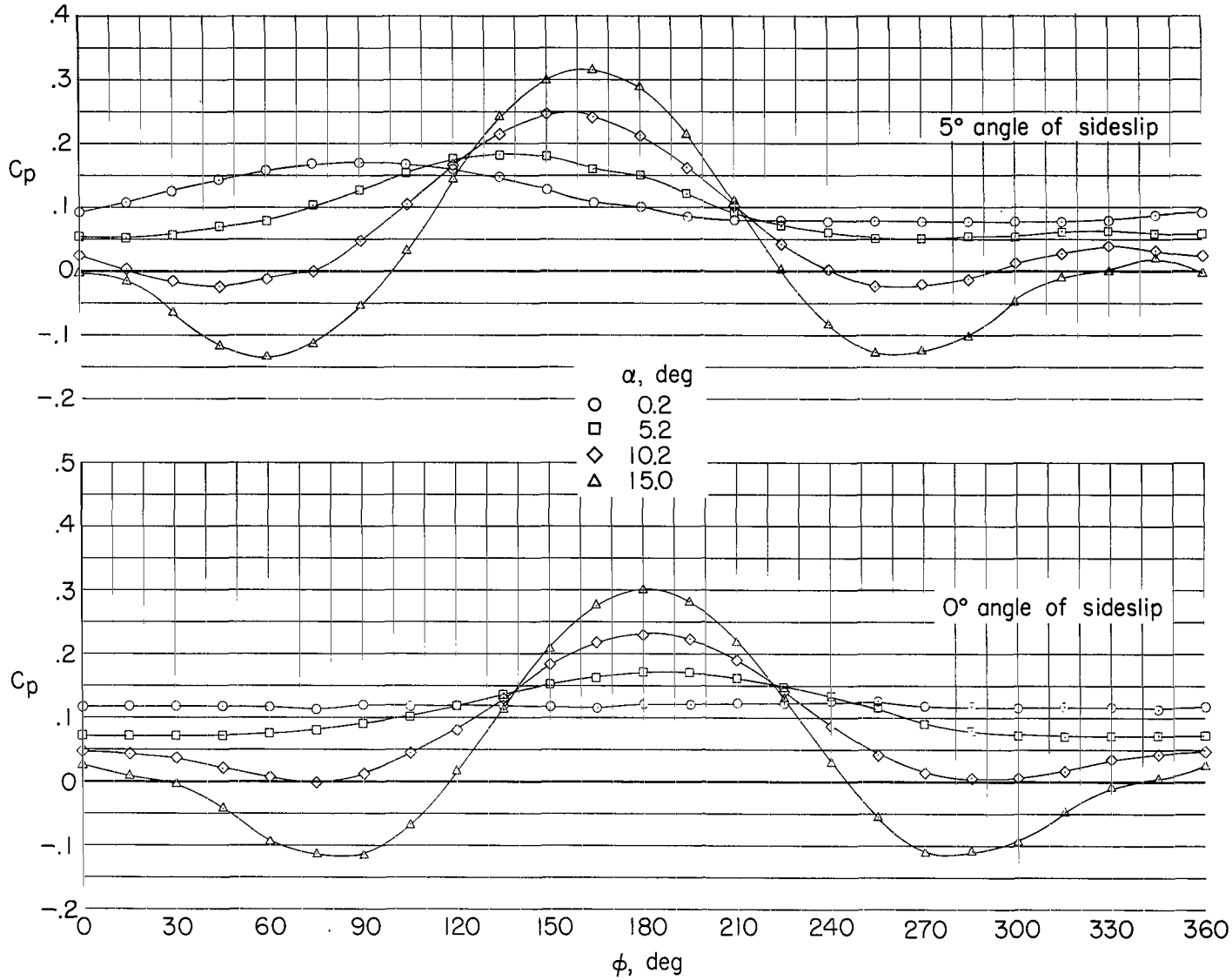

(a) M = 0.30.

Figure 6.- Circumferential pressure distributions at station E.

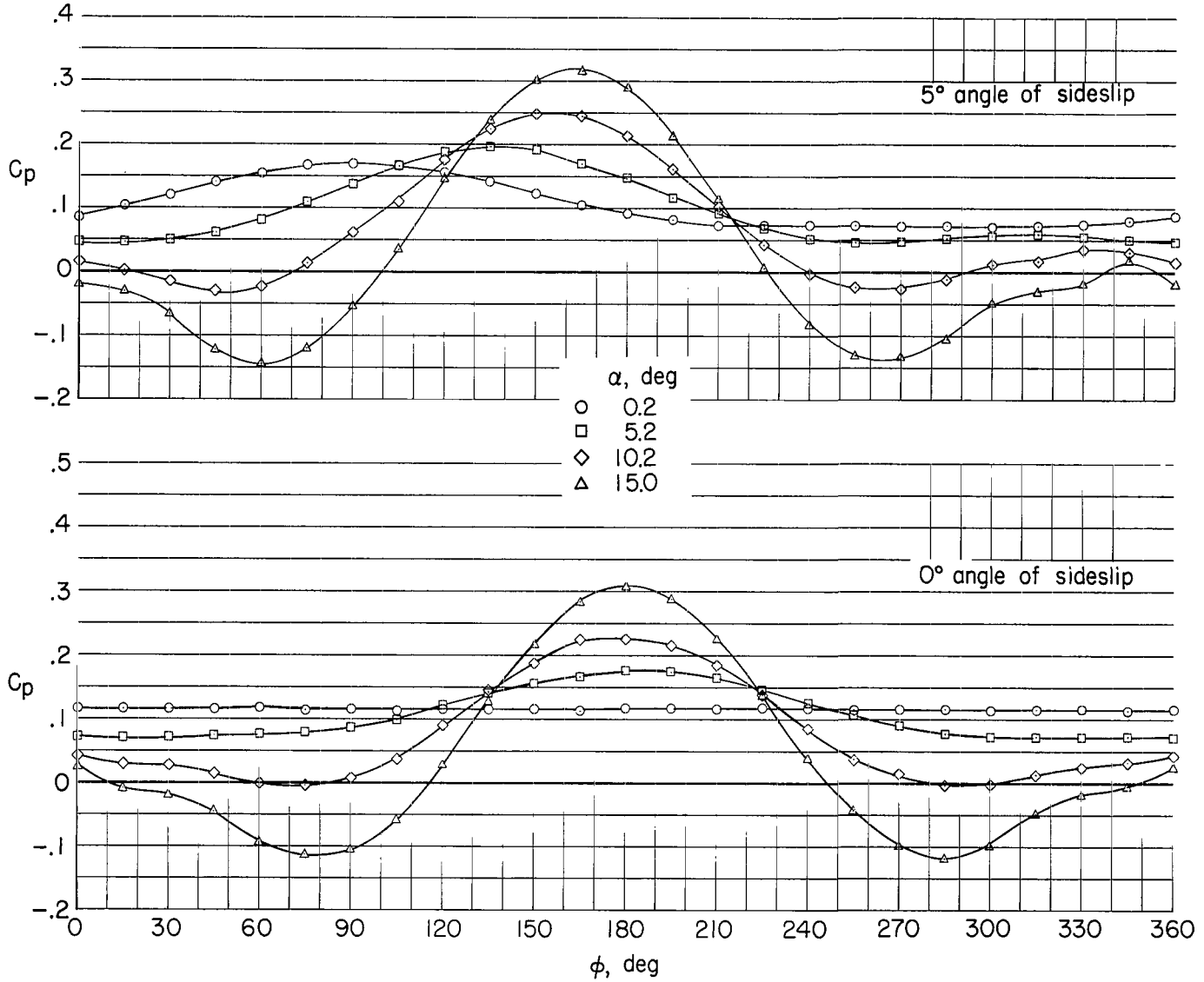

(b) M = 0.50.

Figure 6.- Continued.

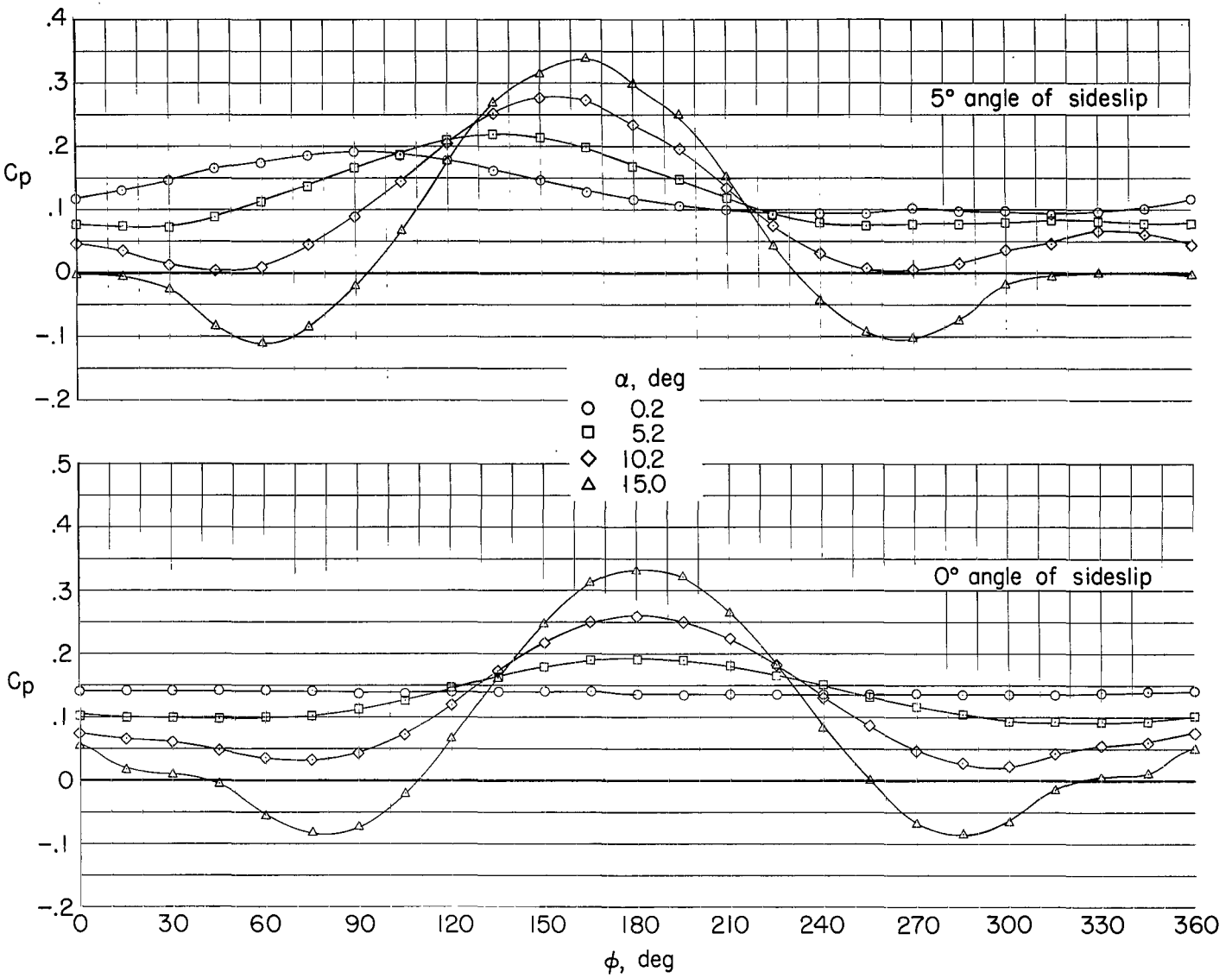

(c) M = 0.80.

Figure 6.- Continued.

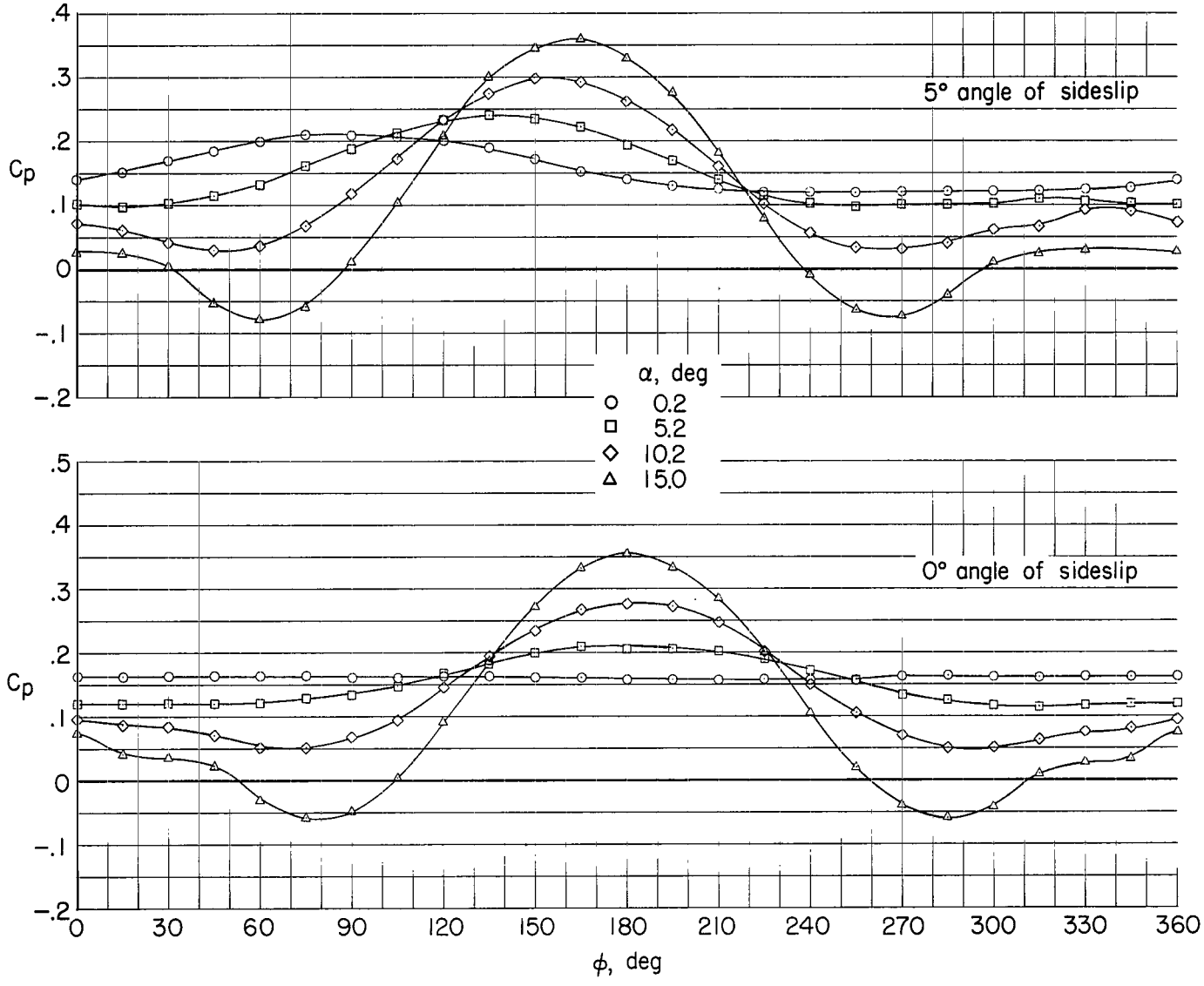

(d) M = 0.90.

Figure 6.- Continued.

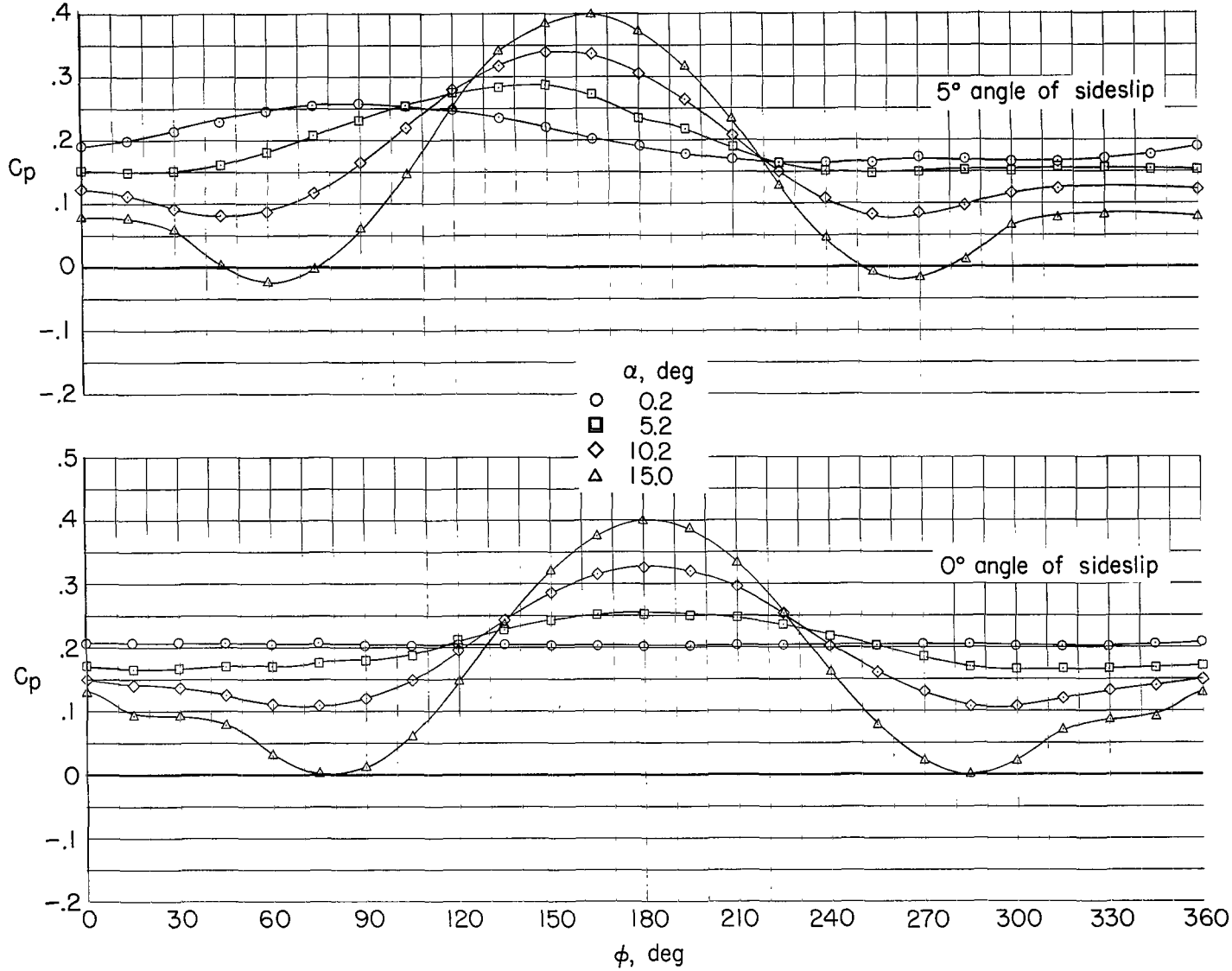

(e) M = 1.00.

Figure 6.- Continued.

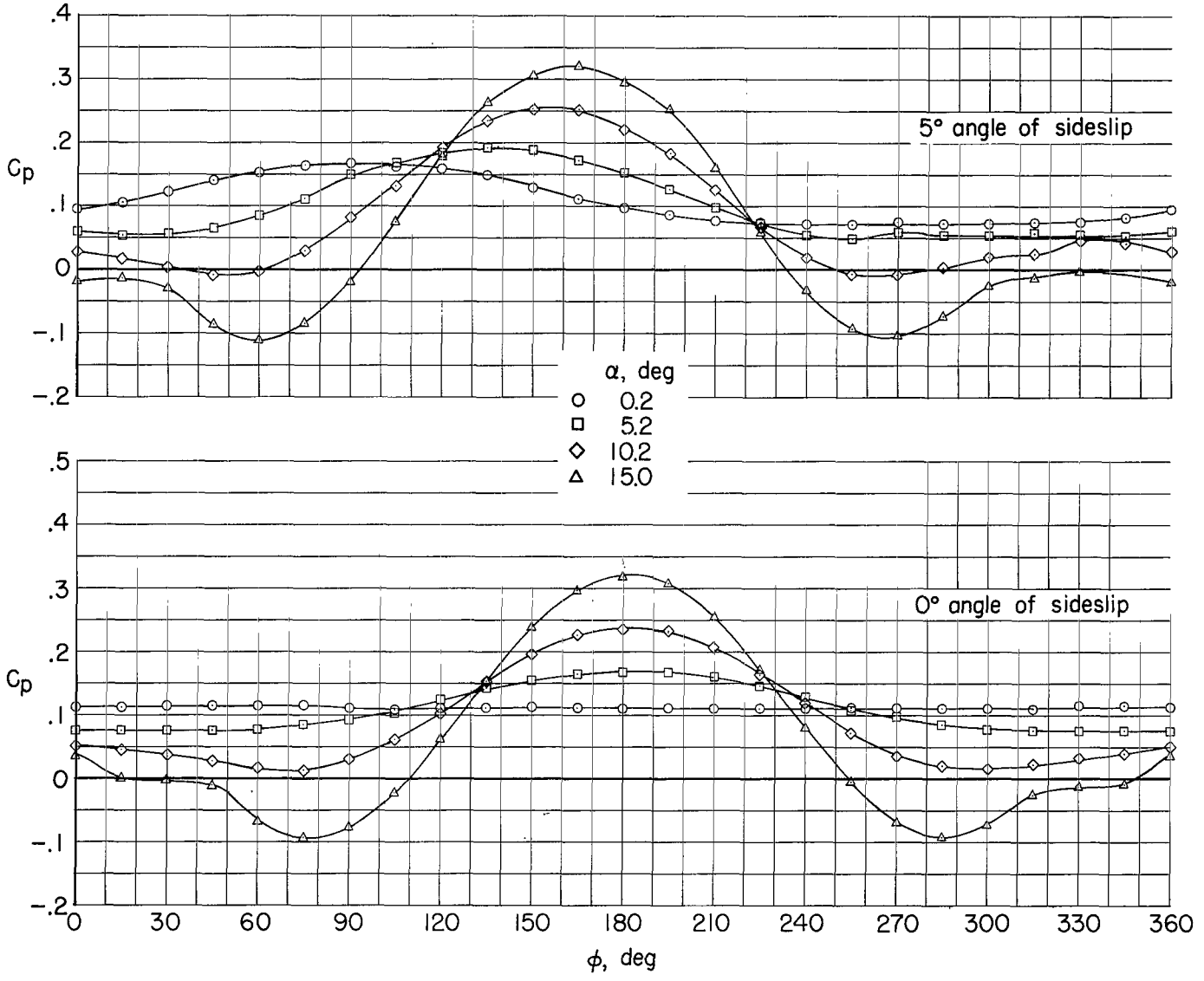

(f) M = 1.10.

Figure 6.- Continued.

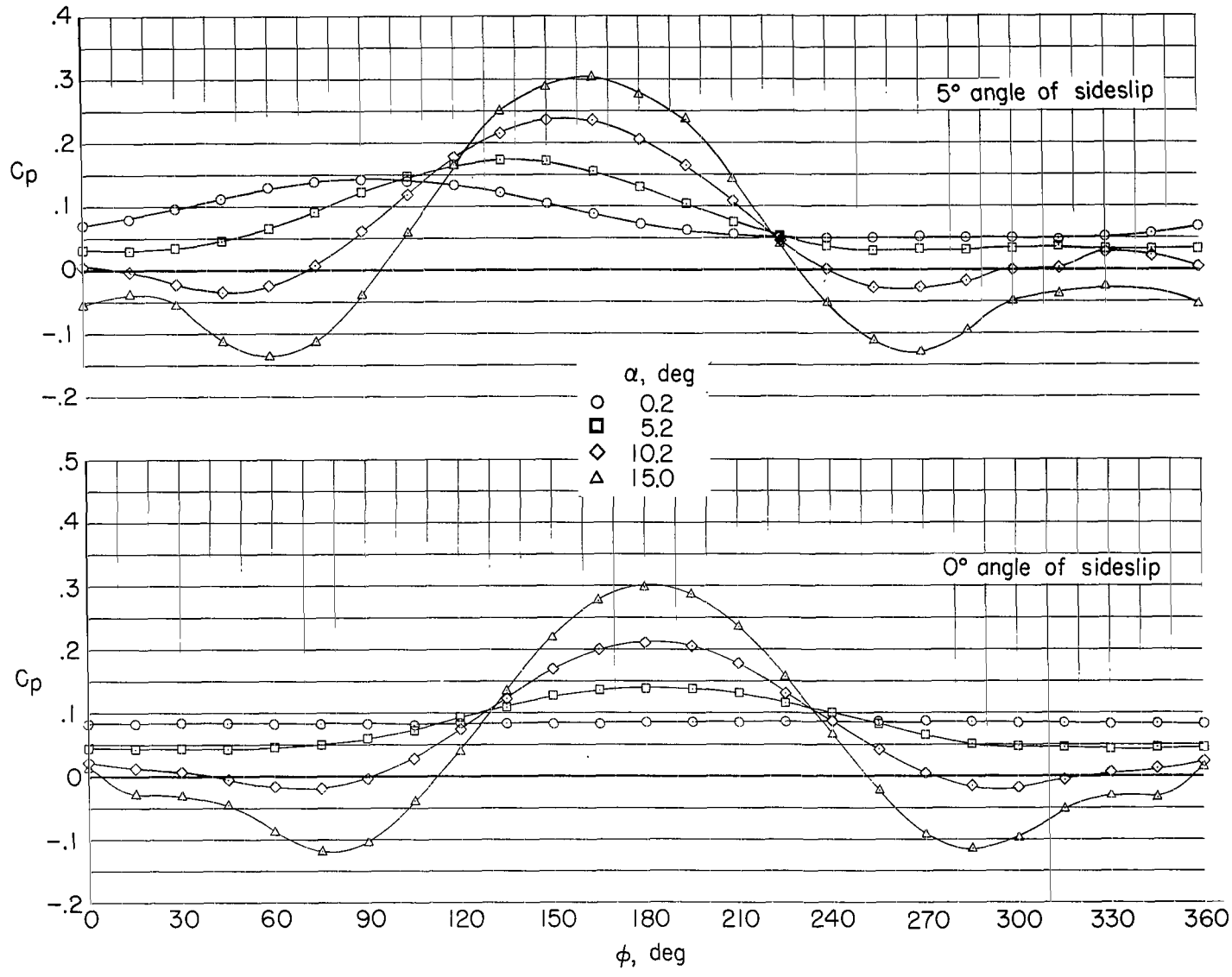

(g) M = 1.20.

Figure 6.- Continued.

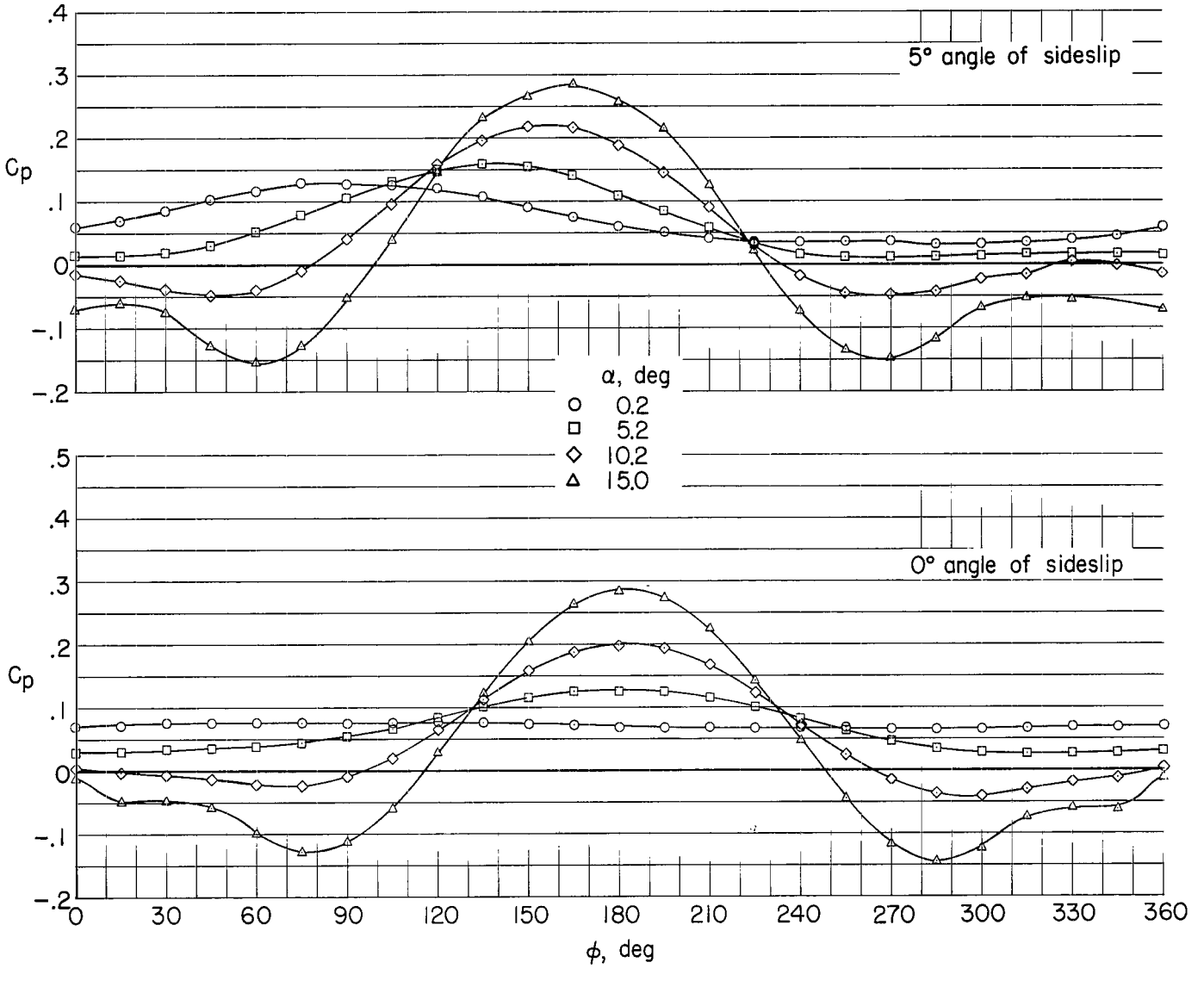

(h) M = 1.29.

Figure 6.- Concluded.

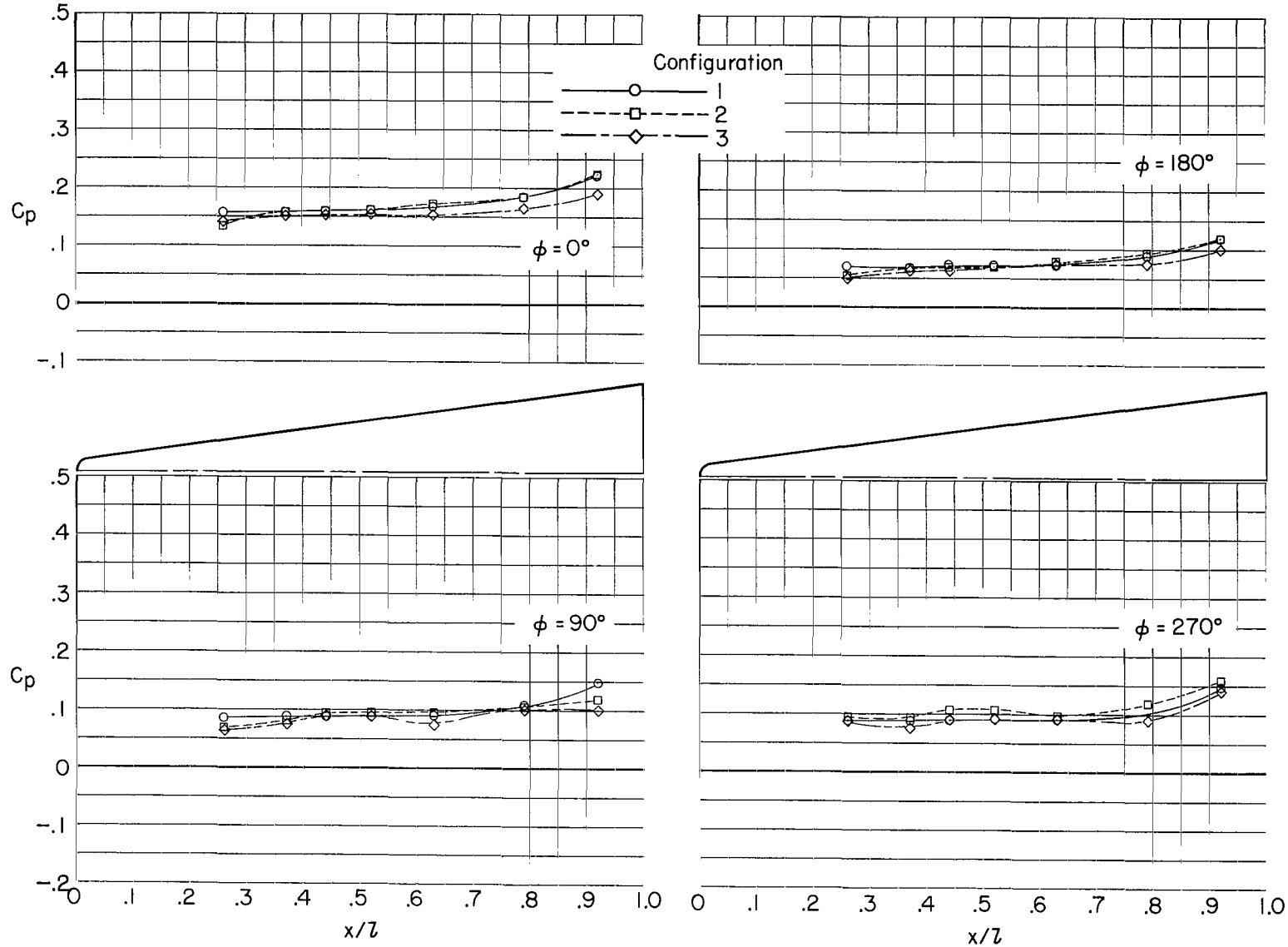

(a) $\alpha = -4.8^0$.

Figure 7.- Comparison of longitudinal pressure distributions for three configurations. M = 0.30; $\beta = 0^0$.

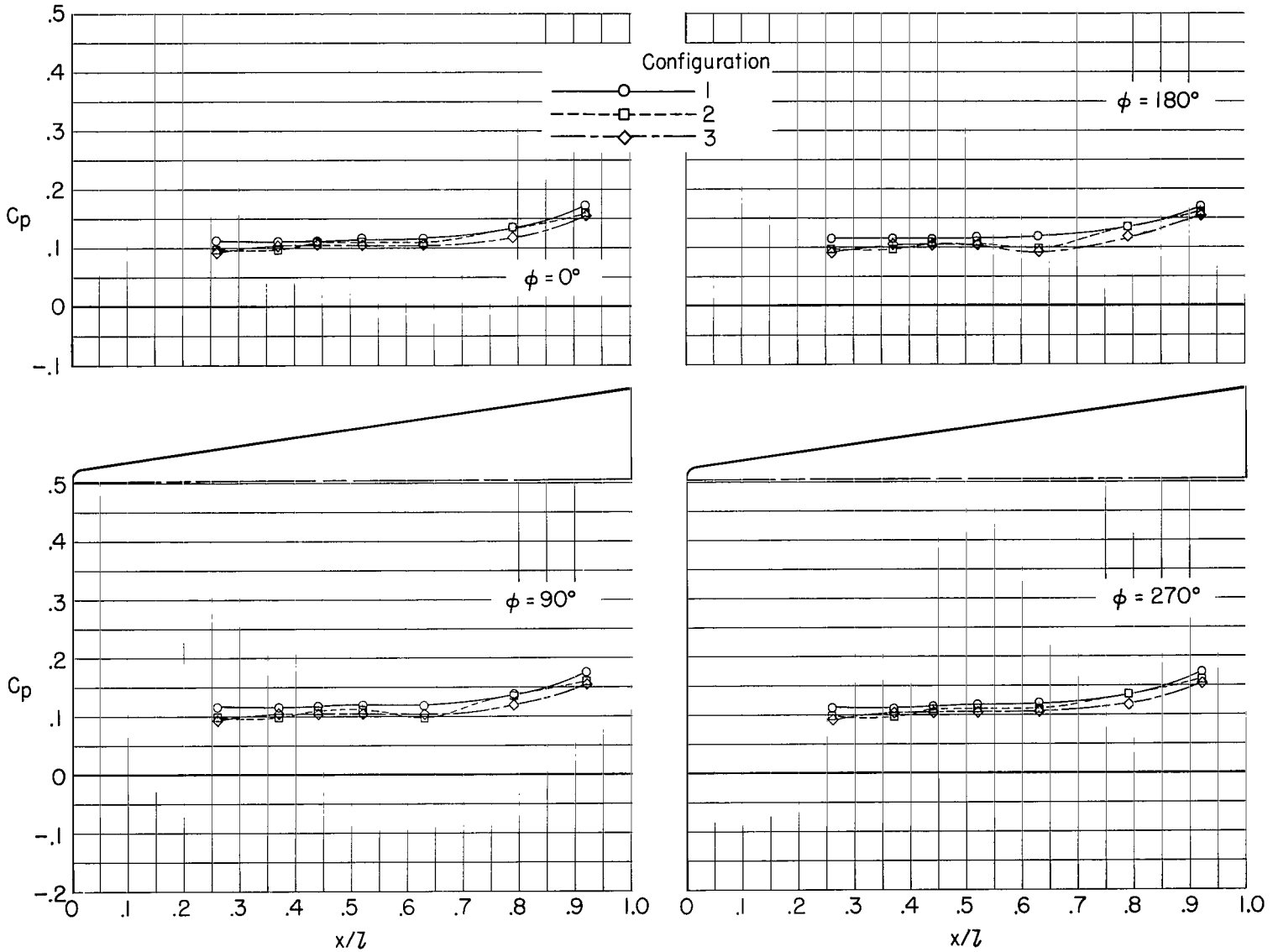

(b) $\alpha = 0.2^0$.

Figure 7.- Continued.

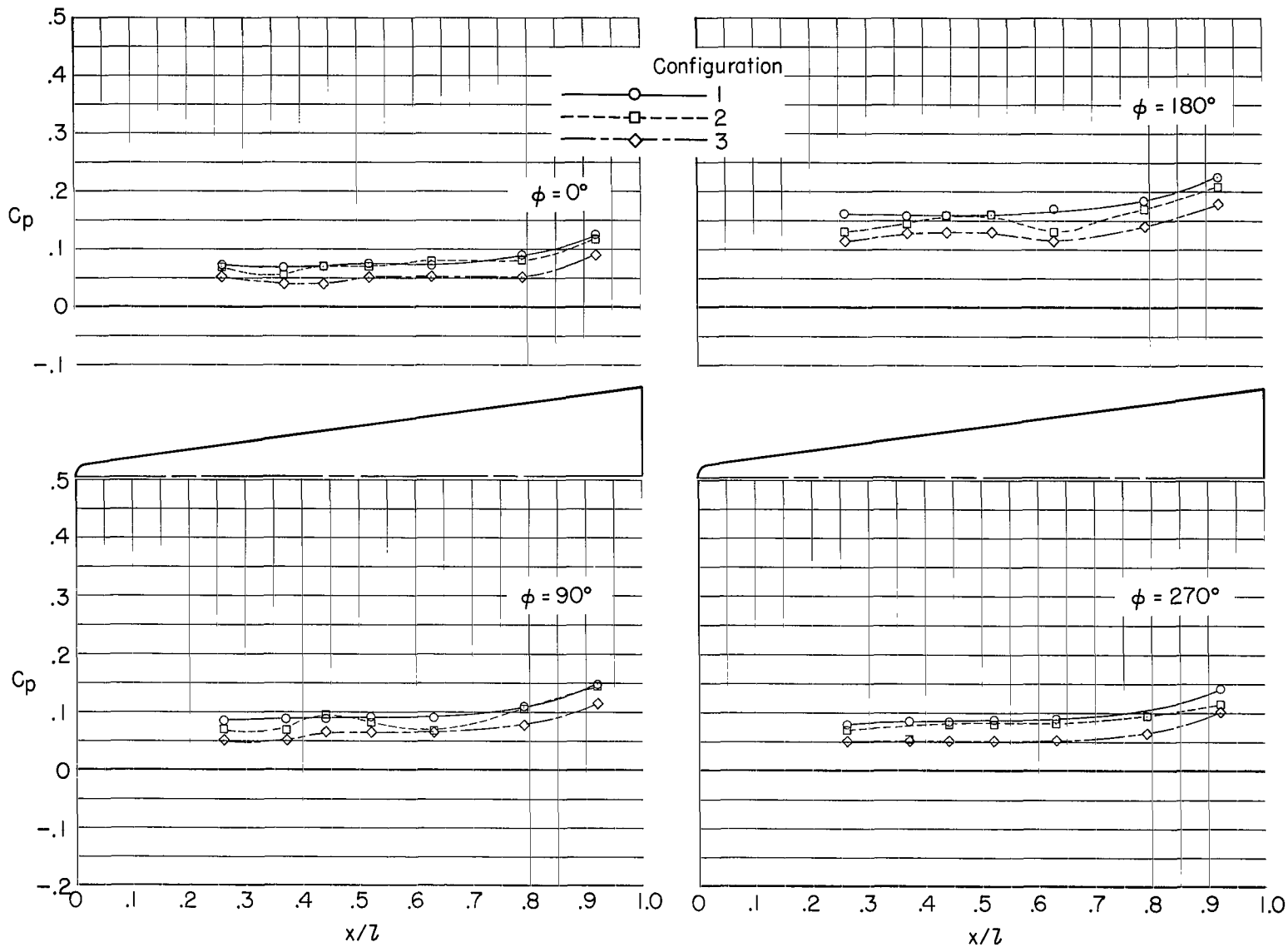

(c) $\alpha = 5.2^0$.

Figure 7.- Continued.

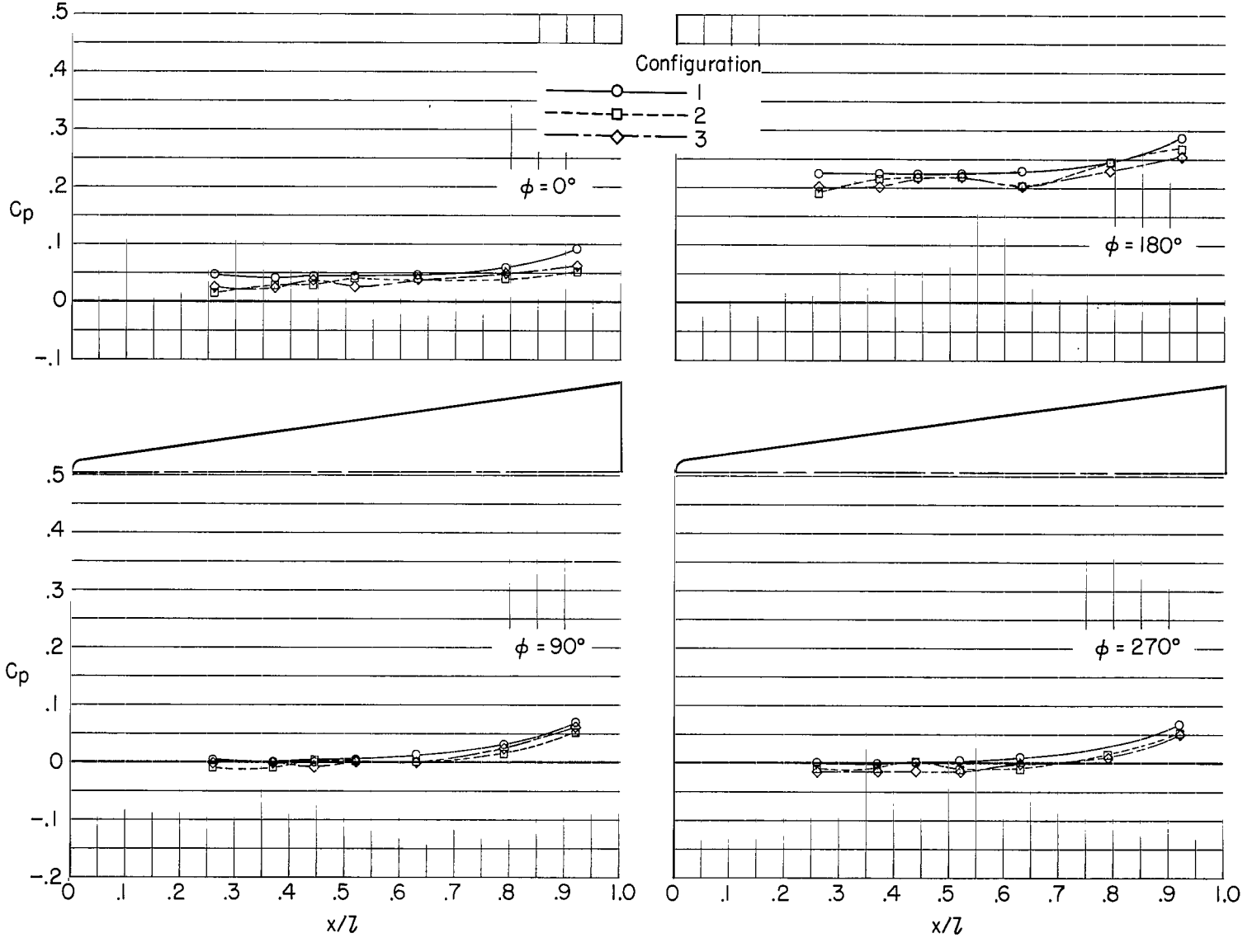

(d) $\alpha = 10.2^{\circ}$.

Figure 7.- Continued.

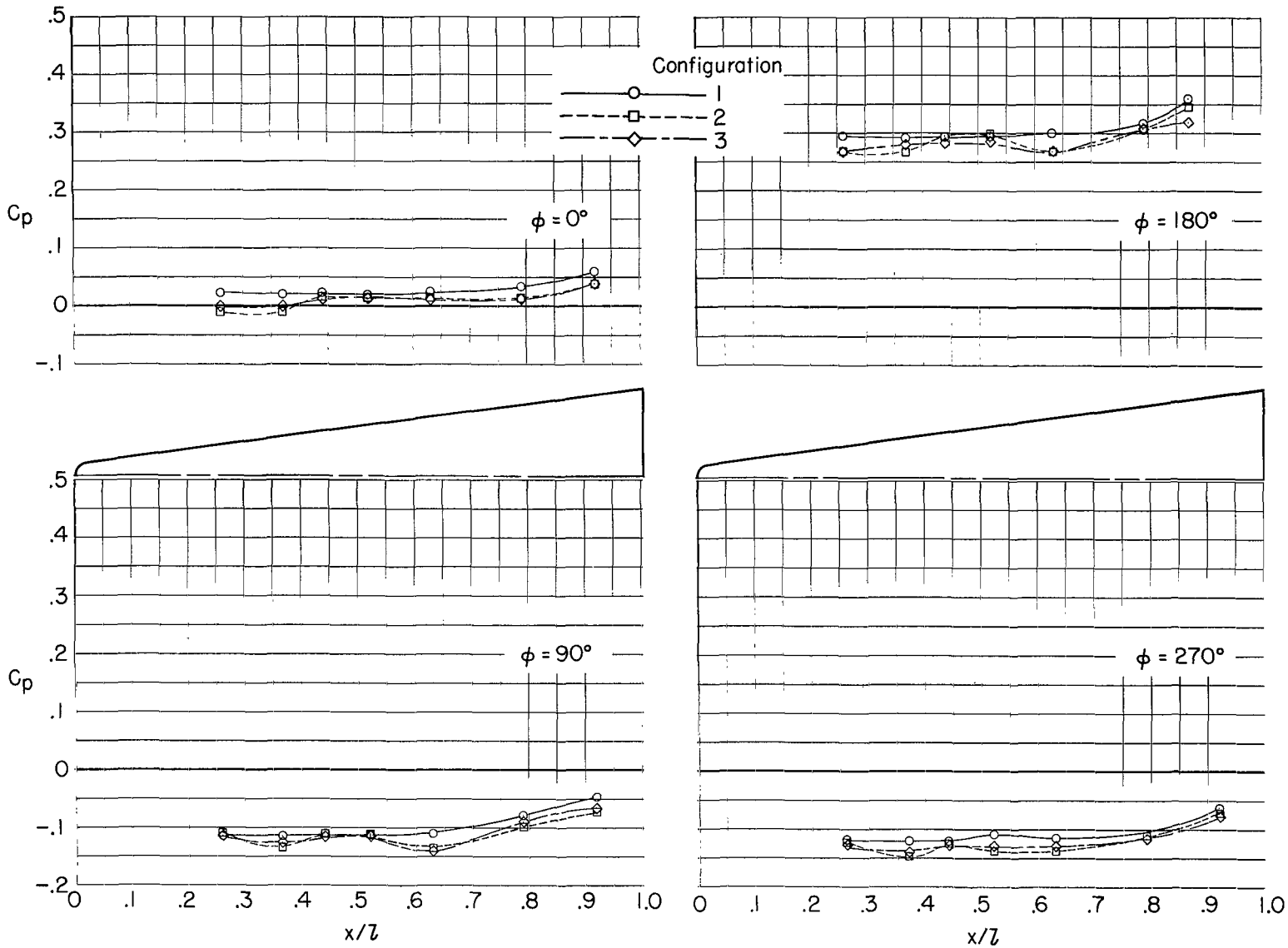

(e) $\alpha = 15.0^0$.

Figure 7.- Concluded.

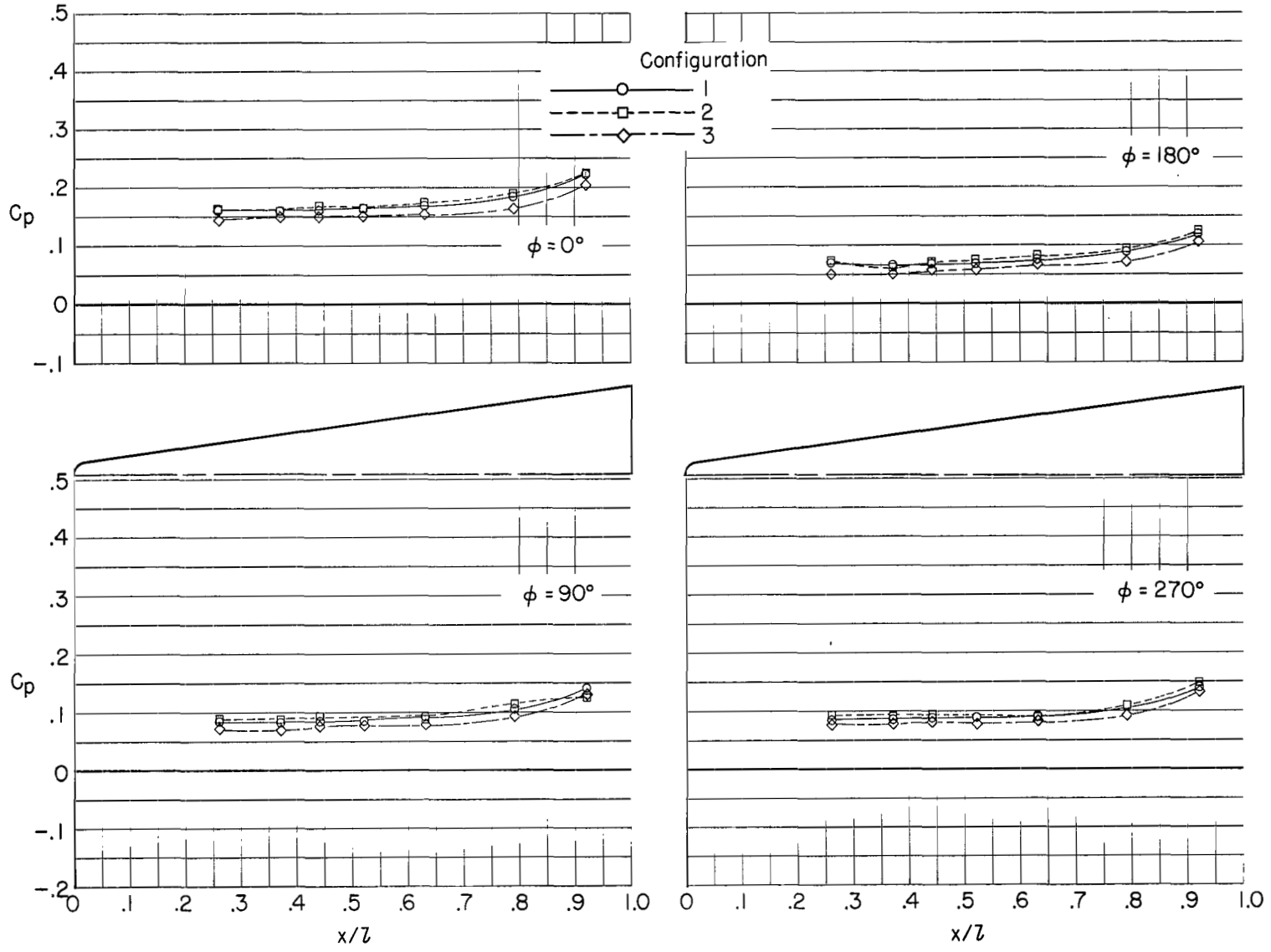

(a) $\alpha = -4.8^0$.

Figure 8.- Comparison of longitudinal pressure distributions for three configurations. M = 0.50; $\beta = 0^0$.

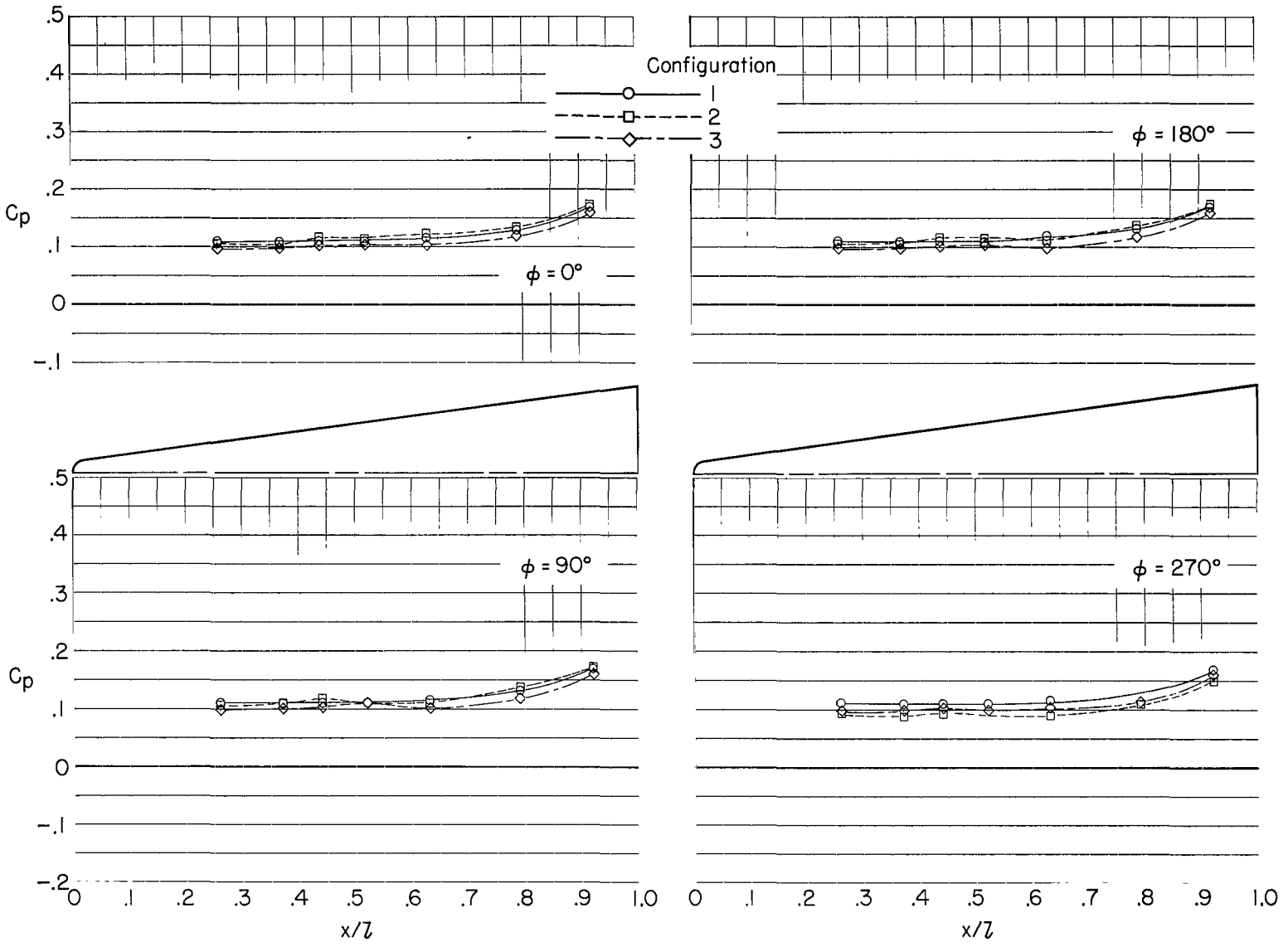

(b) $\alpha = 0.2^0$.

Figure 8.- Continued.

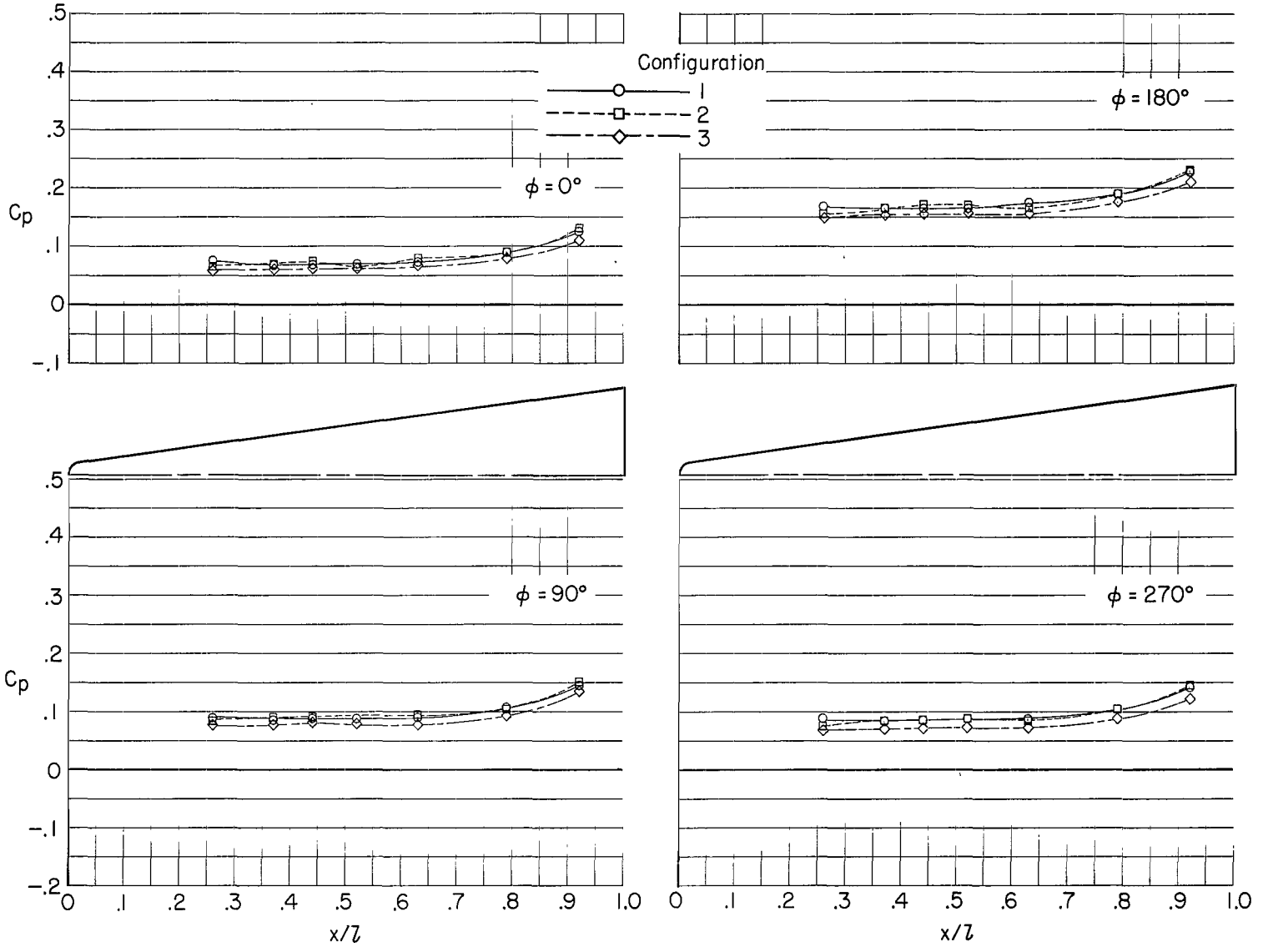

(c) $\alpha = 5.2^0$.

Figure 8.- Continued.

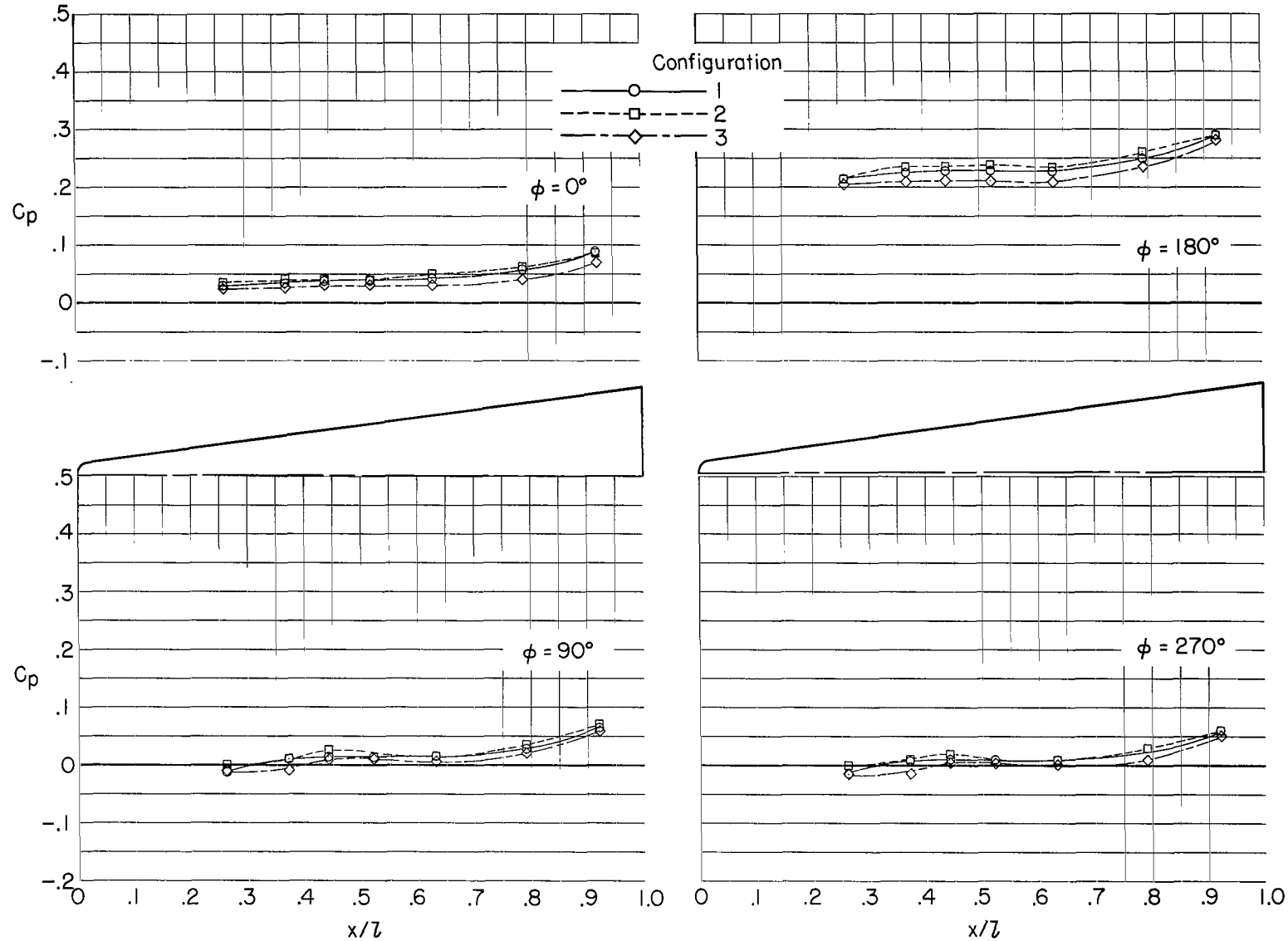

(d) $\alpha = 10.2^0$.

Figure 8.- Continued.

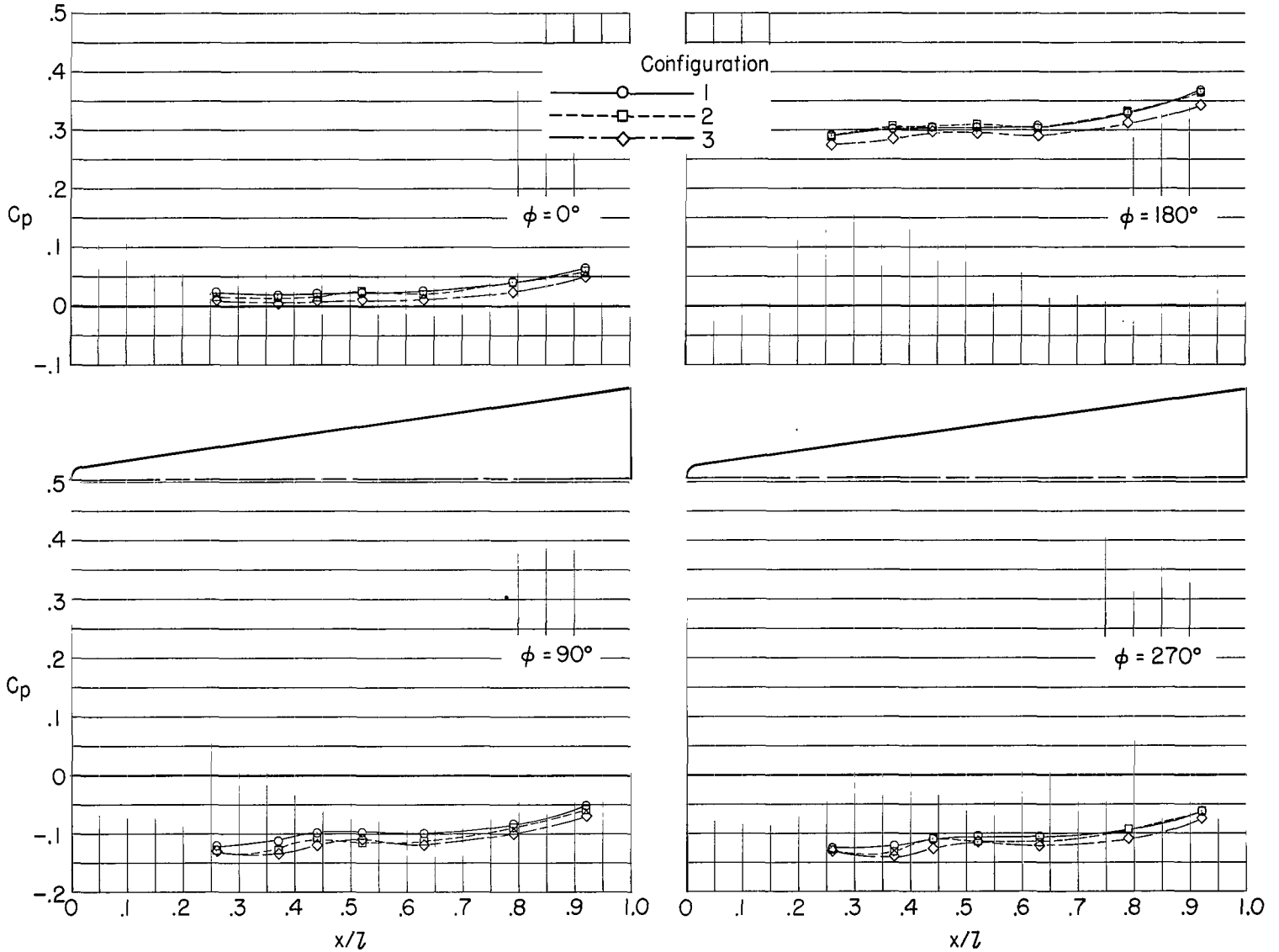

(e) $\alpha = 15.0^0$.

Figure 8.- Concluded.

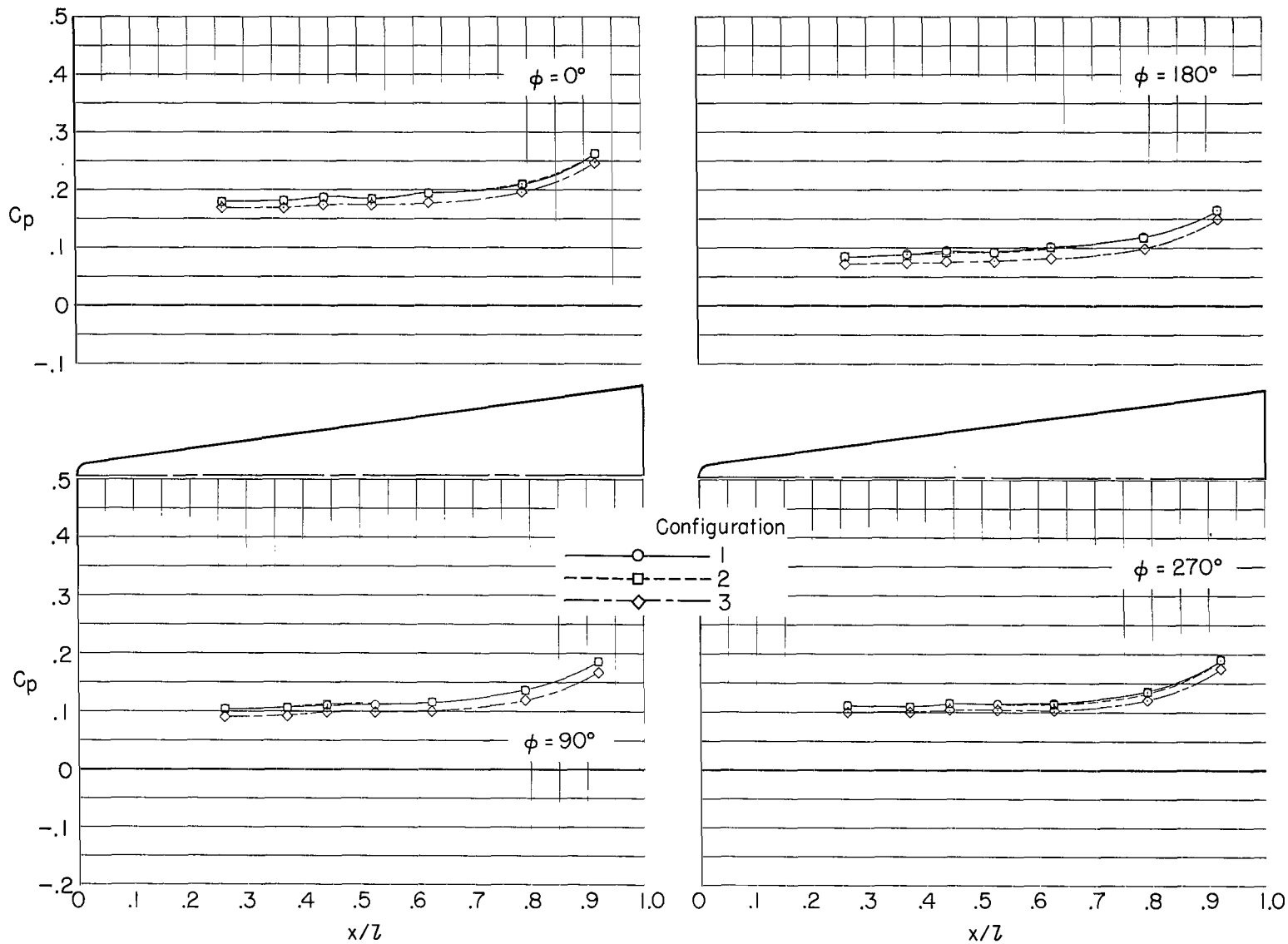

(a) $\alpha = -4.8^0$.

Figure 9.- Comparison of longitudinal pressure distributions for three configurations. M = 0.80; $\beta = 0^0$.

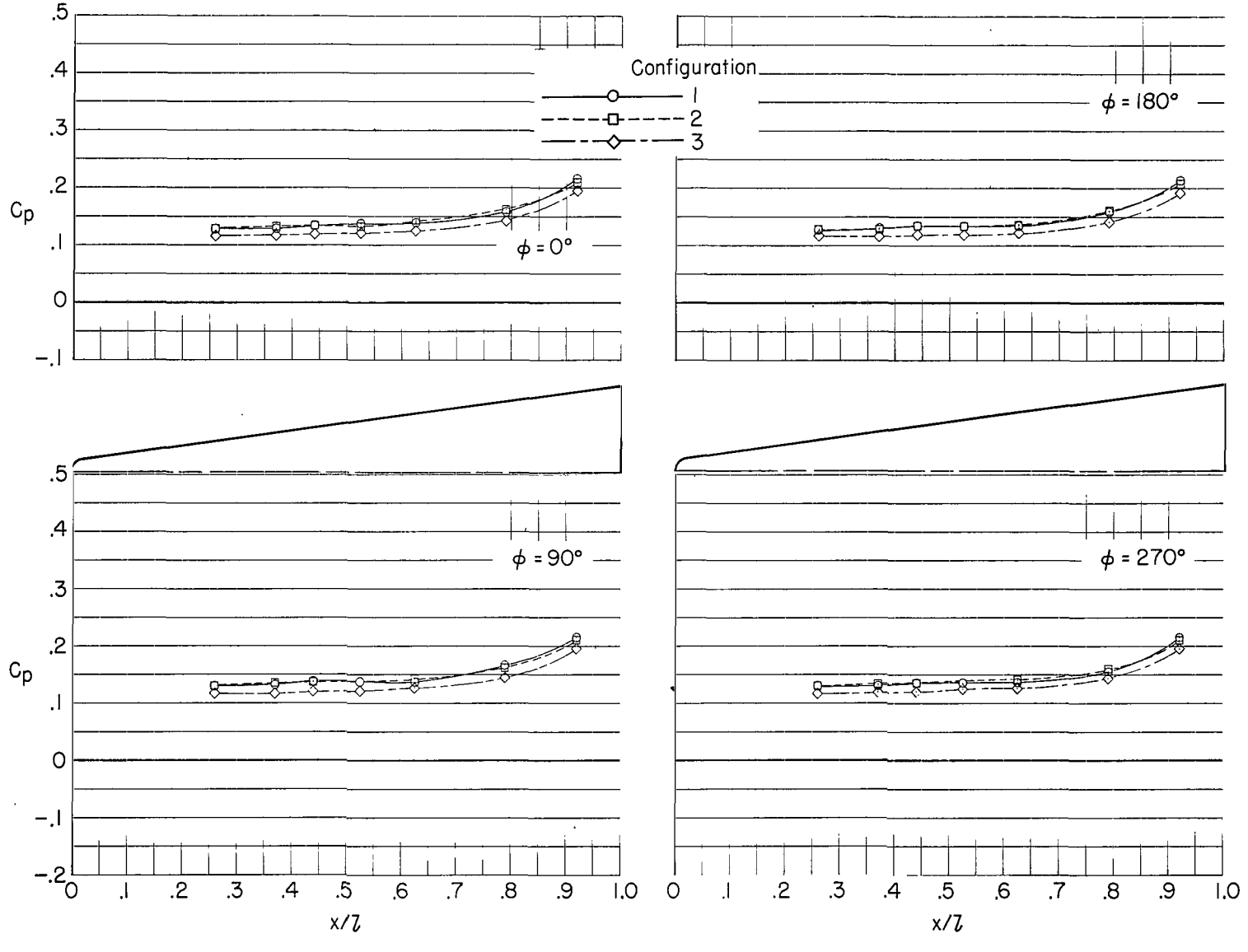

(b) $\alpha = 0.2^{0}$.

Figure 9.- Continued.

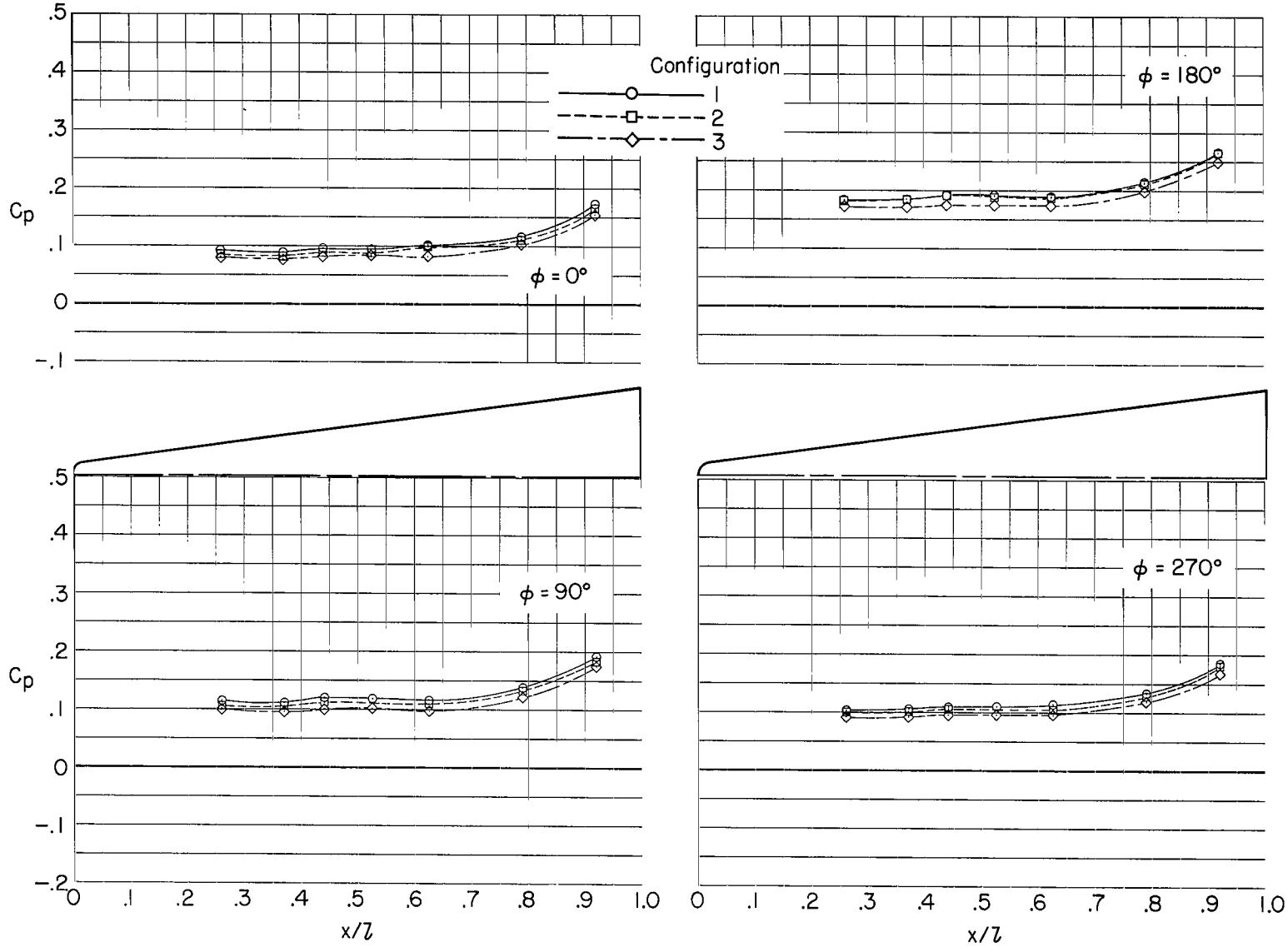

(c) $\alpha = 5.2^0$.

Figure 9.- Continued.

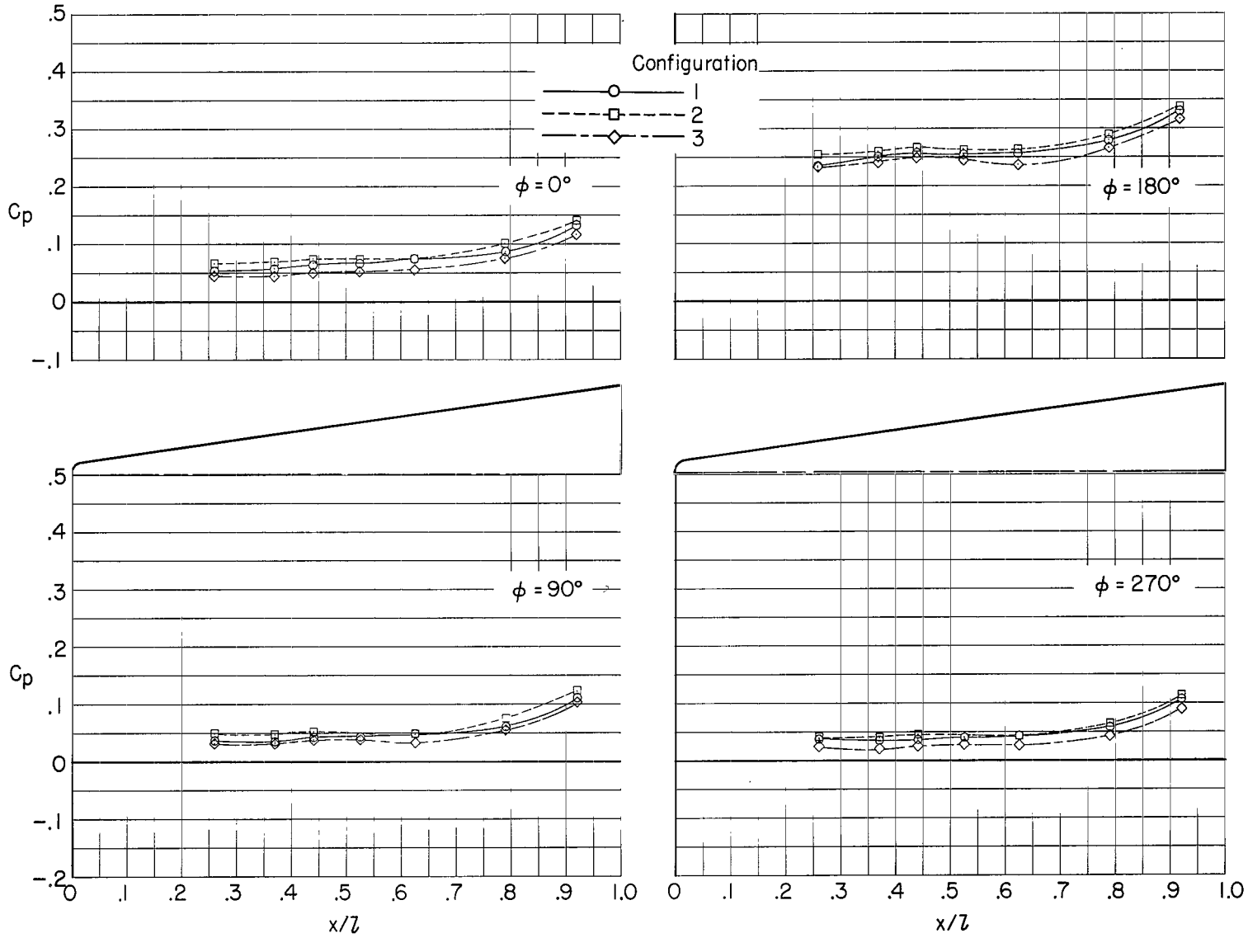

(d) $\alpha = 10.2^0$.

Figure 9.- Continued.

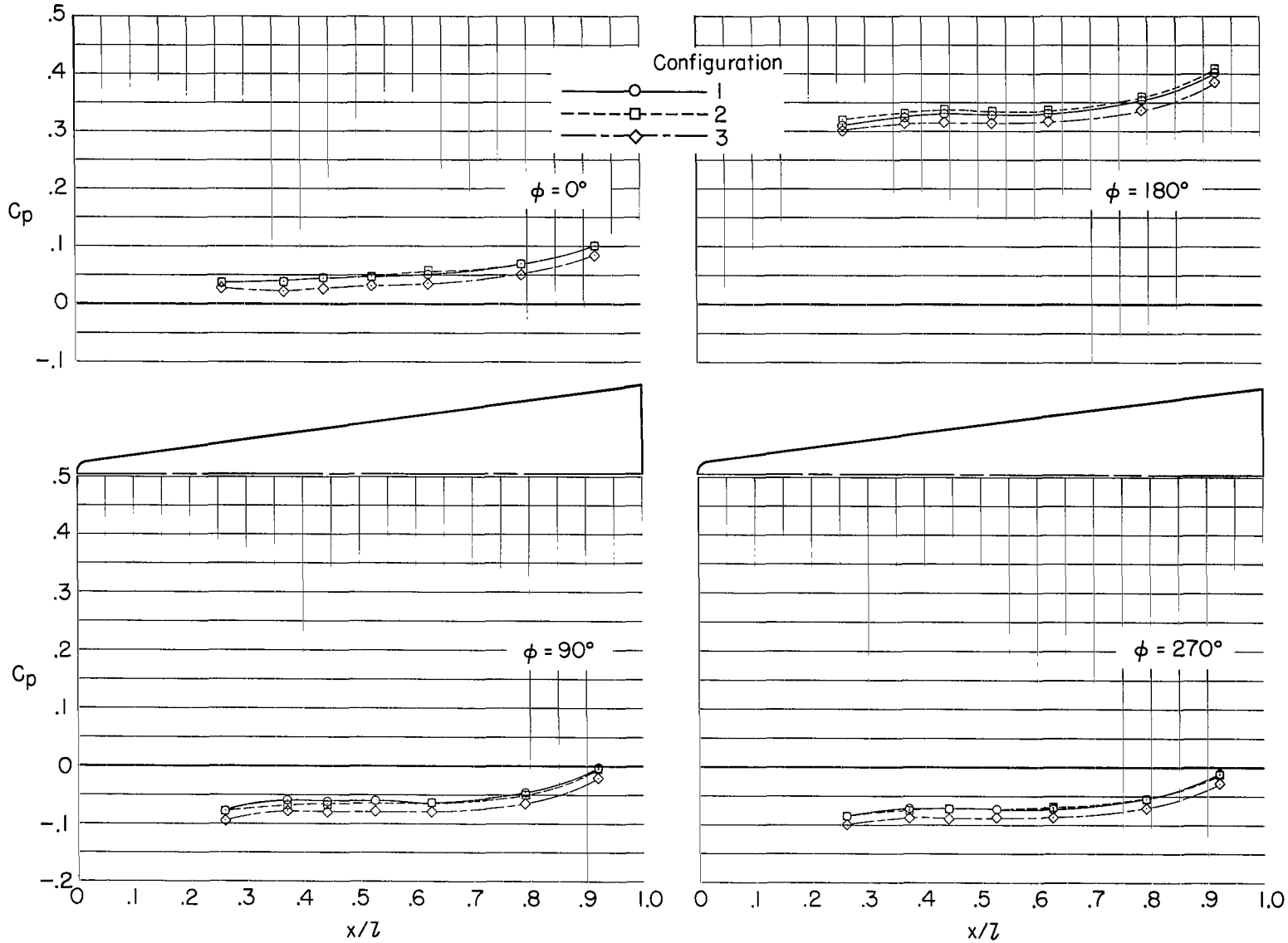

(e) $\alpha = 15.0^0$.

Figure 9.- Concluded.

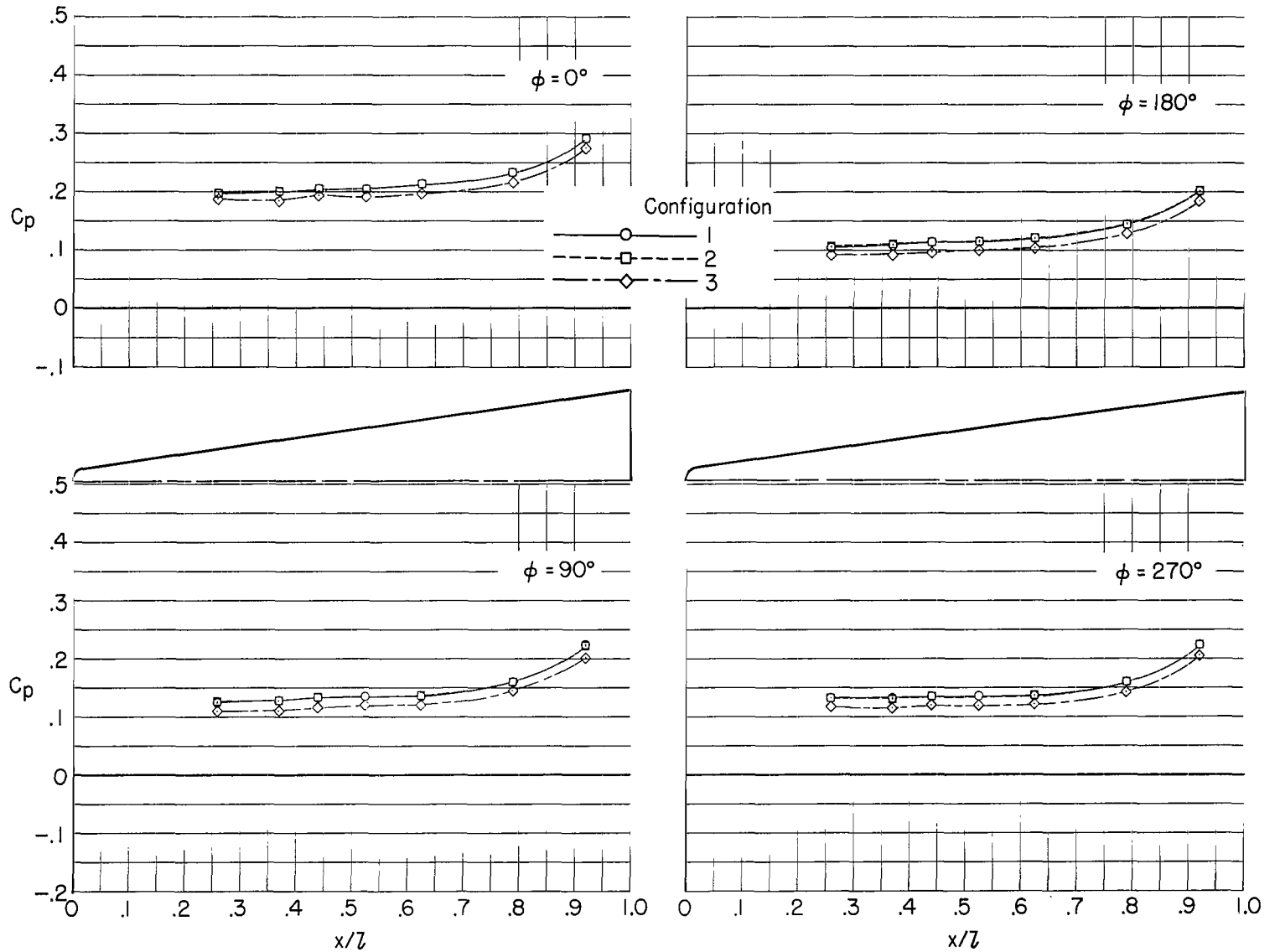

(a) $\alpha = -4.8^{0}$.

Figure 10.- Comparison of longitudinal pressure distributions for three configurations. $M = 0.90$; $\beta = 0^{0}$.

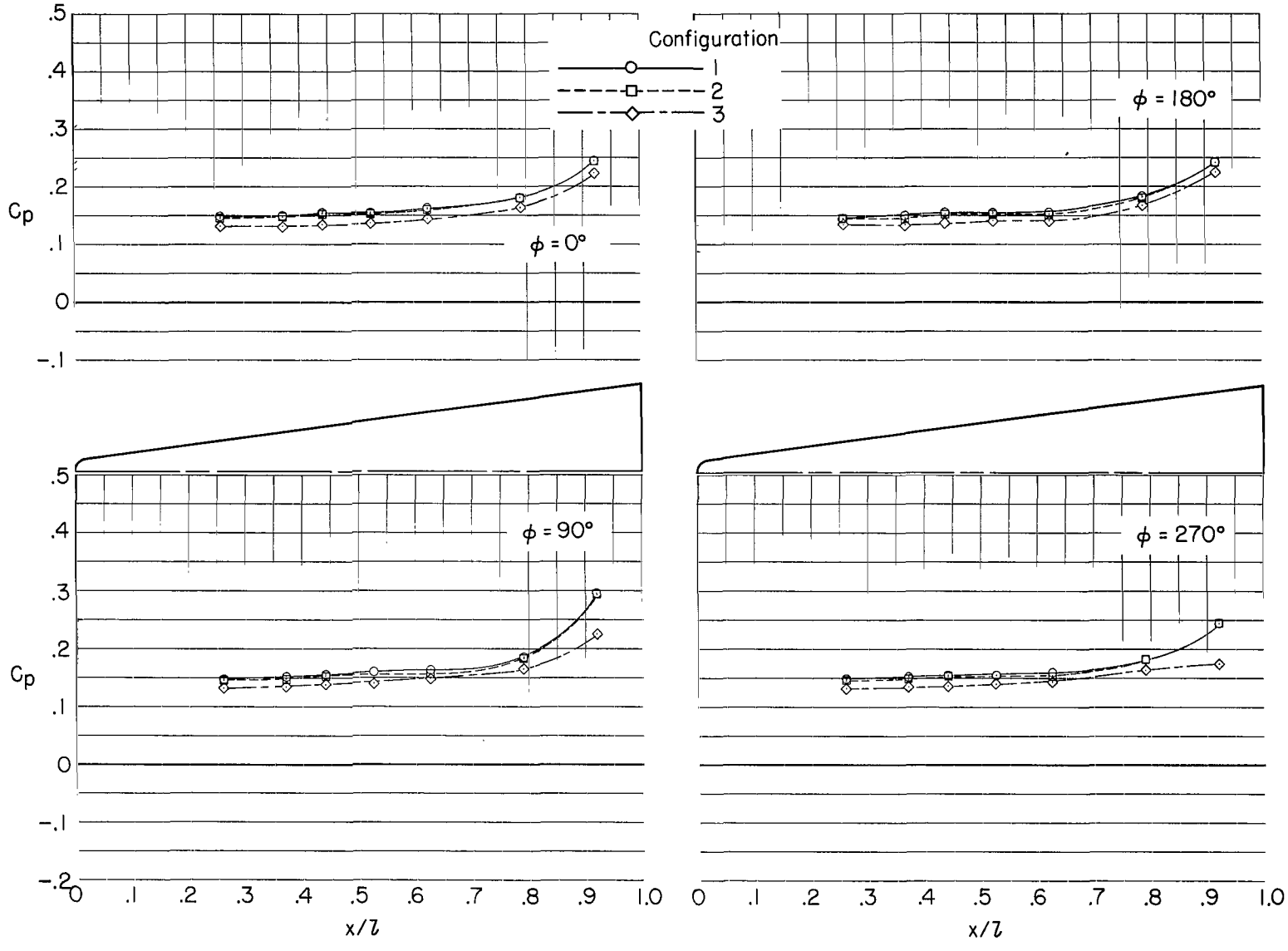

(b) $\alpha = 0.2^0$.

Figure 10.- Continued.

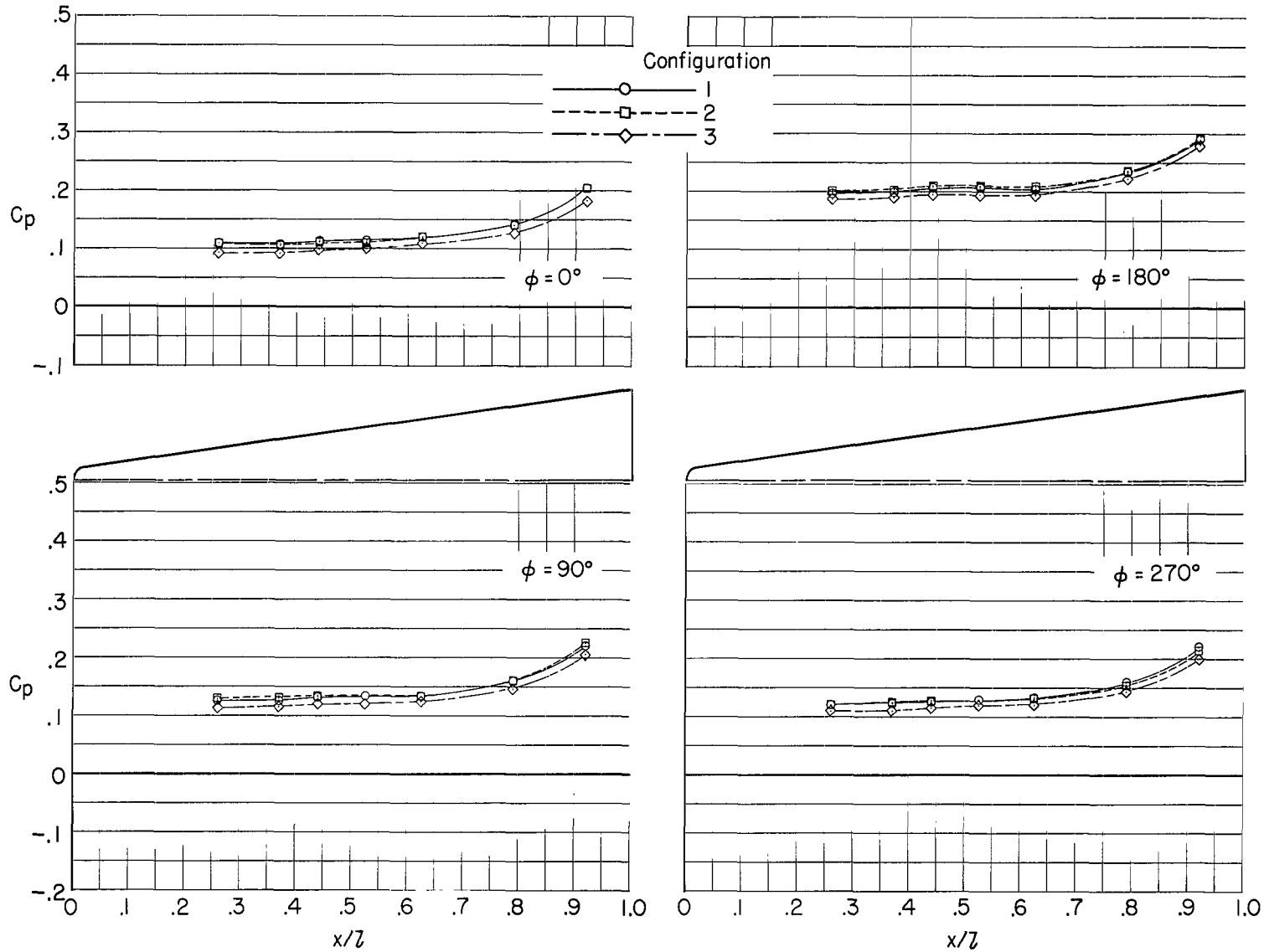

(c) $\alpha = 5.2^0$.

Figure 10.- Continued.

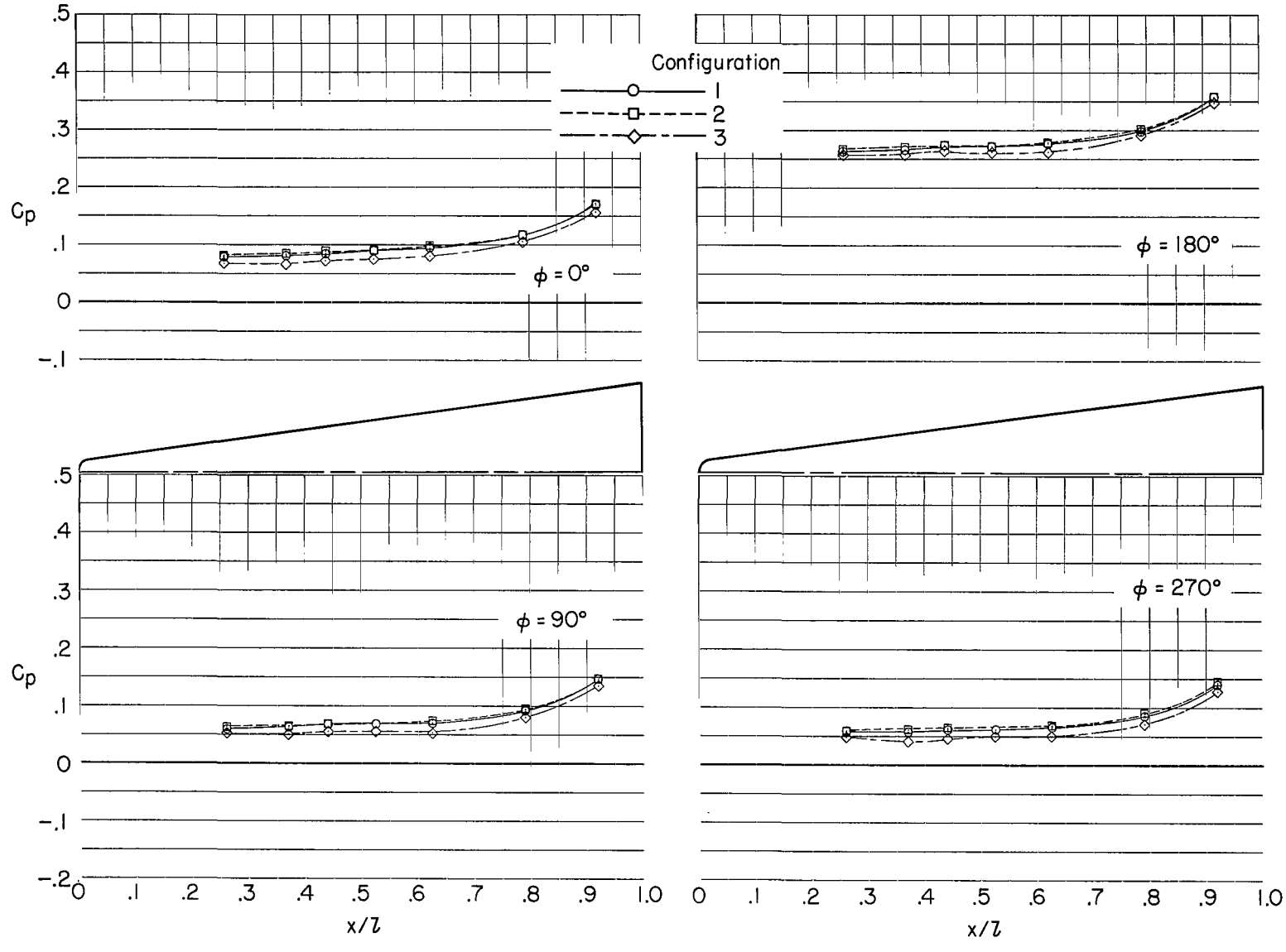

(d) $\alpha = 10.2^0$.

Figure 10.- Continued.

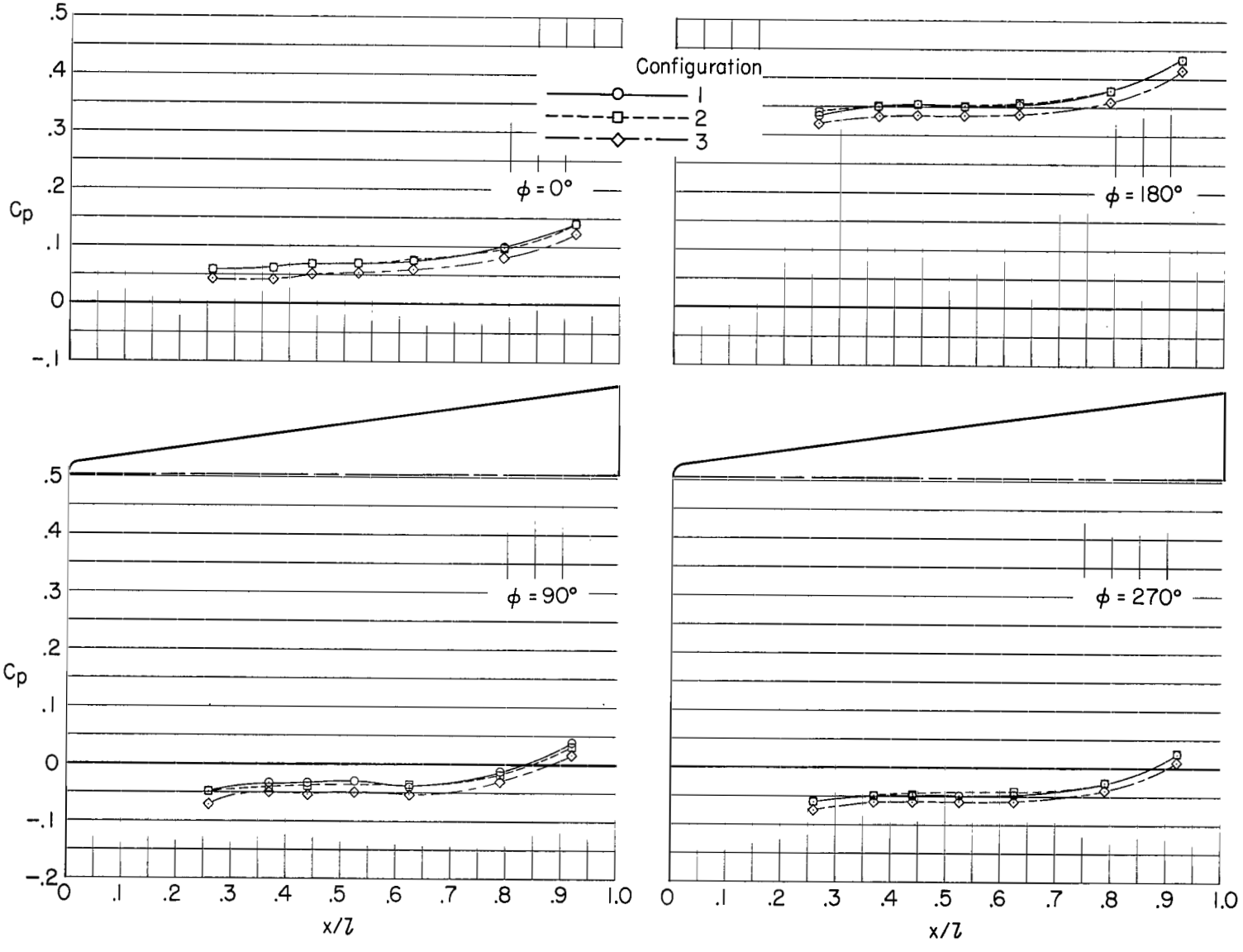

(e) $\alpha = 15.0^0$.

Figure 10.- Concluded.

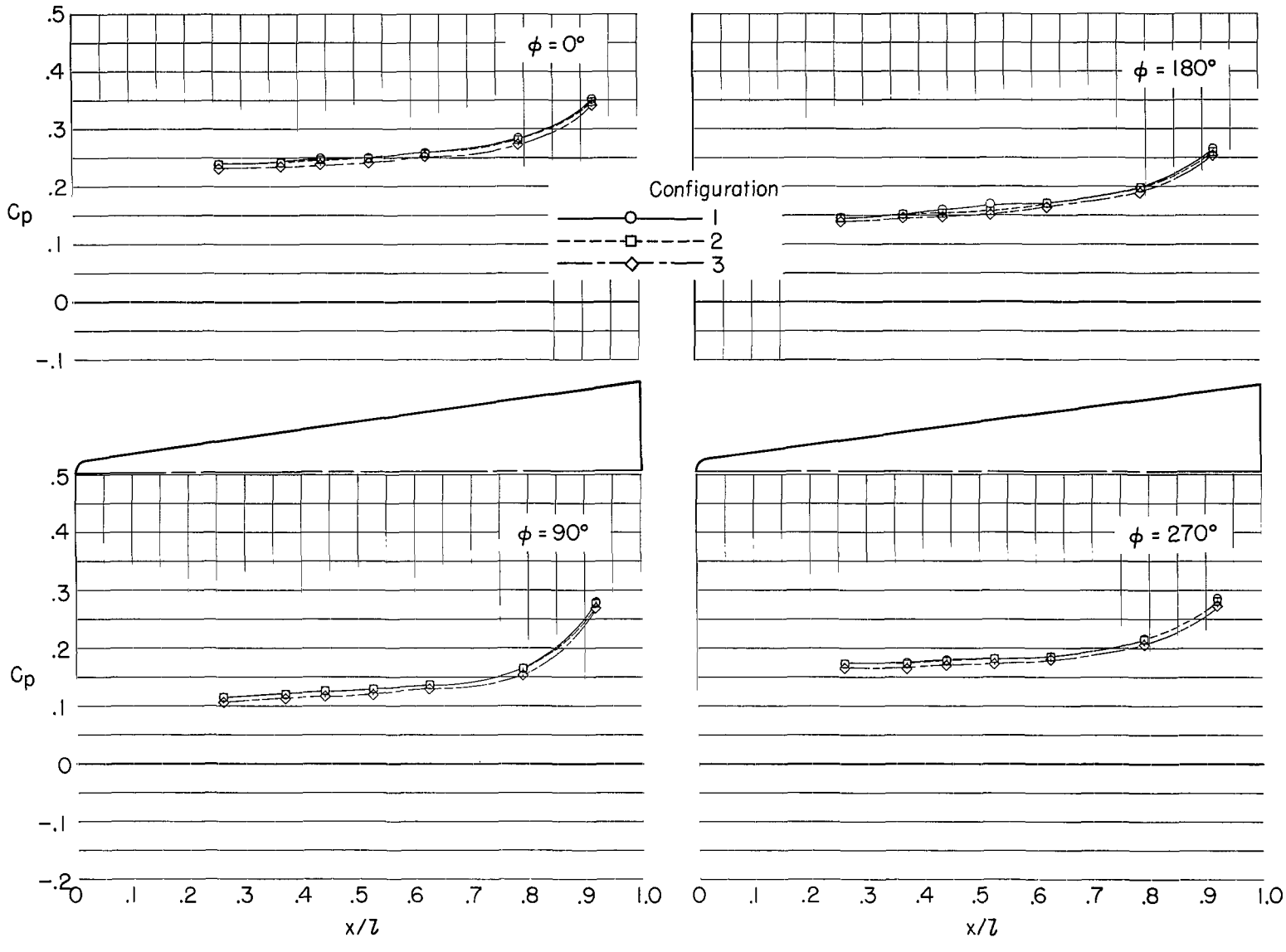

(a) $\alpha = -4.8^0$.

Figure 11.- Comparison of lontitudinal pressure distributions for three configurations. M = 1.00; $\beta = 0^0$.

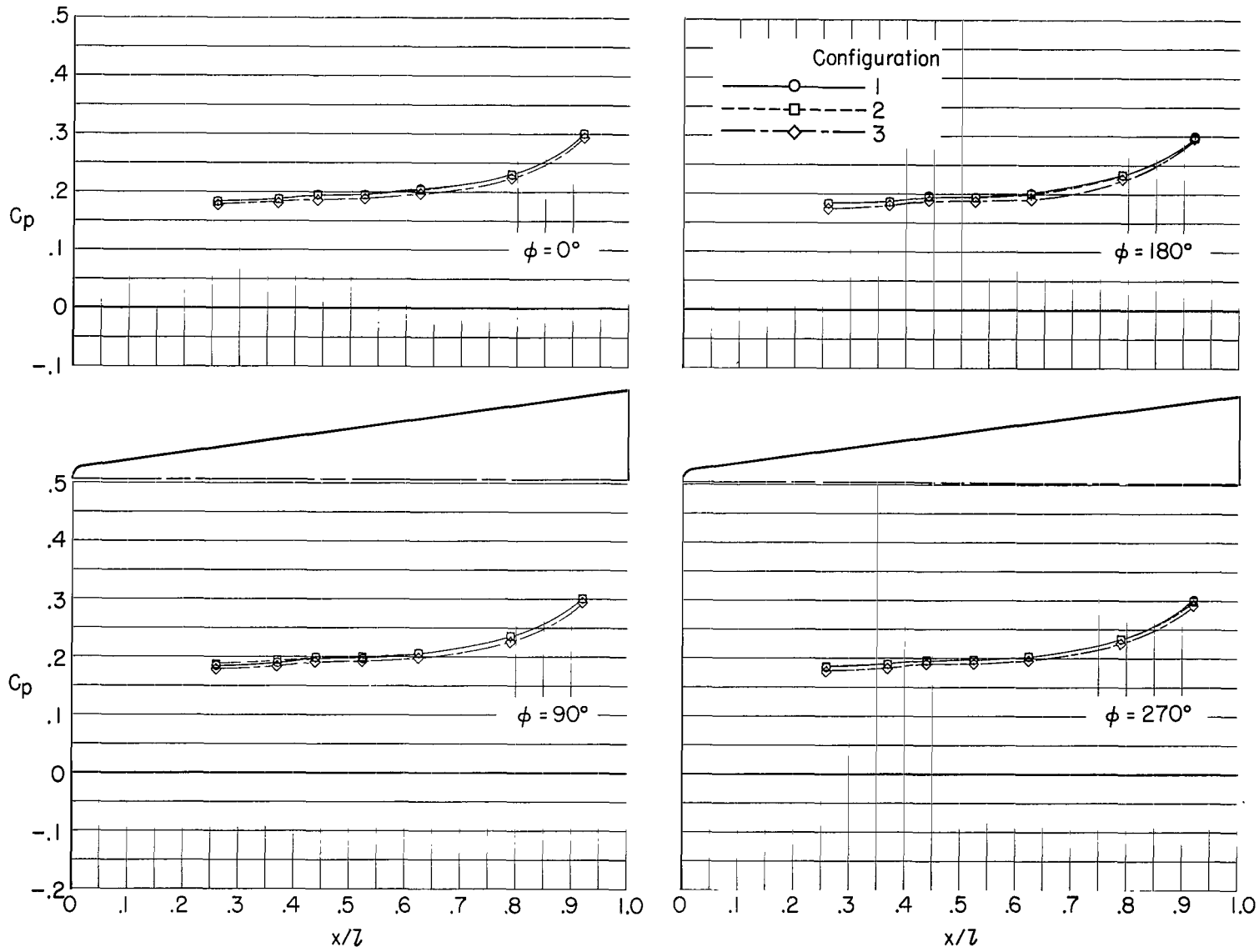

(b) $\alpha = 0.2^0$.

Figure 11.- Continued.

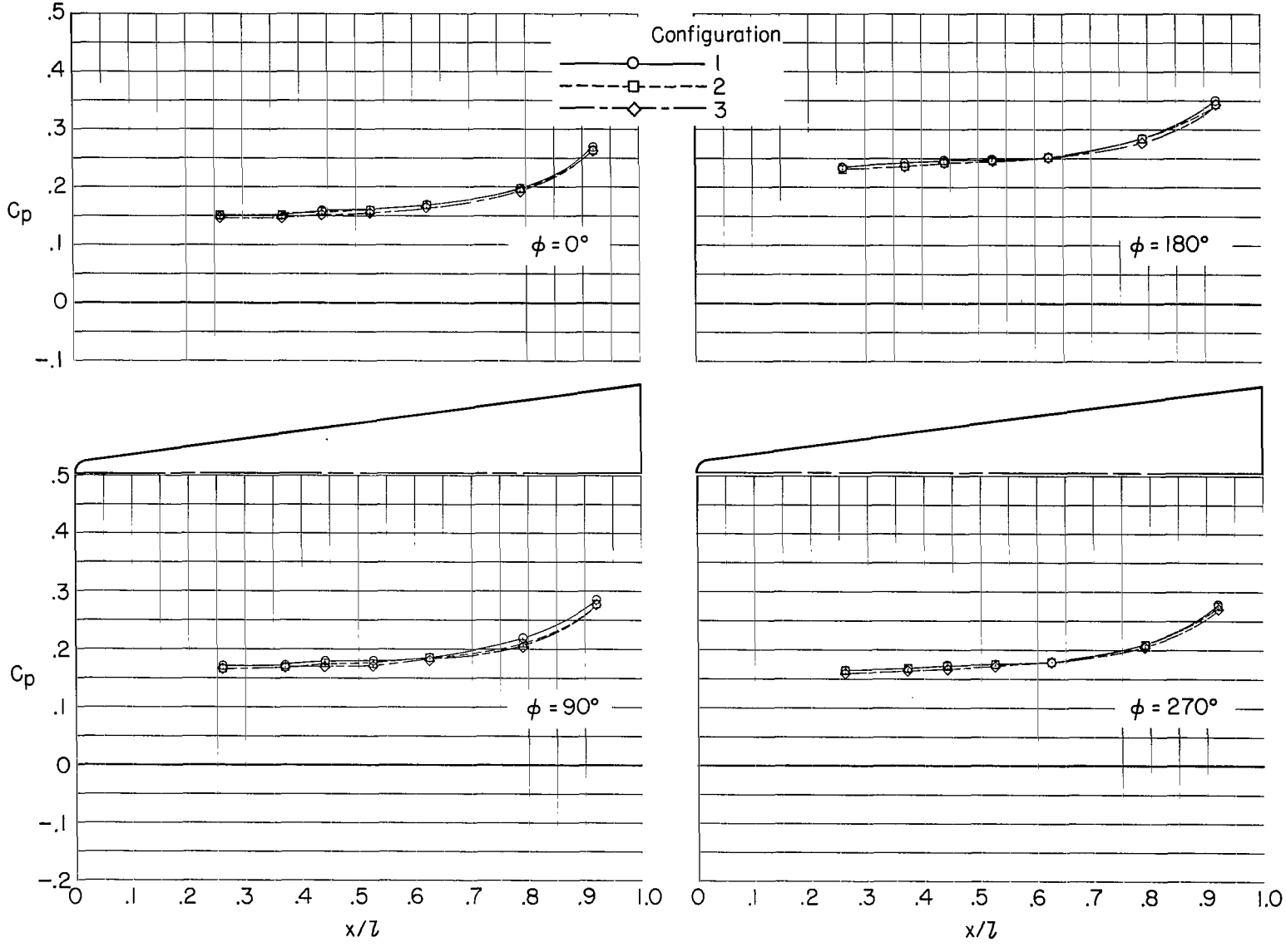

(c) $\alpha = 5.2^0$.

Figure 11.- Continued.

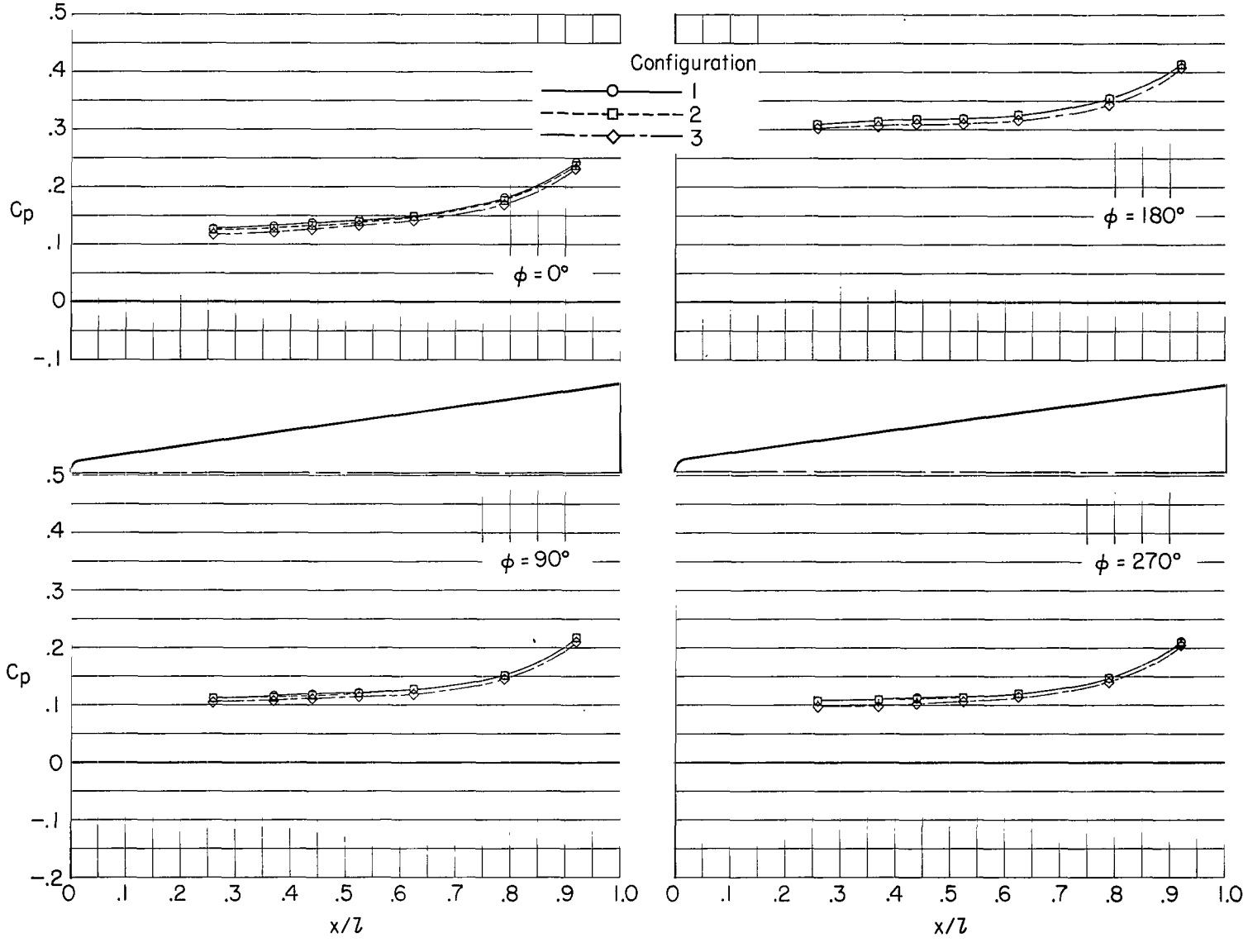

(d) $\alpha = 10.2^0$.

Figure 11.- Continued.

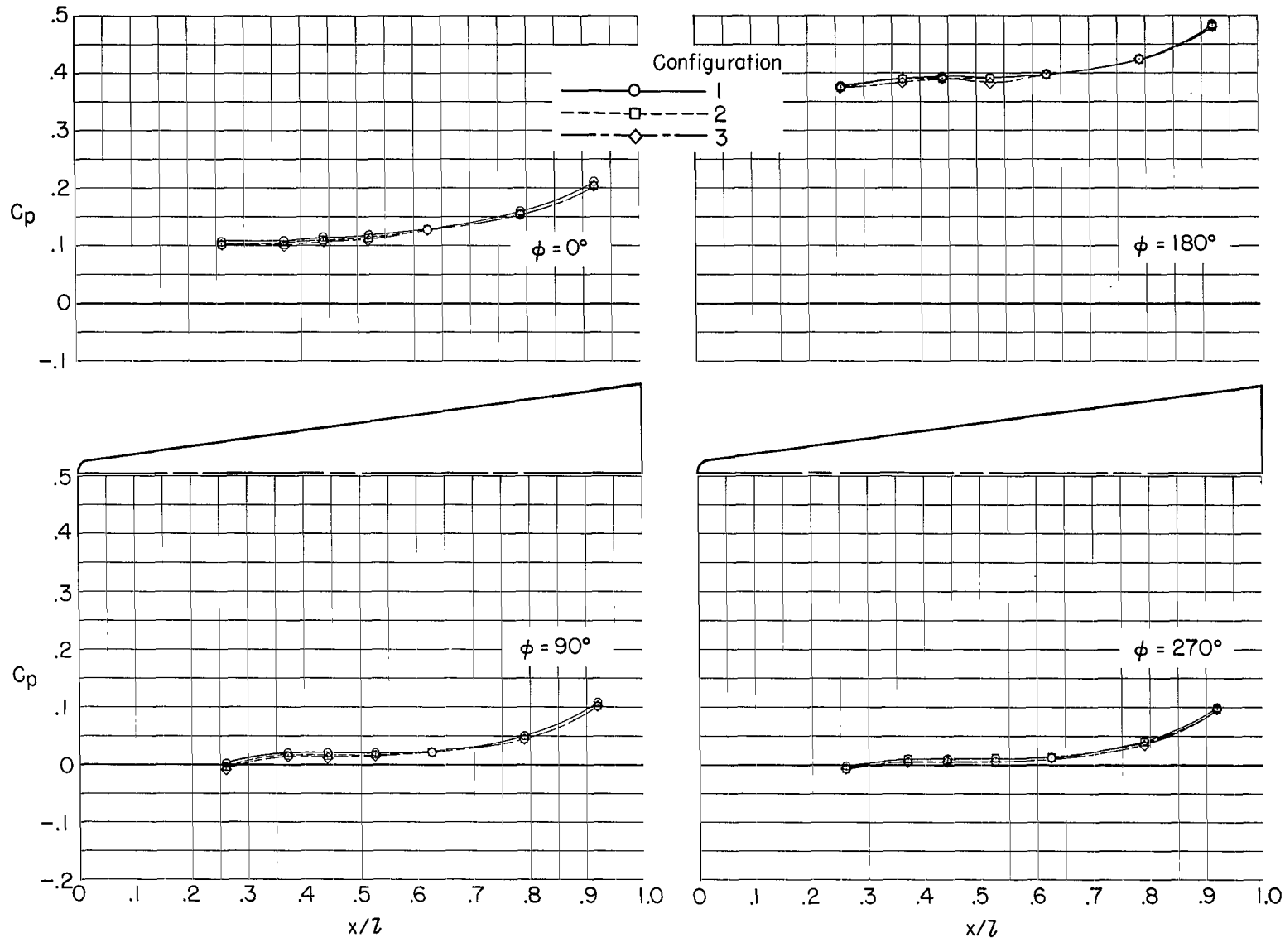

(e) $\alpha = 15.0^0$.

Figure 11.- Concluded.

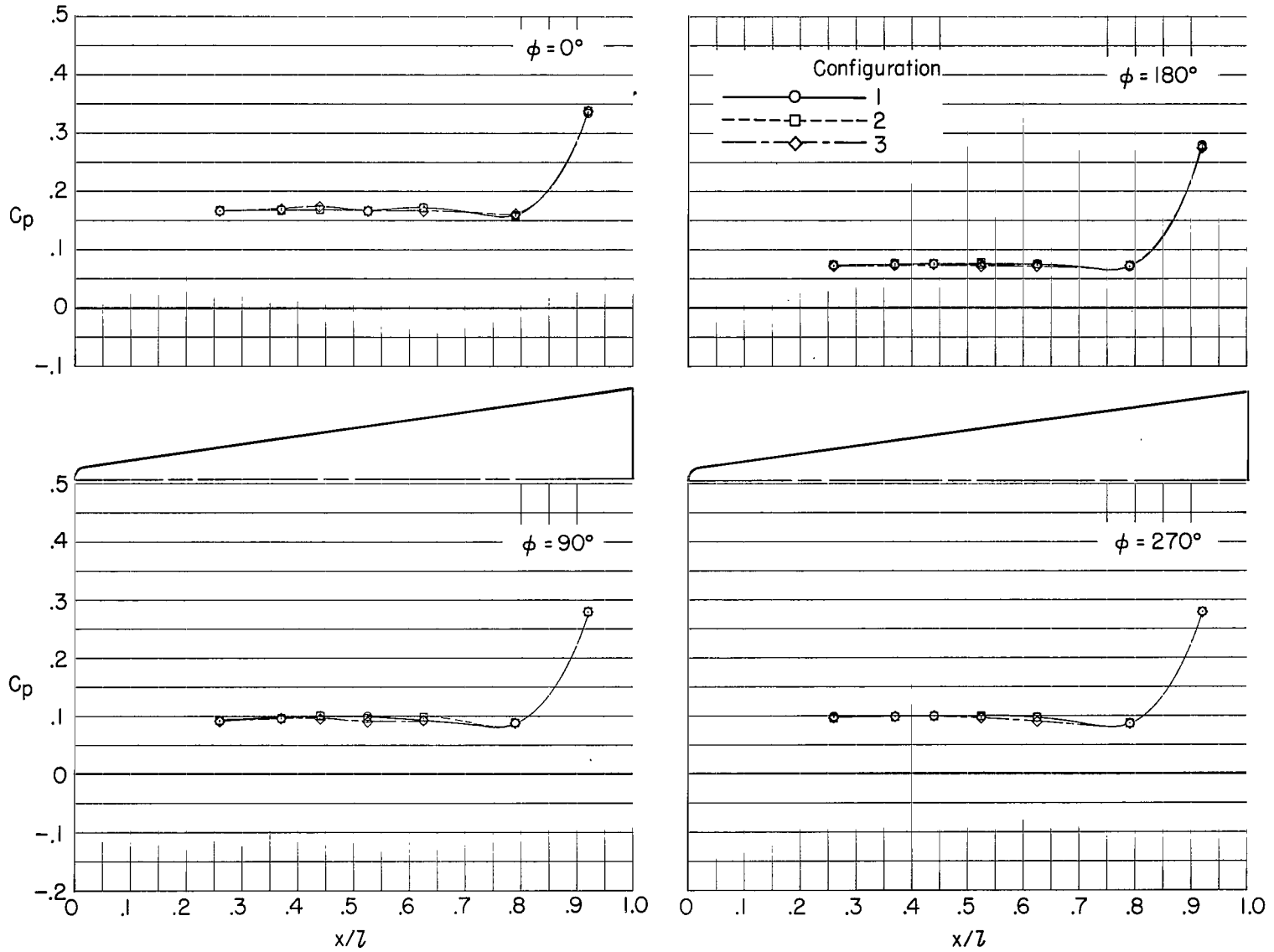

(a) $\alpha = -4.8^0$.

Figure 12.- Comparison of longitudinal pressure distributions for three configurations. M = 1.10; $\beta = 0^0$.

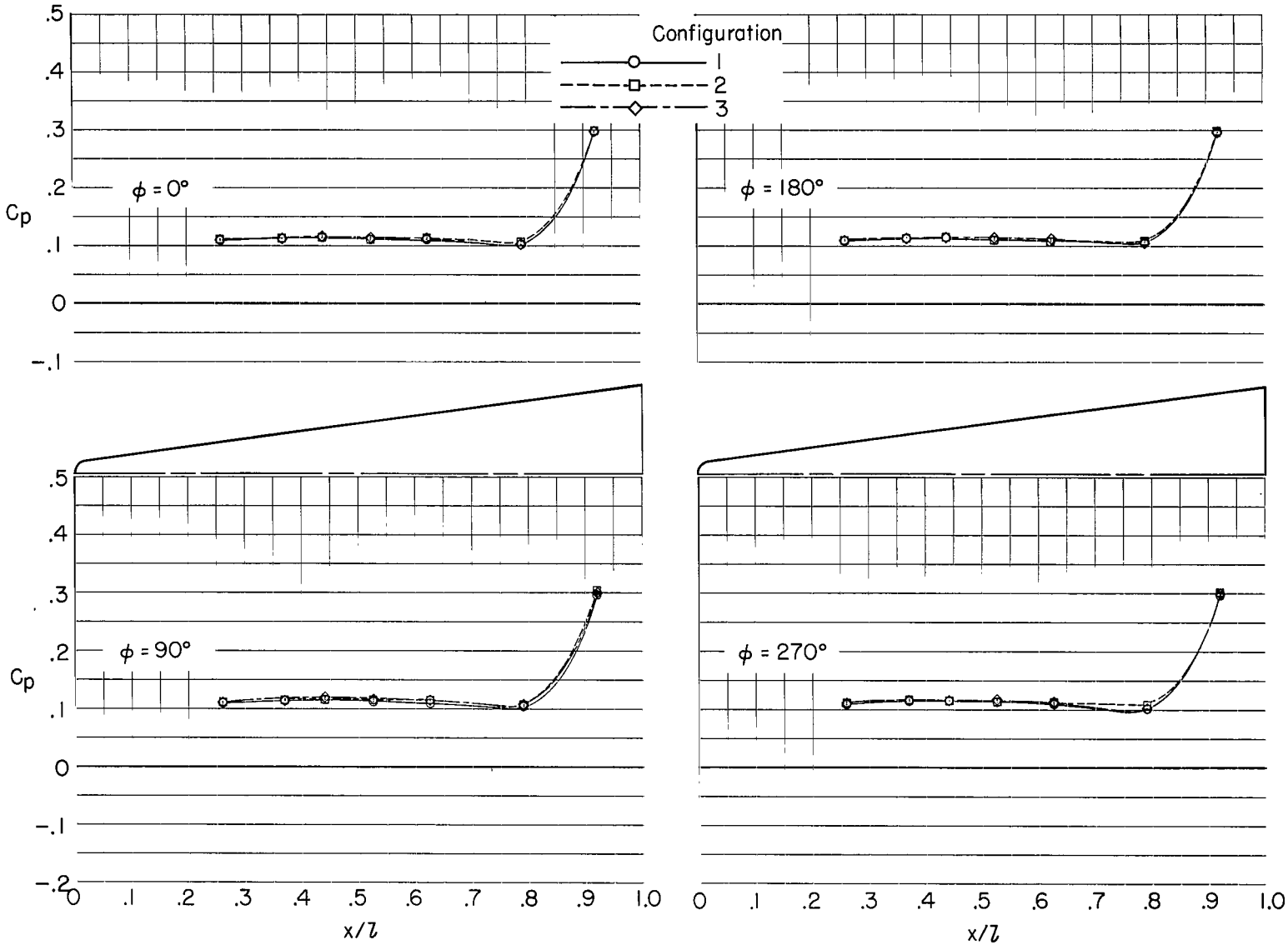

(b) $\alpha = 0.2^0$.

Figure 12.- Continued.

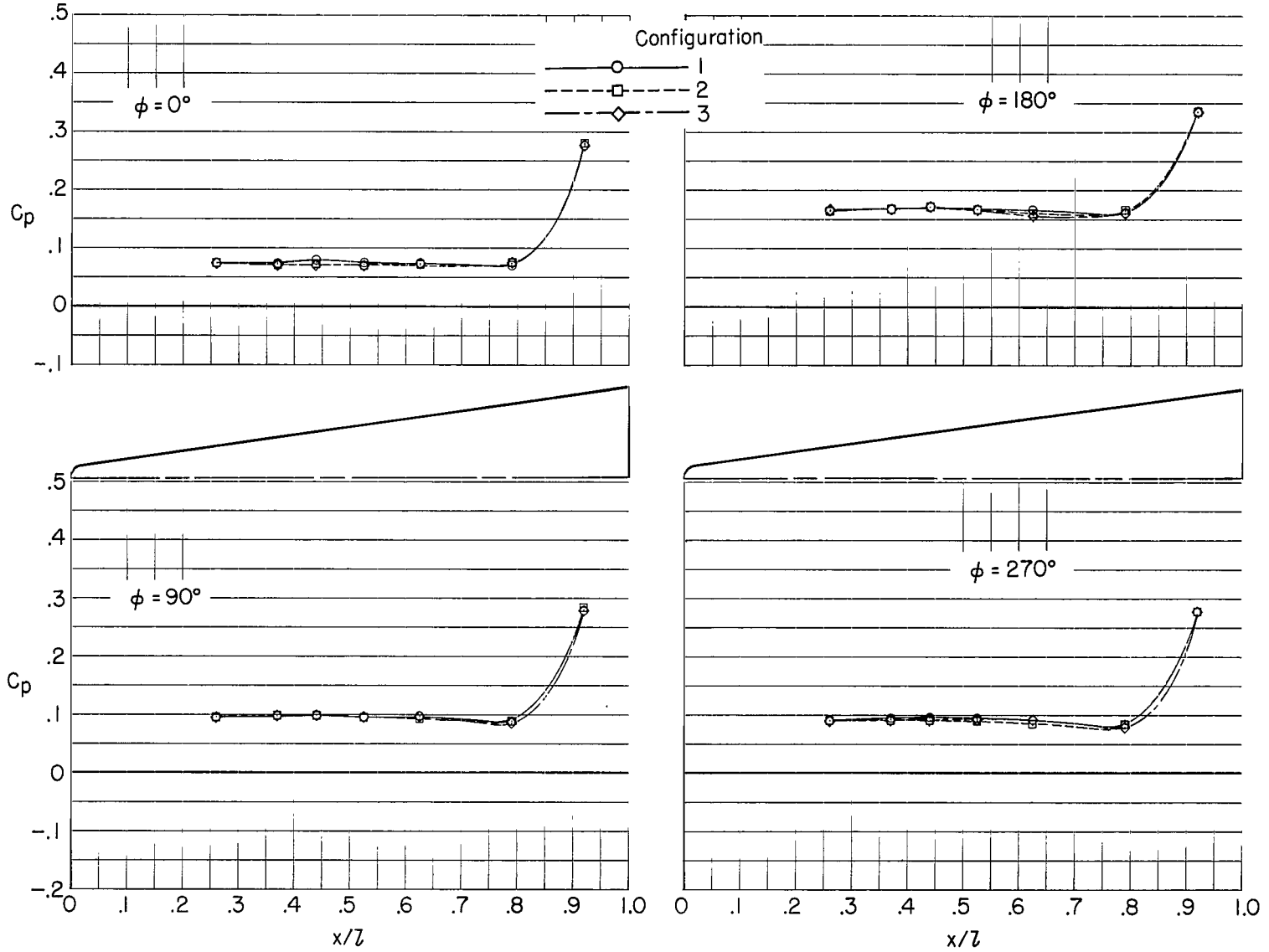

(c) $\alpha = 5.2^0$.

Figure 12.- Continued.

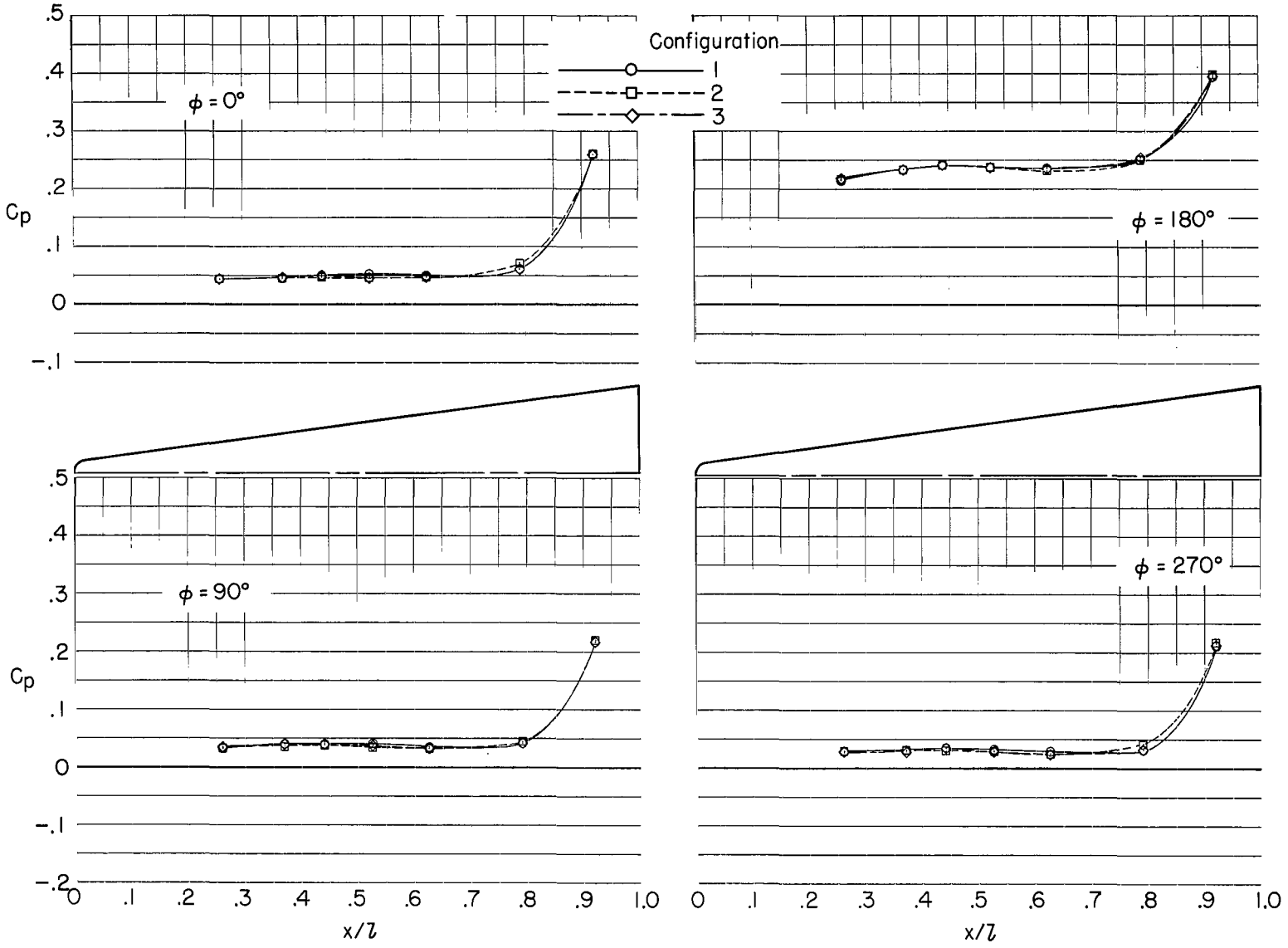

(d) $\alpha = 10.2^{0}$.

Figure 12.- Continued.

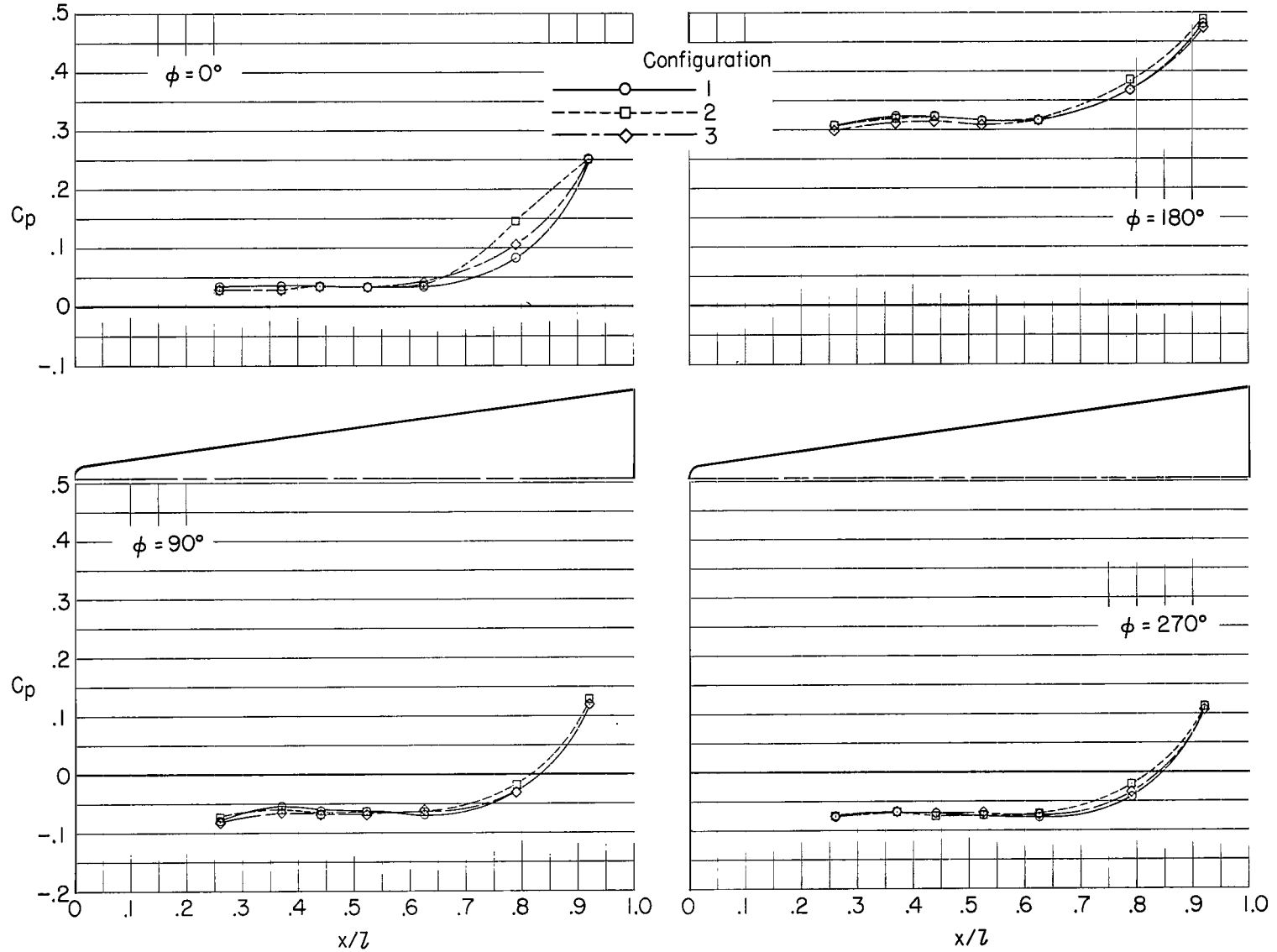

(e) $\alpha = 15.0^0$.

Figure 12.- Concluded.

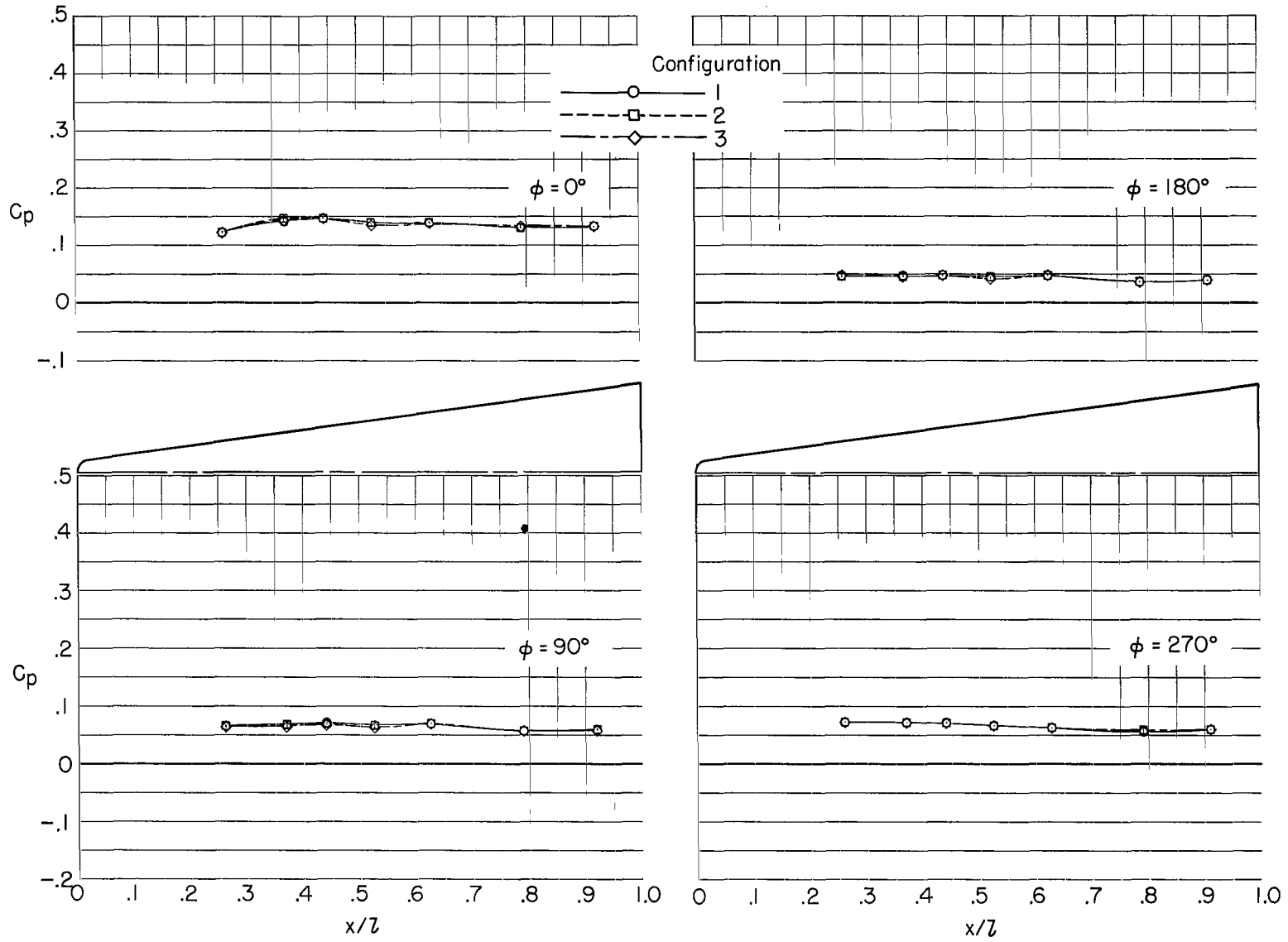

(a) $\alpha = -4.8^0$.

Figure 13.- Comparison of longitudinal pressure distributions for three configurations. M = 1.20; $\beta = 0^0$.

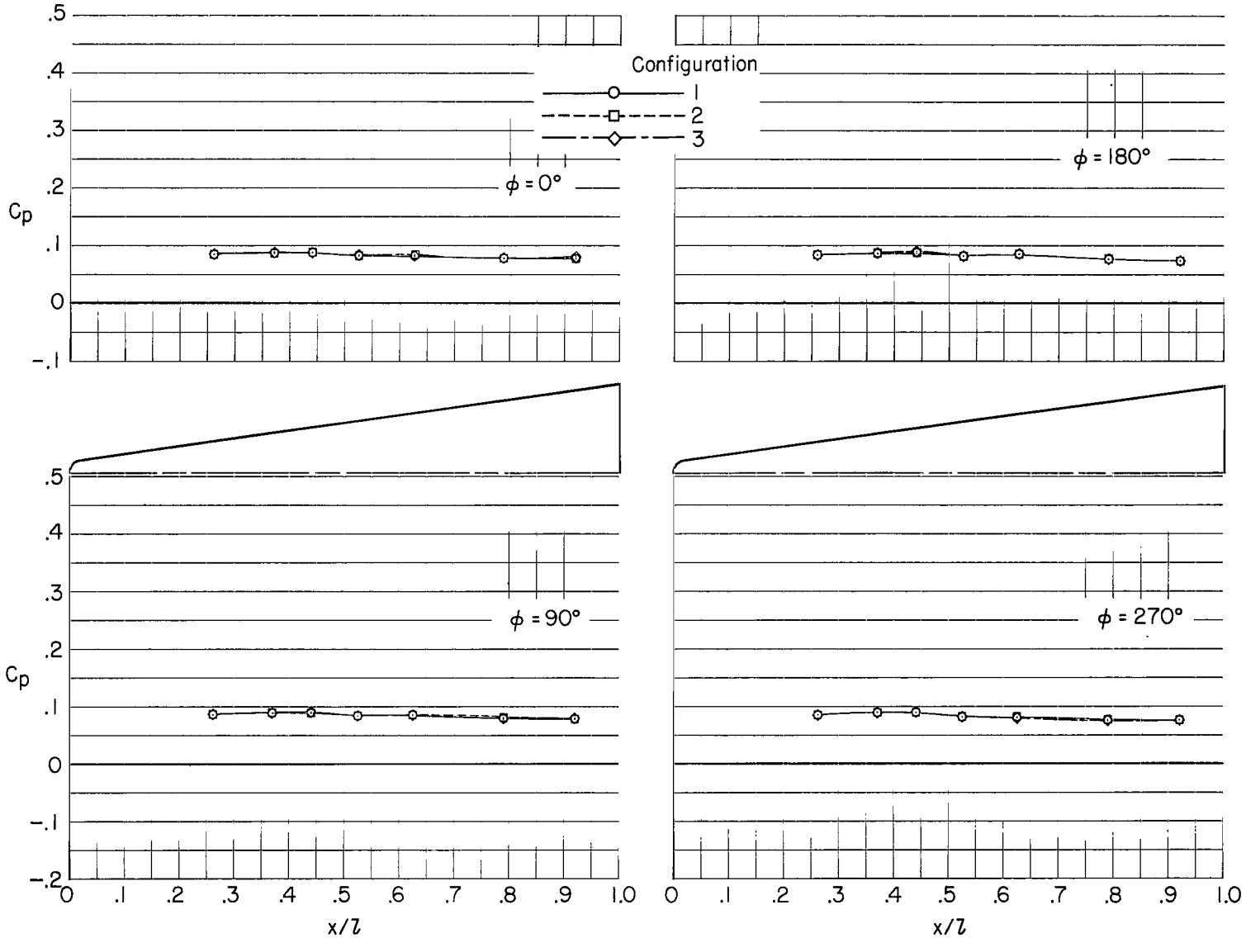

(b) $\alpha = 0.2^0$.

Figure 13.- Continued.

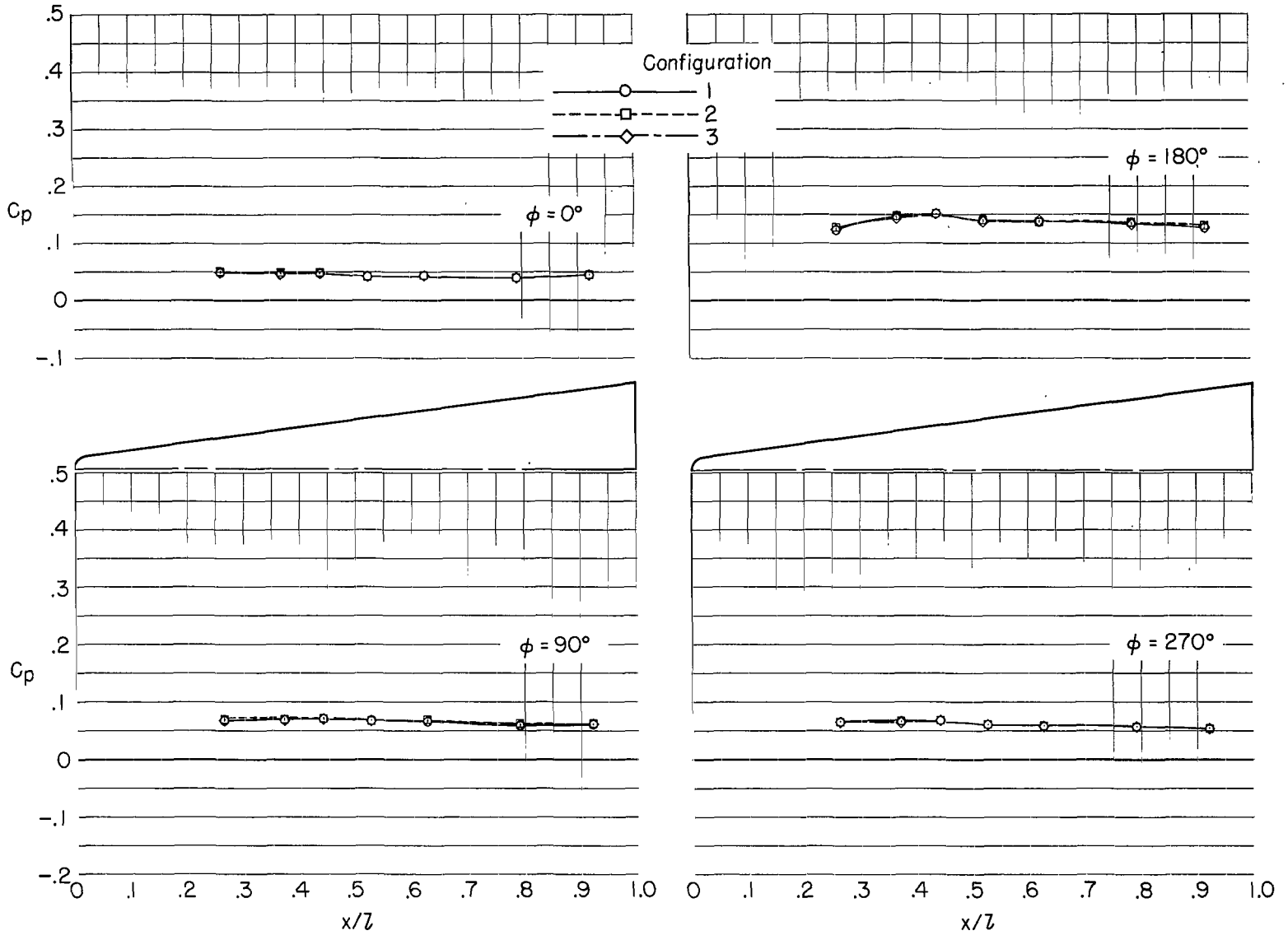

(c) $\alpha = 5.2^0$.

Figure 13.- Continued.

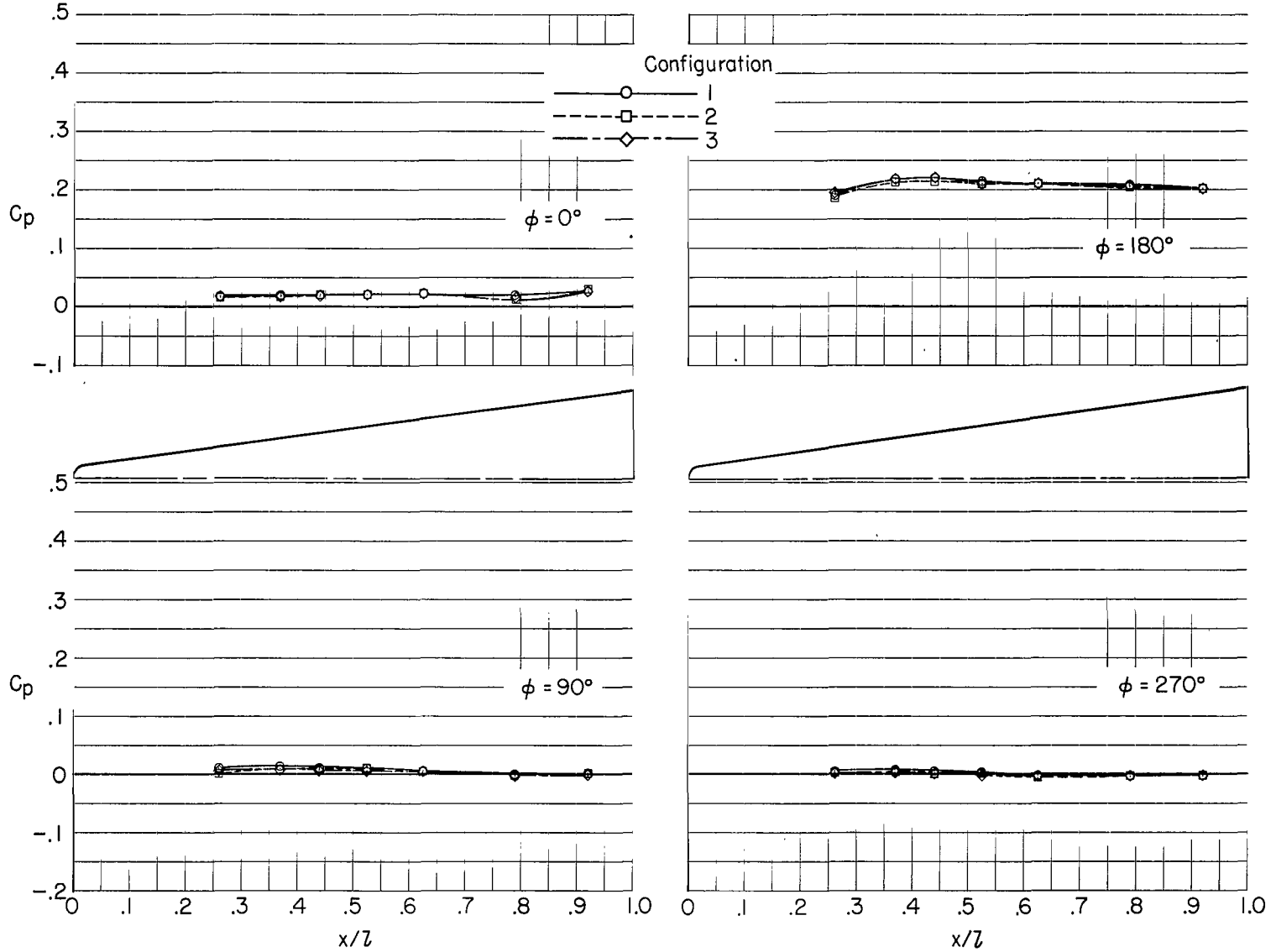

(d) $\alpha = 10.2^0$.

Figure 13.- Continued.

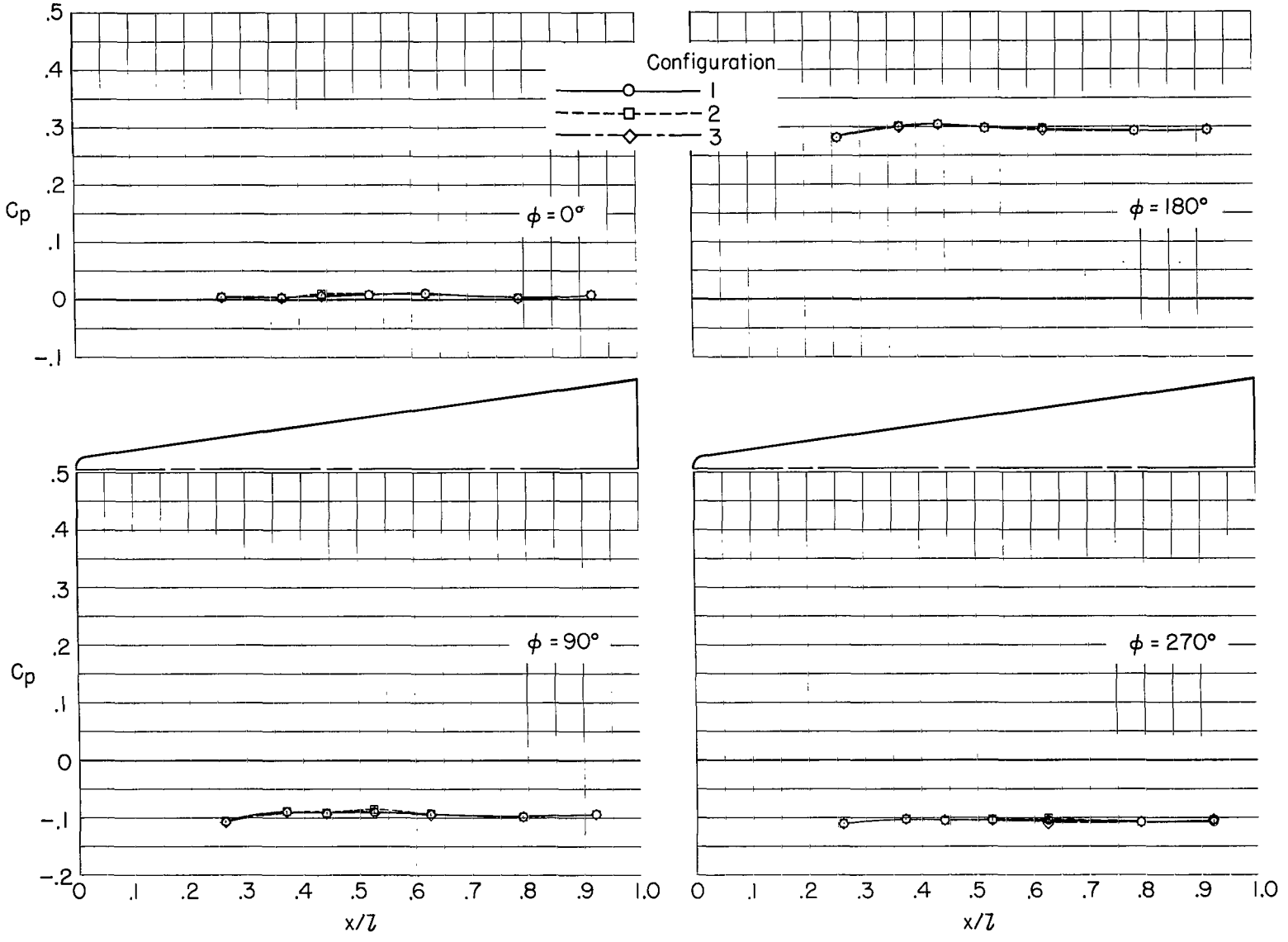

(e) $\alpha = 15.0^0$.

Figure 13.- Concluded.

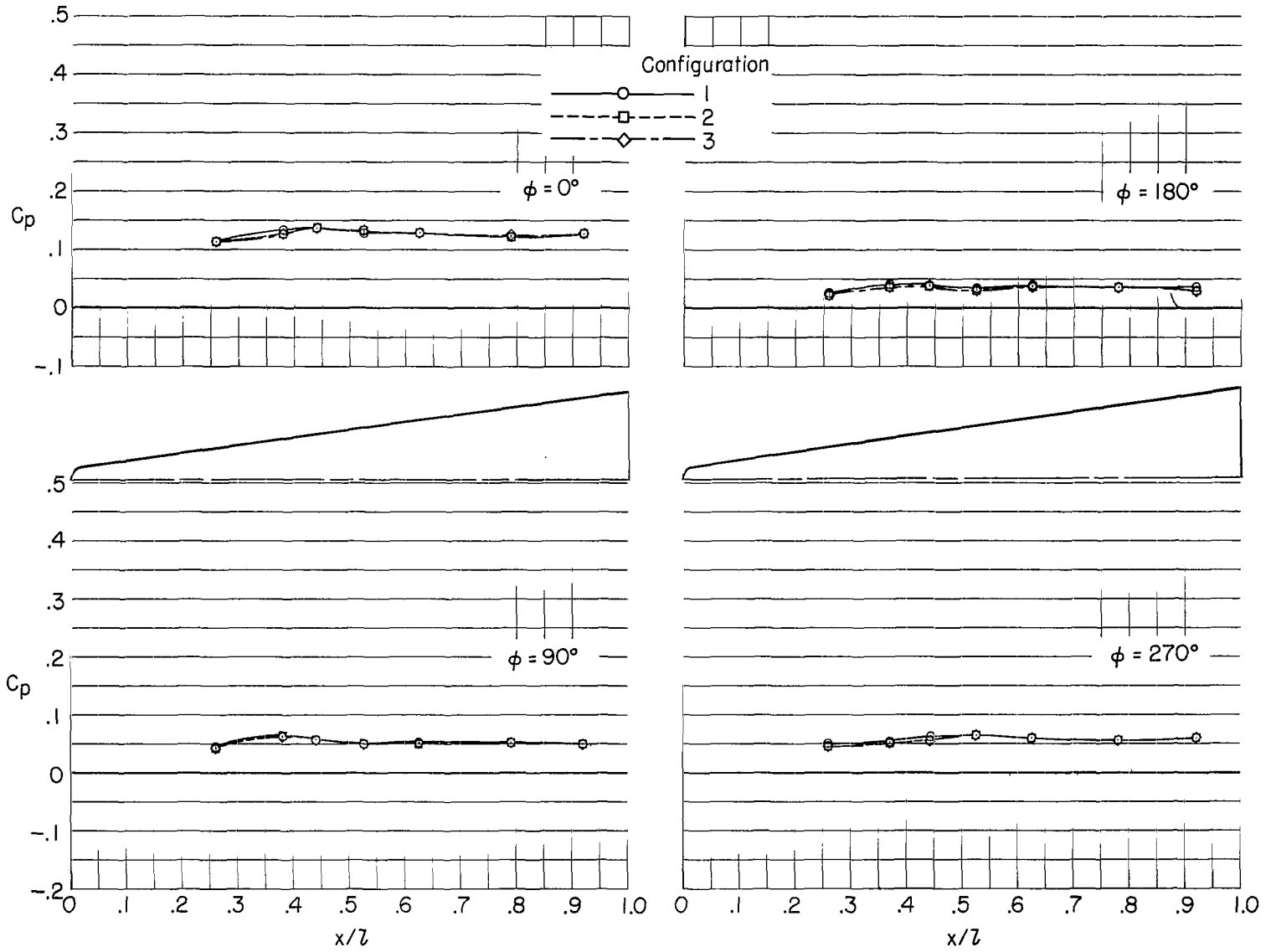

(a) $\alpha = -4.8^0$.

Figure 14.- Comparison of longitudinal pressure distributions for three configurations. M = 1.29; $\beta = 0^0$.

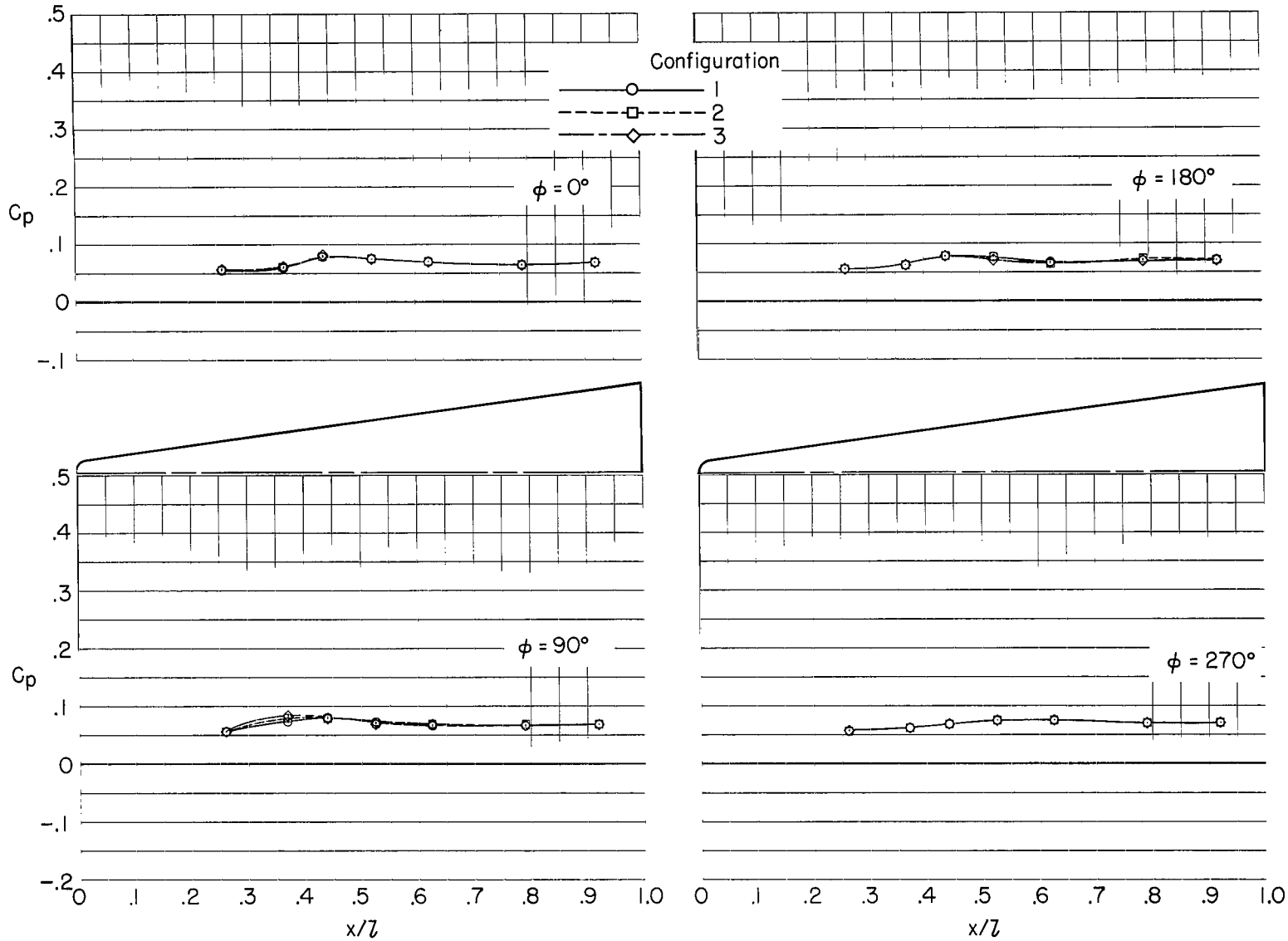

(b) $\alpha = 0.2^0$.

Figure 14.- Continued.

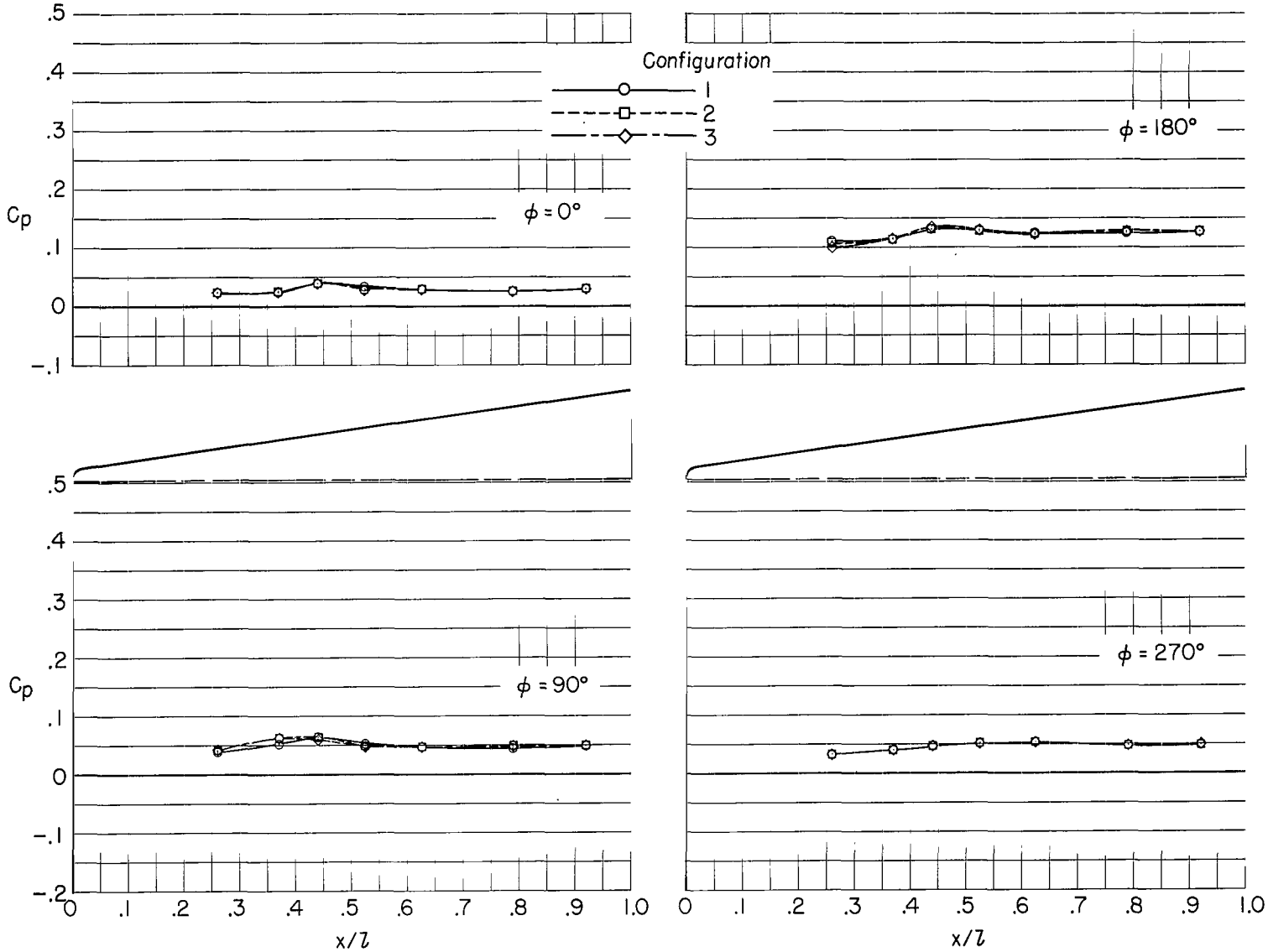

(c) $\alpha = 5.2^0$.

Figure 14.- Continued.

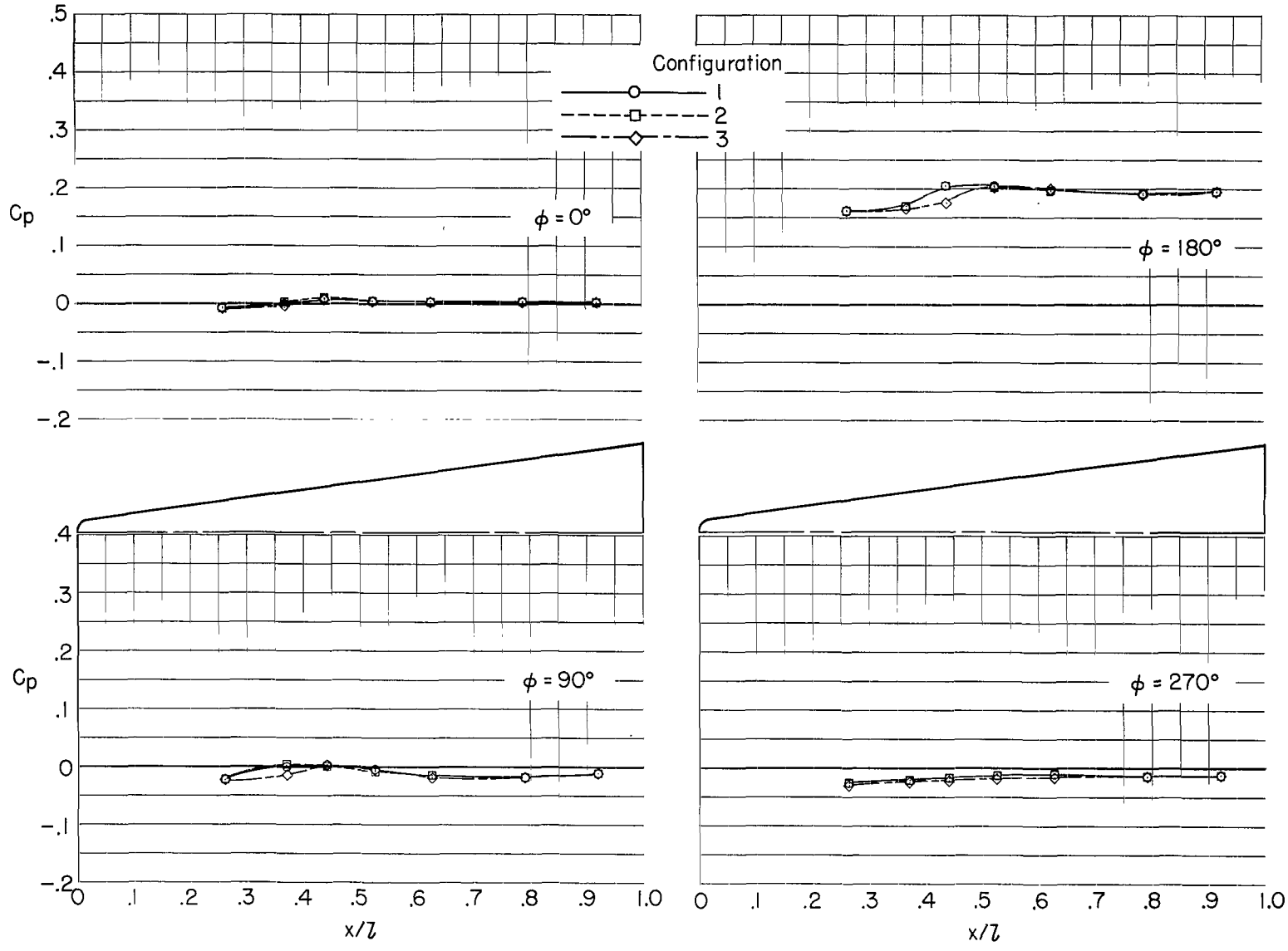

(d) $\alpha = 10.2^{0}$.

Figure 14.- Continued.

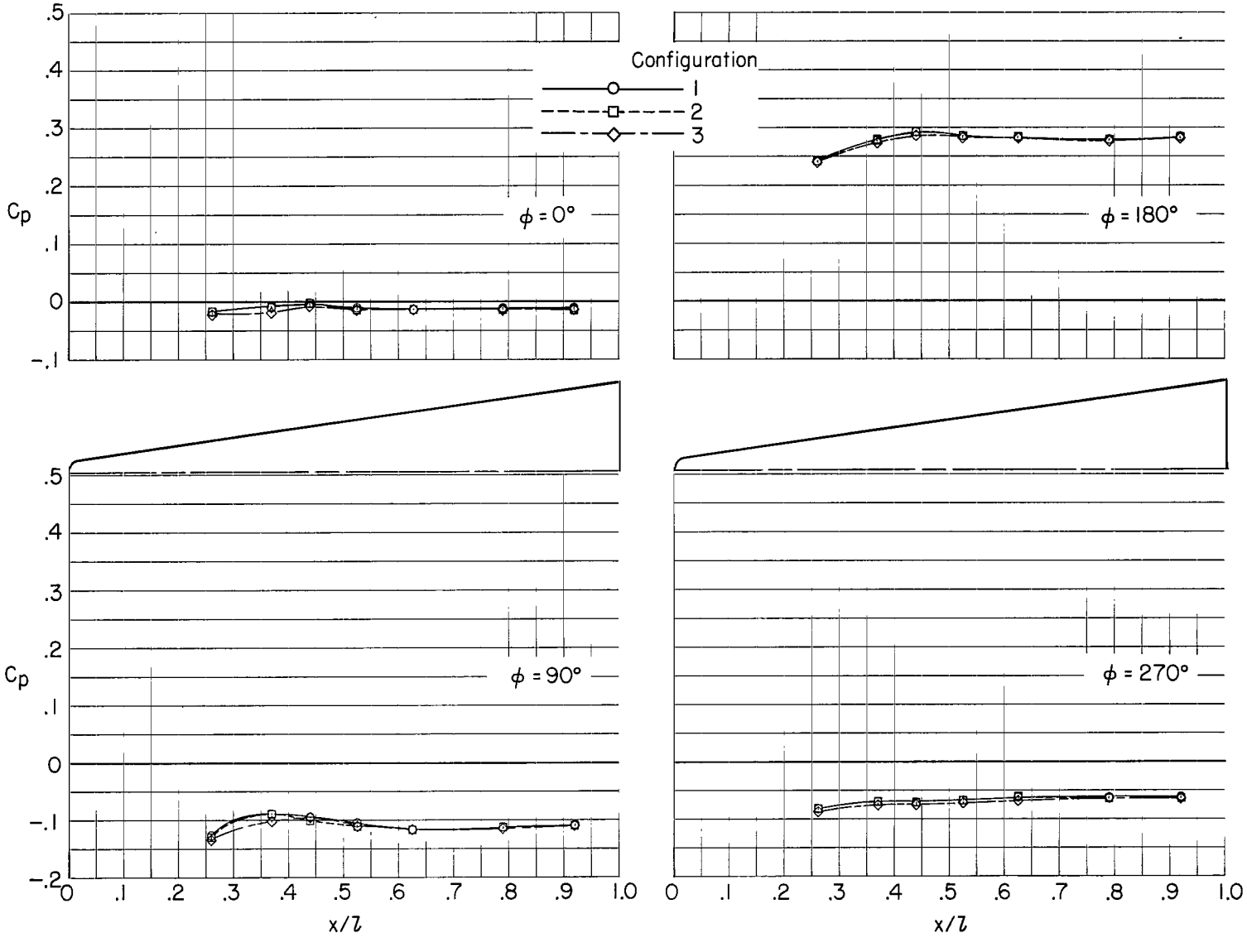

(e) $\alpha = 15.0^0$.

Figure 14.- Concluded.

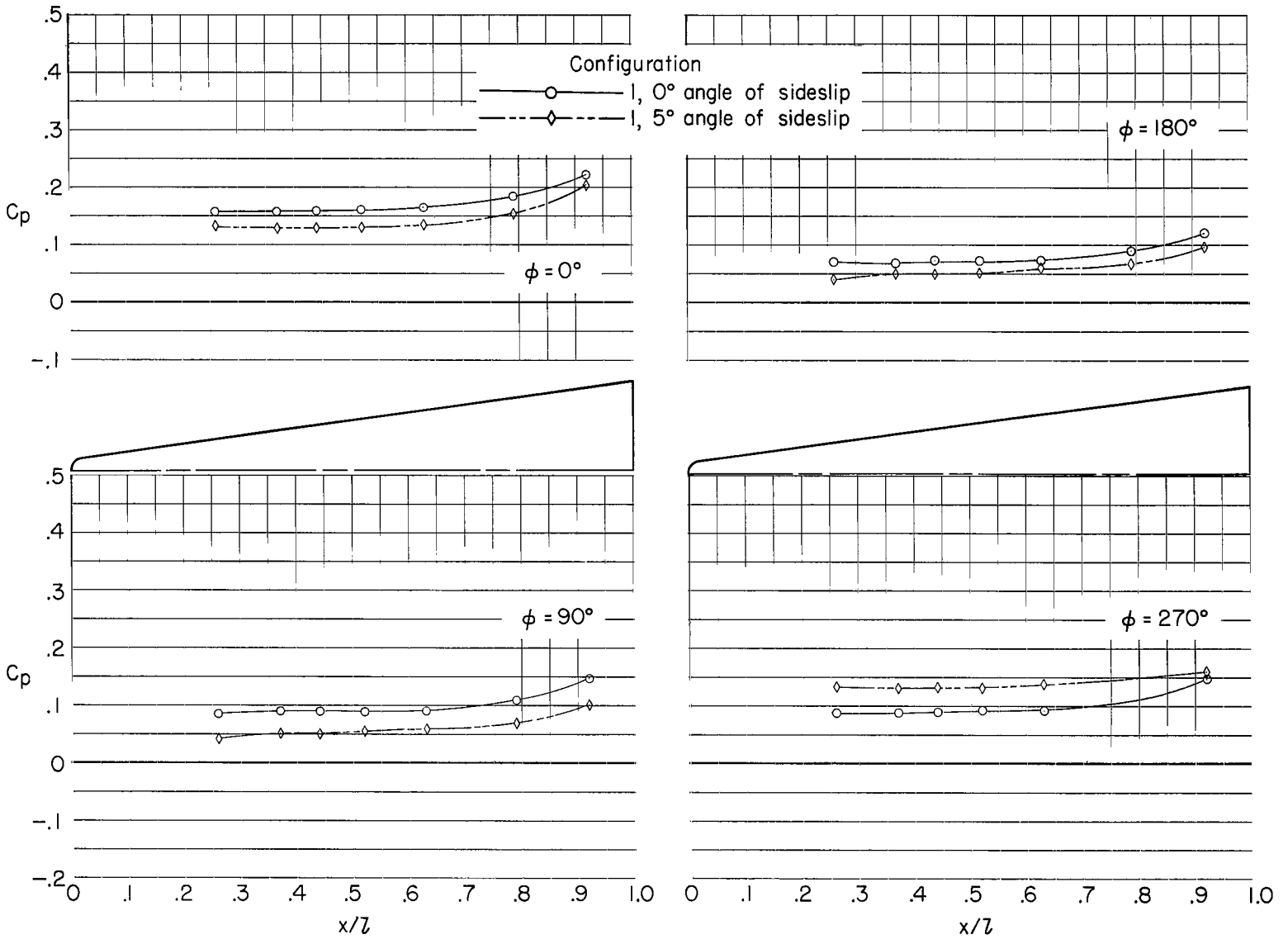

(a) $\alpha = -4.8^0$.

Figure 15.- Longitudinal pressure distributions. M = 0.30.

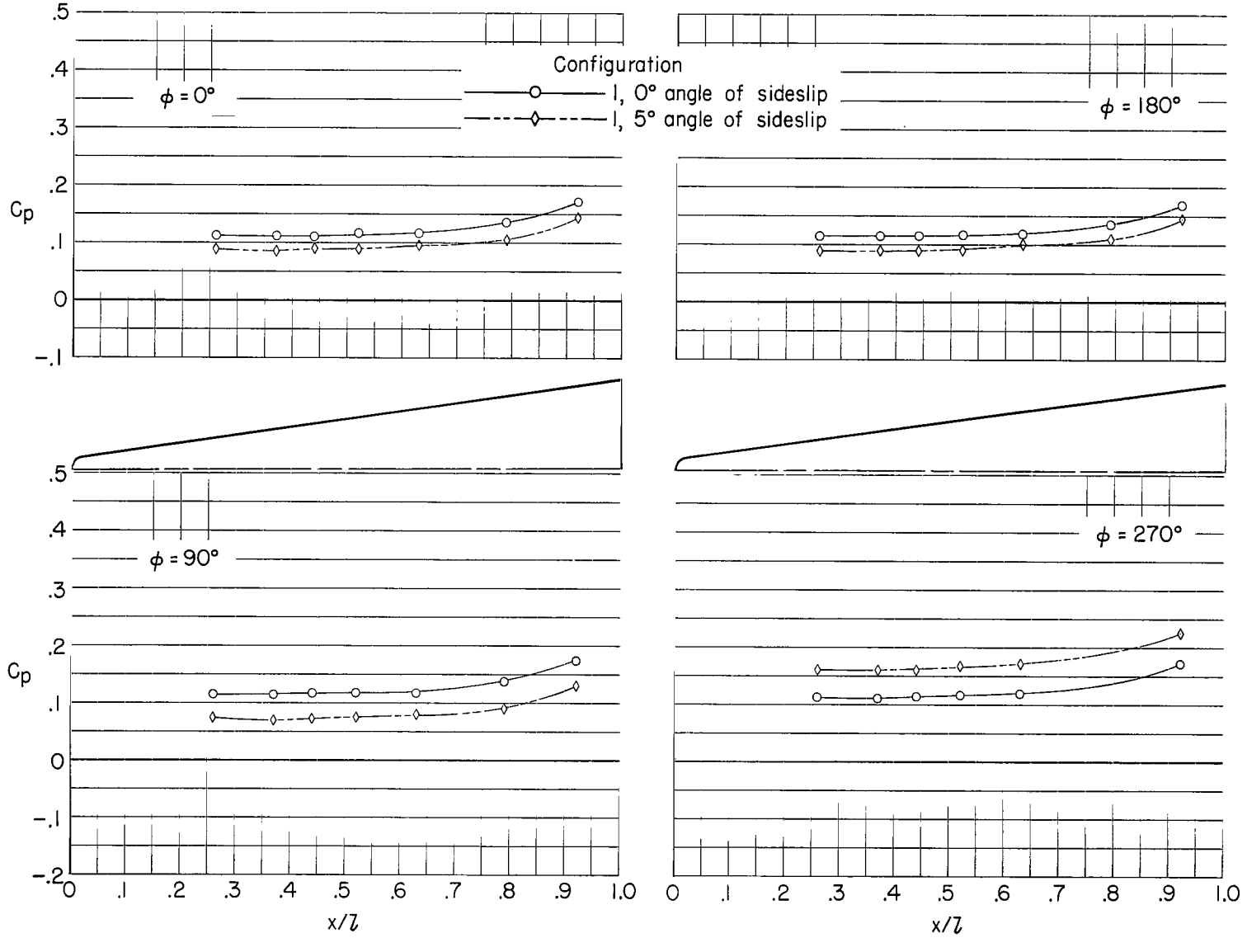

(b) $\alpha = 0.2^{\circ}$.

Figure 15.- Continued.

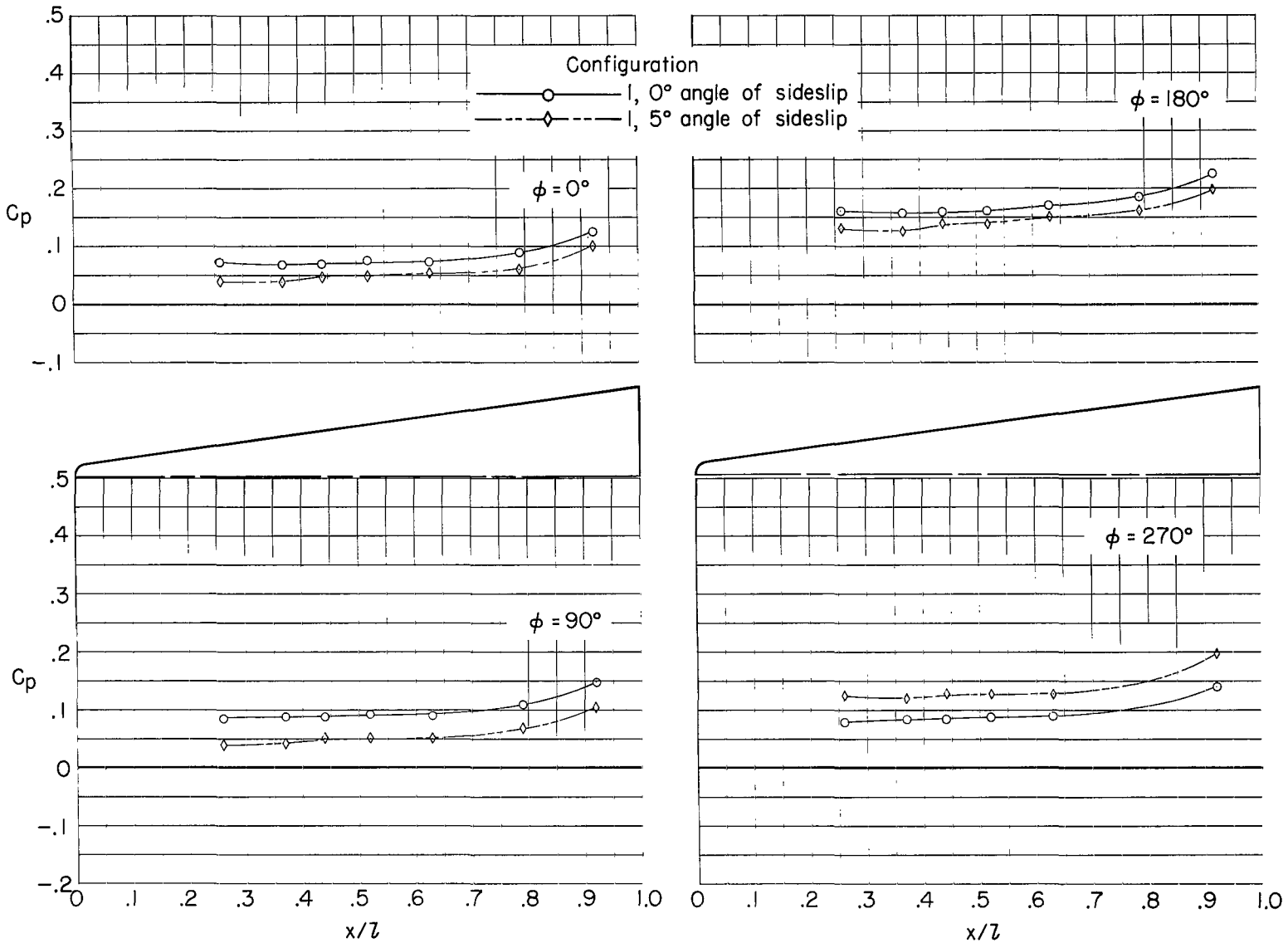

(c) $\alpha = 5.2^0$.

Figure 15.- Continued.

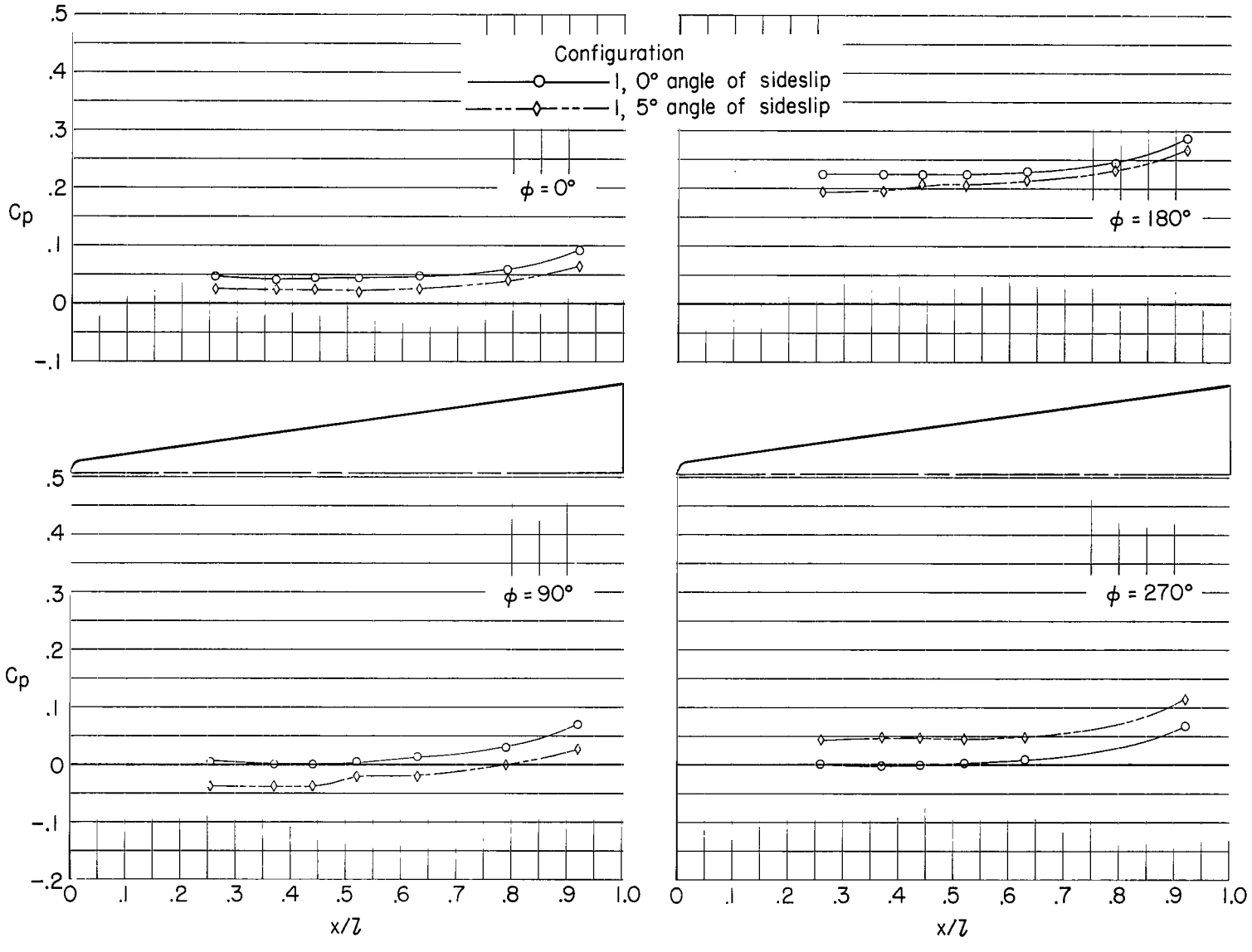

(d) $\alpha = 10.2^0$.

Figure 15.- Continued.

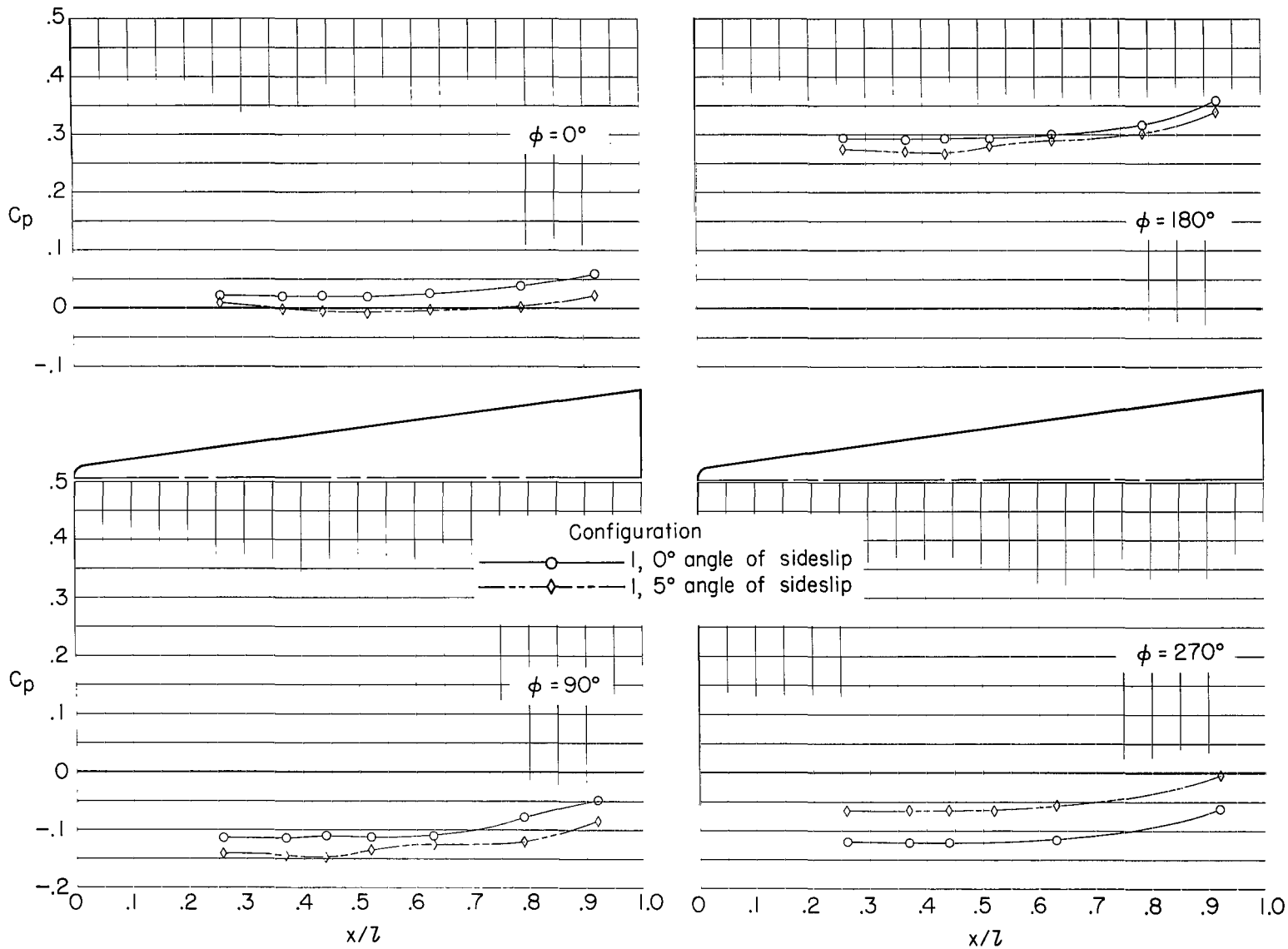

(e) $\alpha = 15.0^{0}$.

Figure 15.- Concluded.

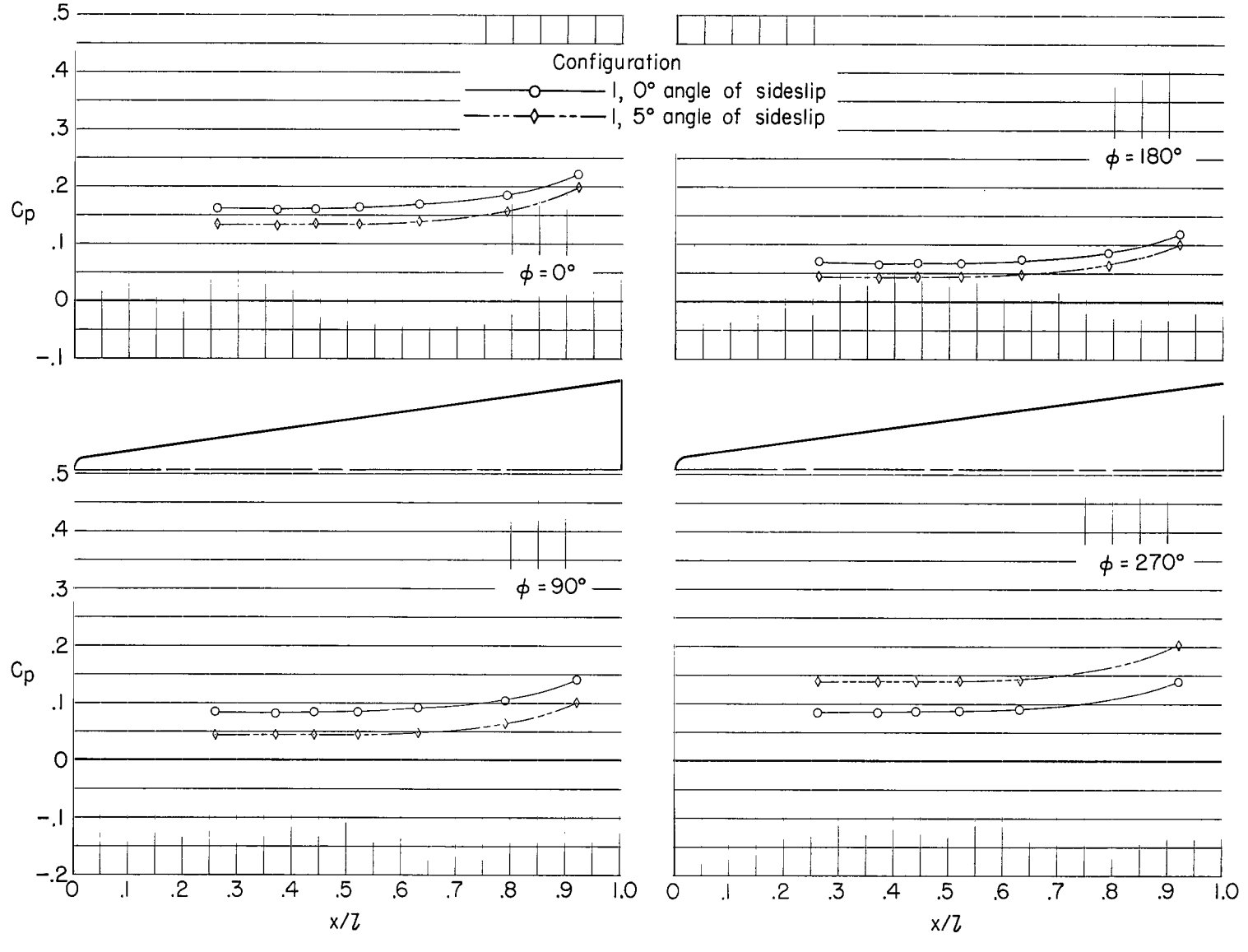

(a) $\alpha = -4.8^0$.

Figure 16.- Longitudinal pressure distributions. M = 0.50.

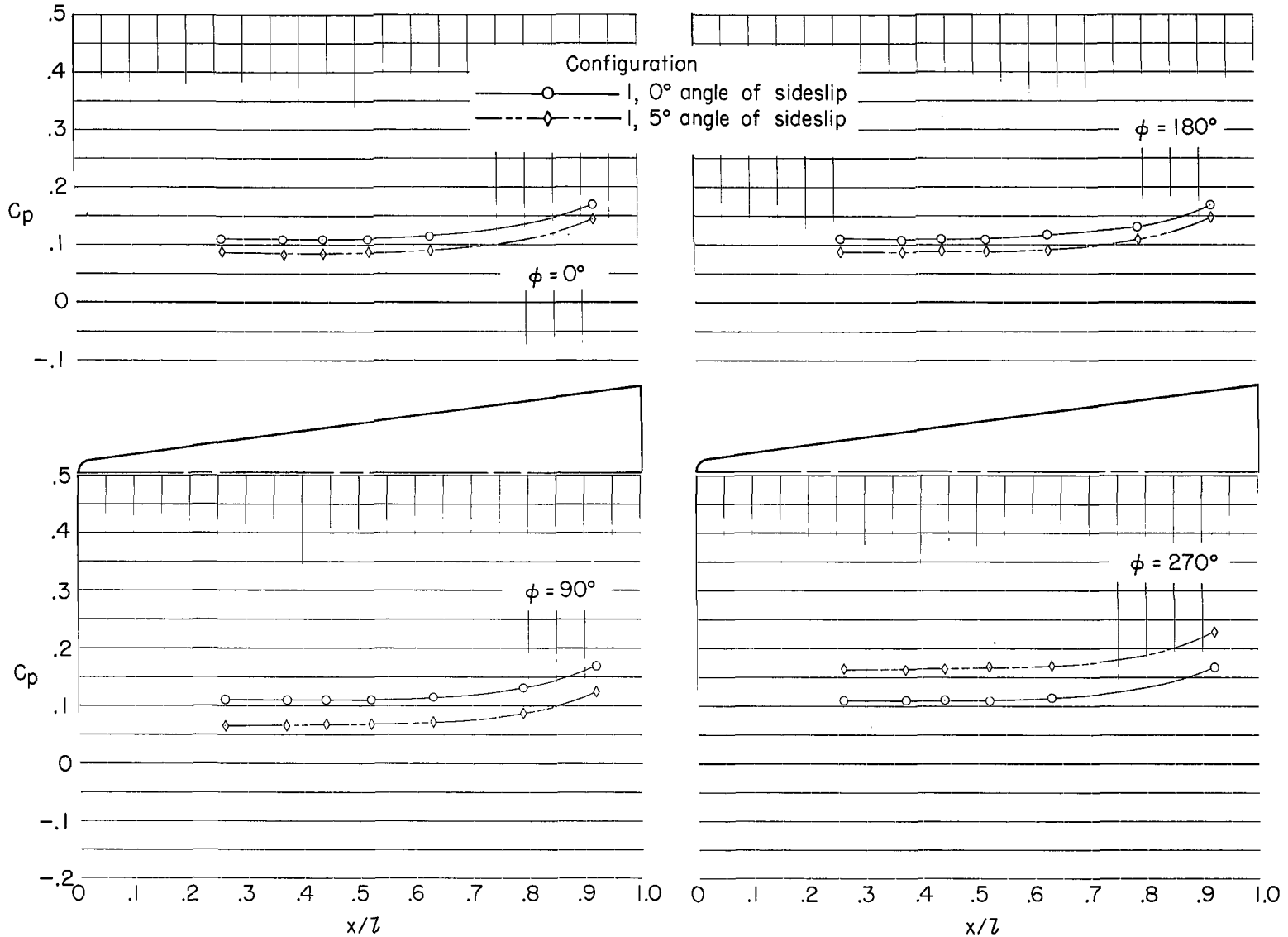

(b) $\alpha = 0.2^0$.

Figure 16.- Continued.

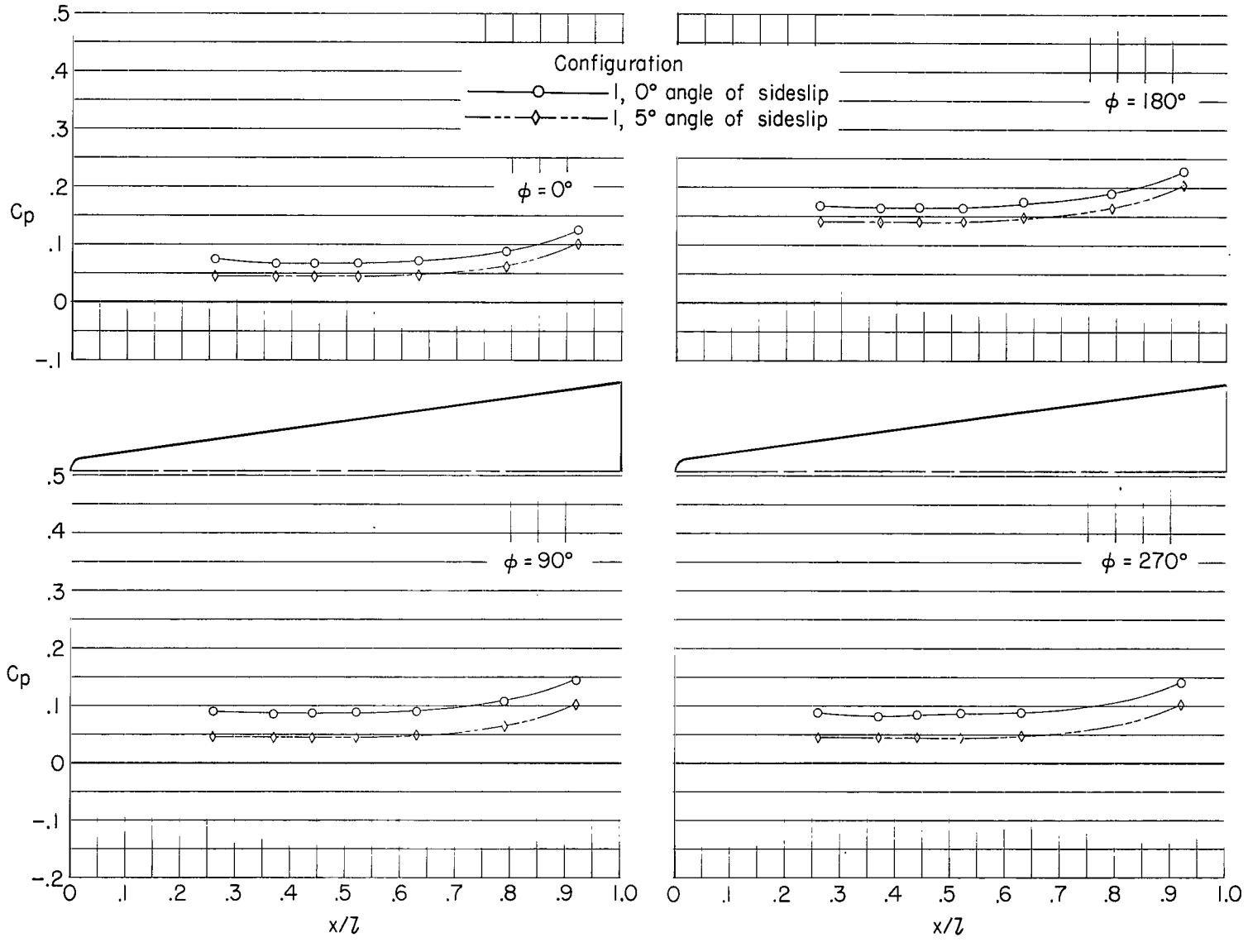

(c) $\alpha = 5.2^0$.

Figure 16.- Continued.

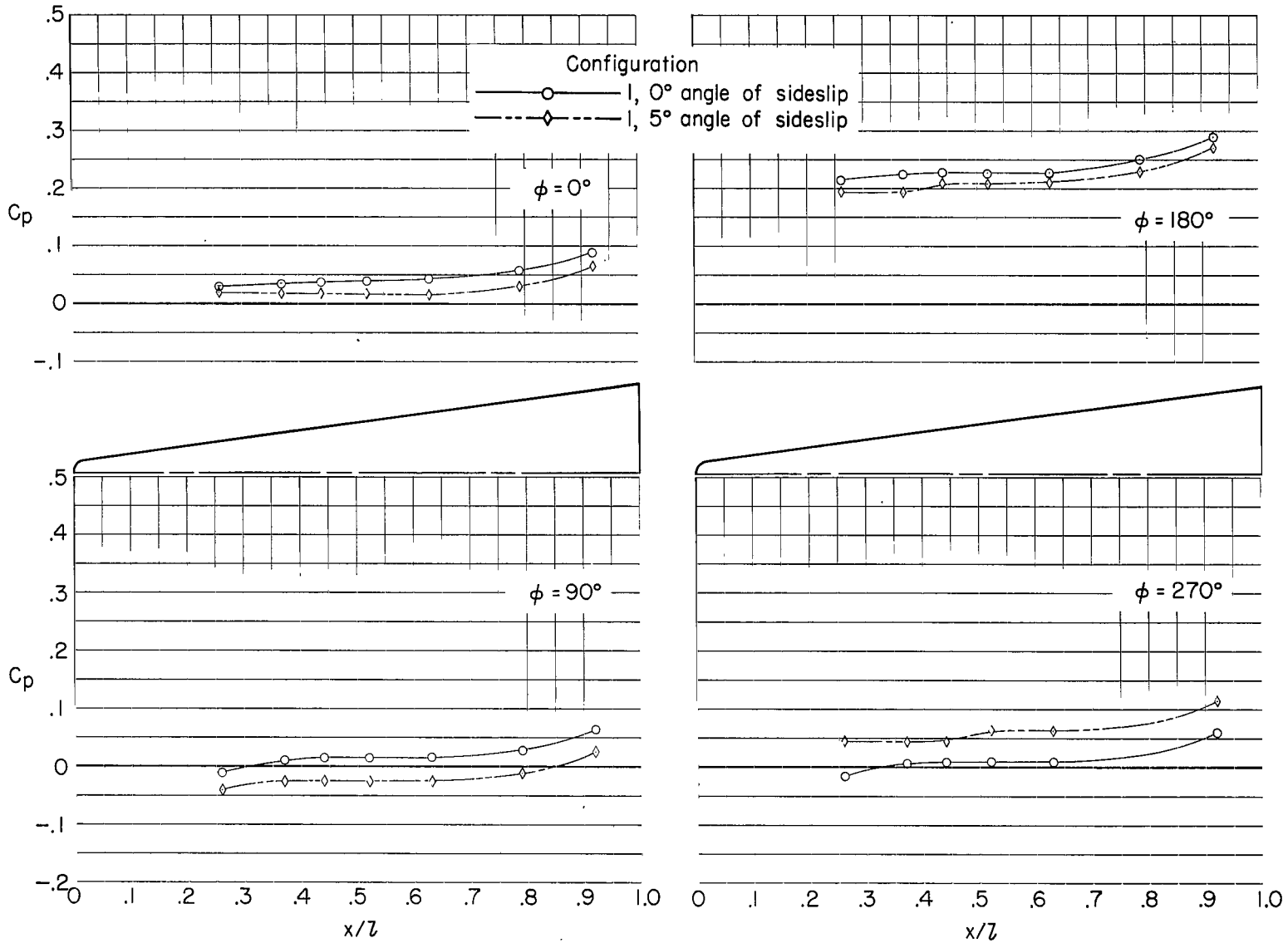

(d) $\alpha = 10.2^{0}$.

Figure 16.- Continued.

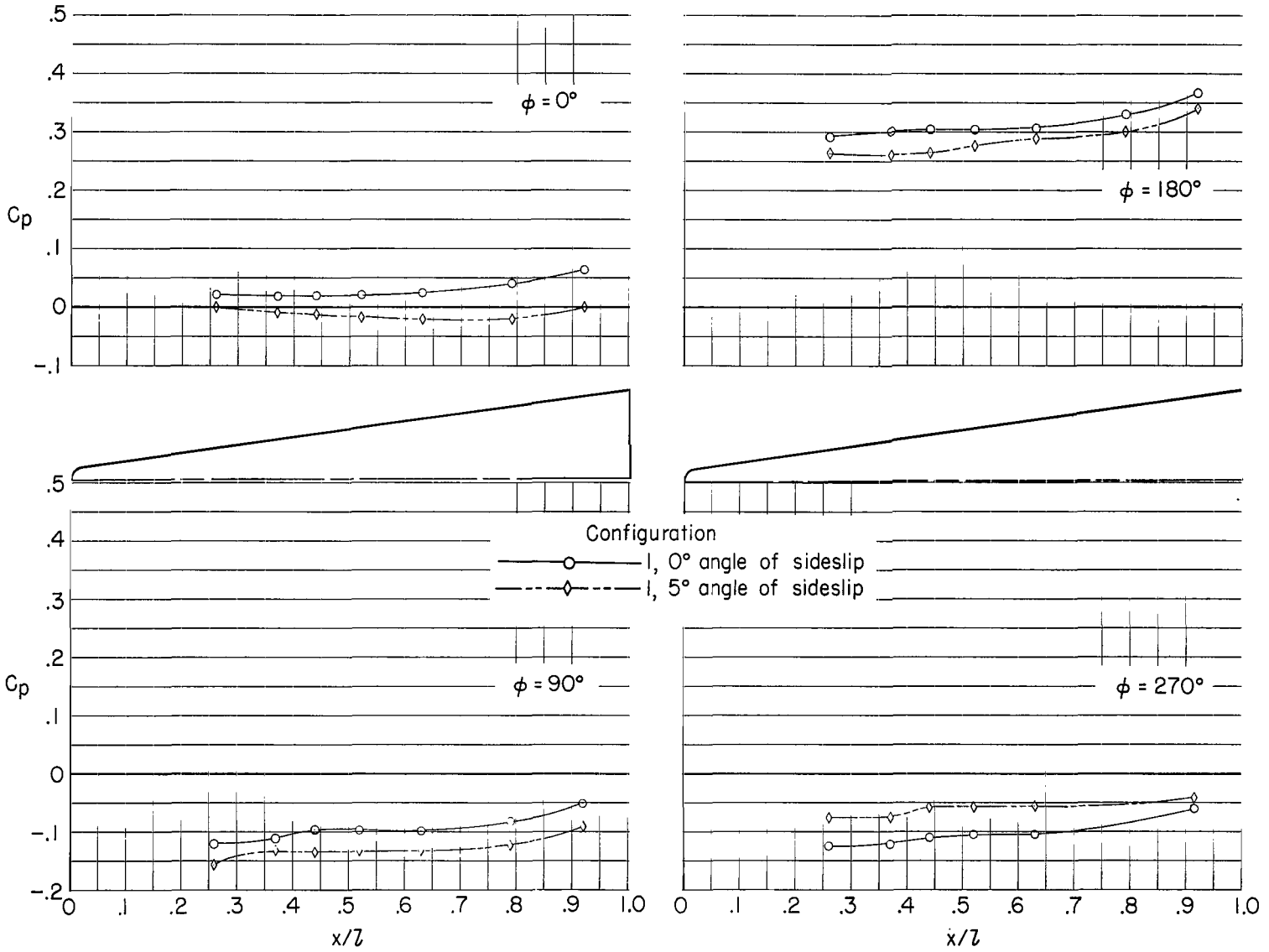

(e) $\alpha = 15.0^0$.

Figure 16.- Concluded.

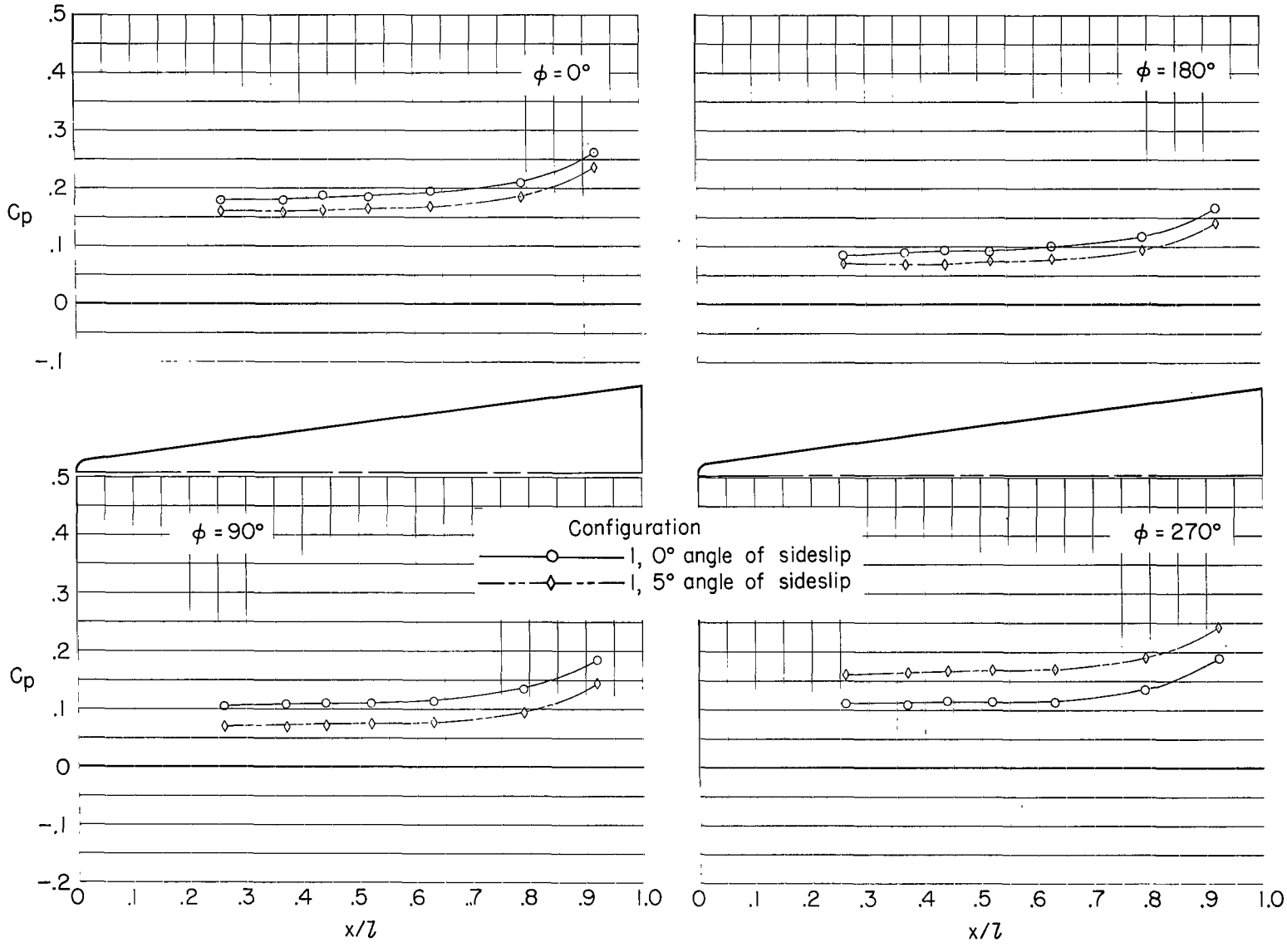

(a) $\alpha = -4.8^{0}$.

Figure 17.- Longitudinal pressure distributions. M = 0.80.

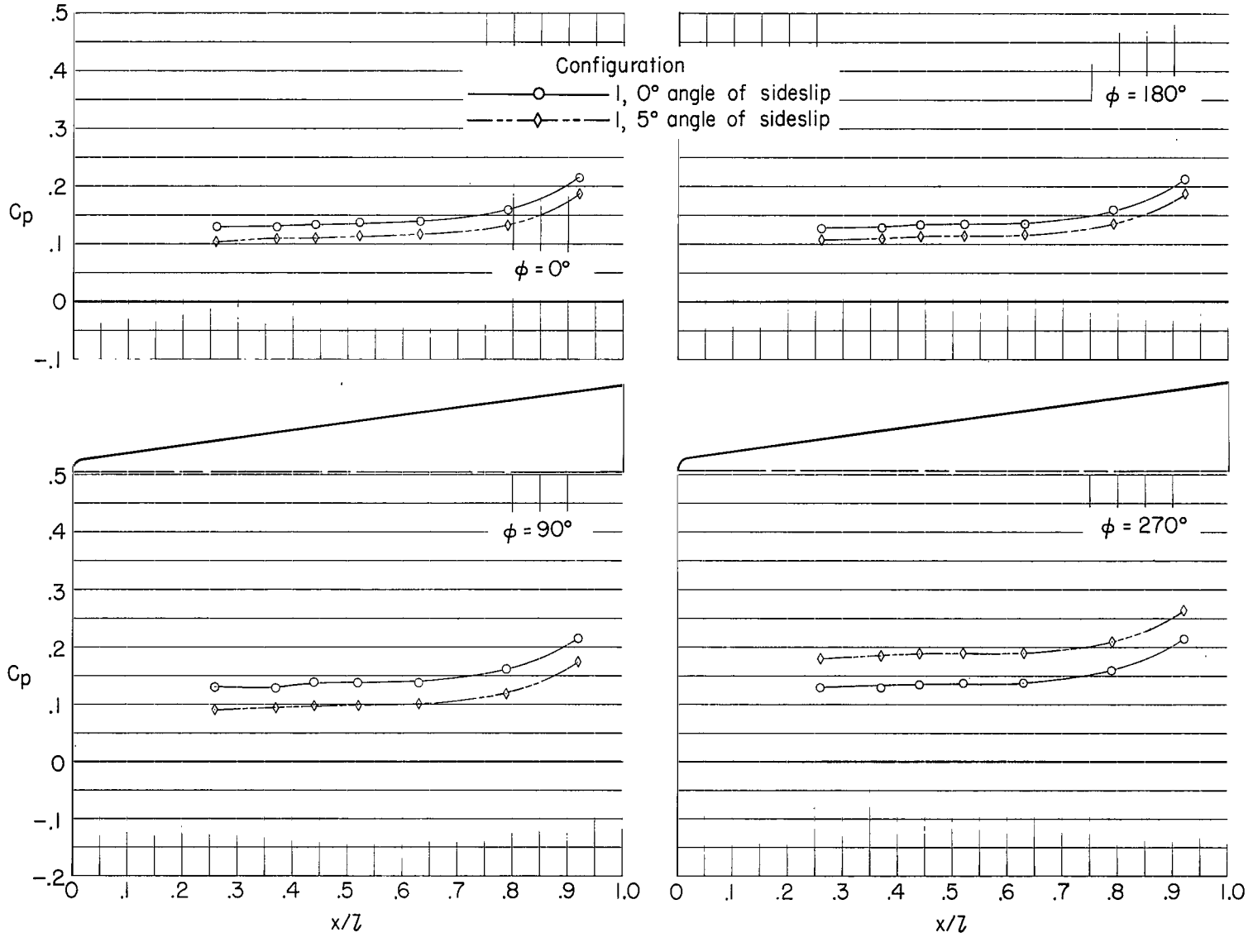

(b) $\alpha = 0.2^0$.

Figure 17.- Continued.

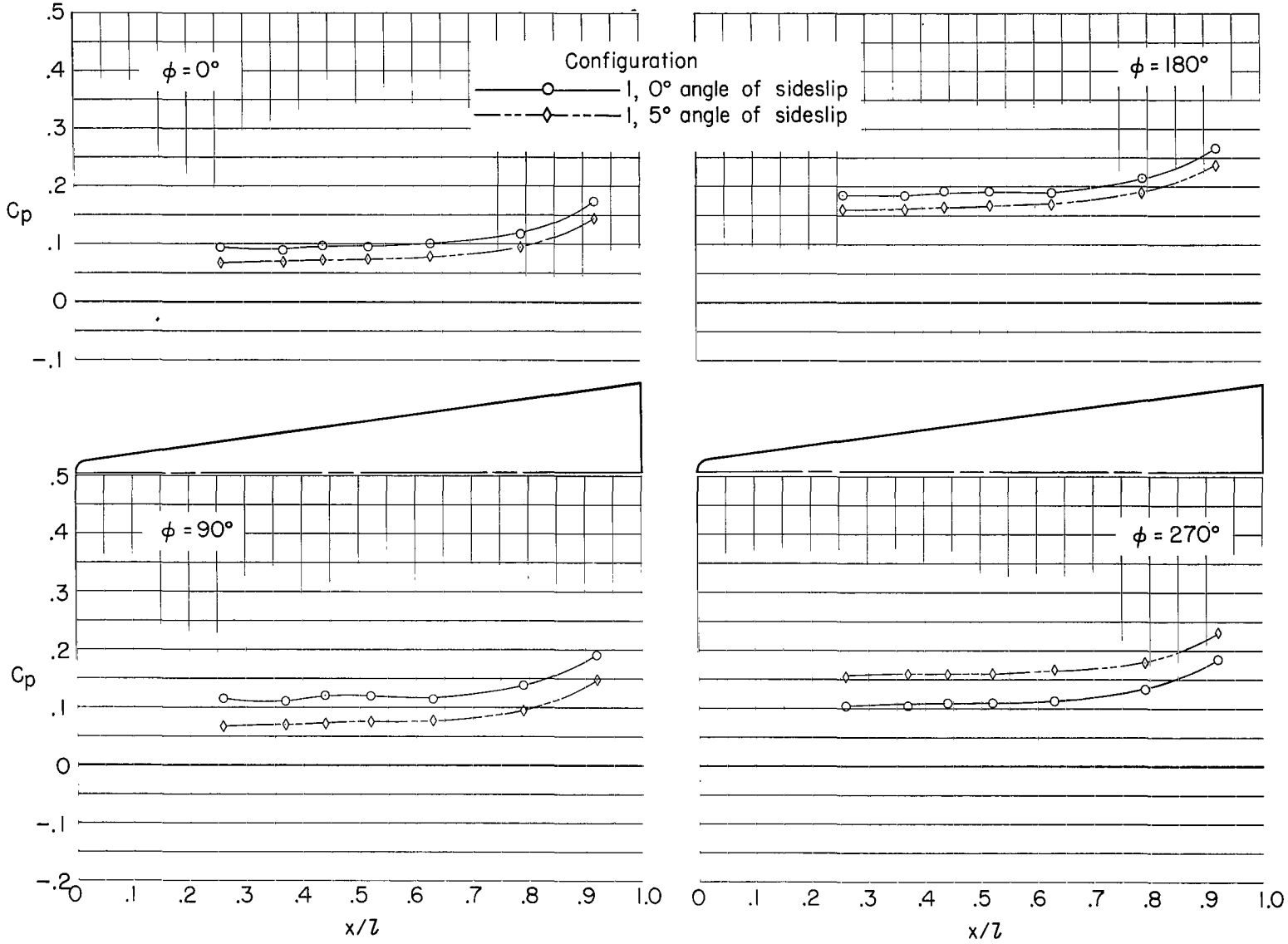

(c) $\alpha = 5.2^{0}$.

Figure 17.- Continued.

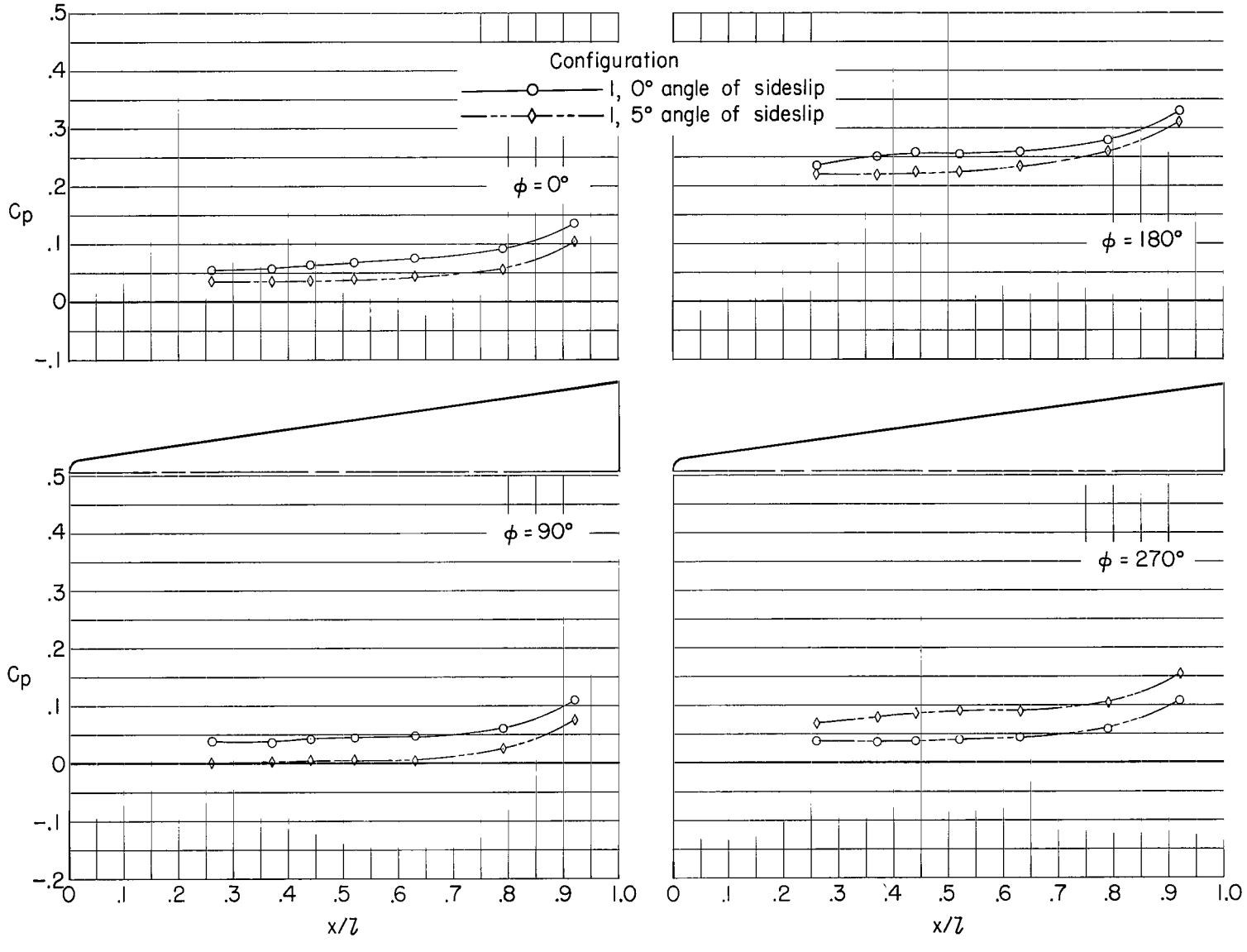

(d) $\alpha = 10.2^0$.

Figure 17.- Continued.

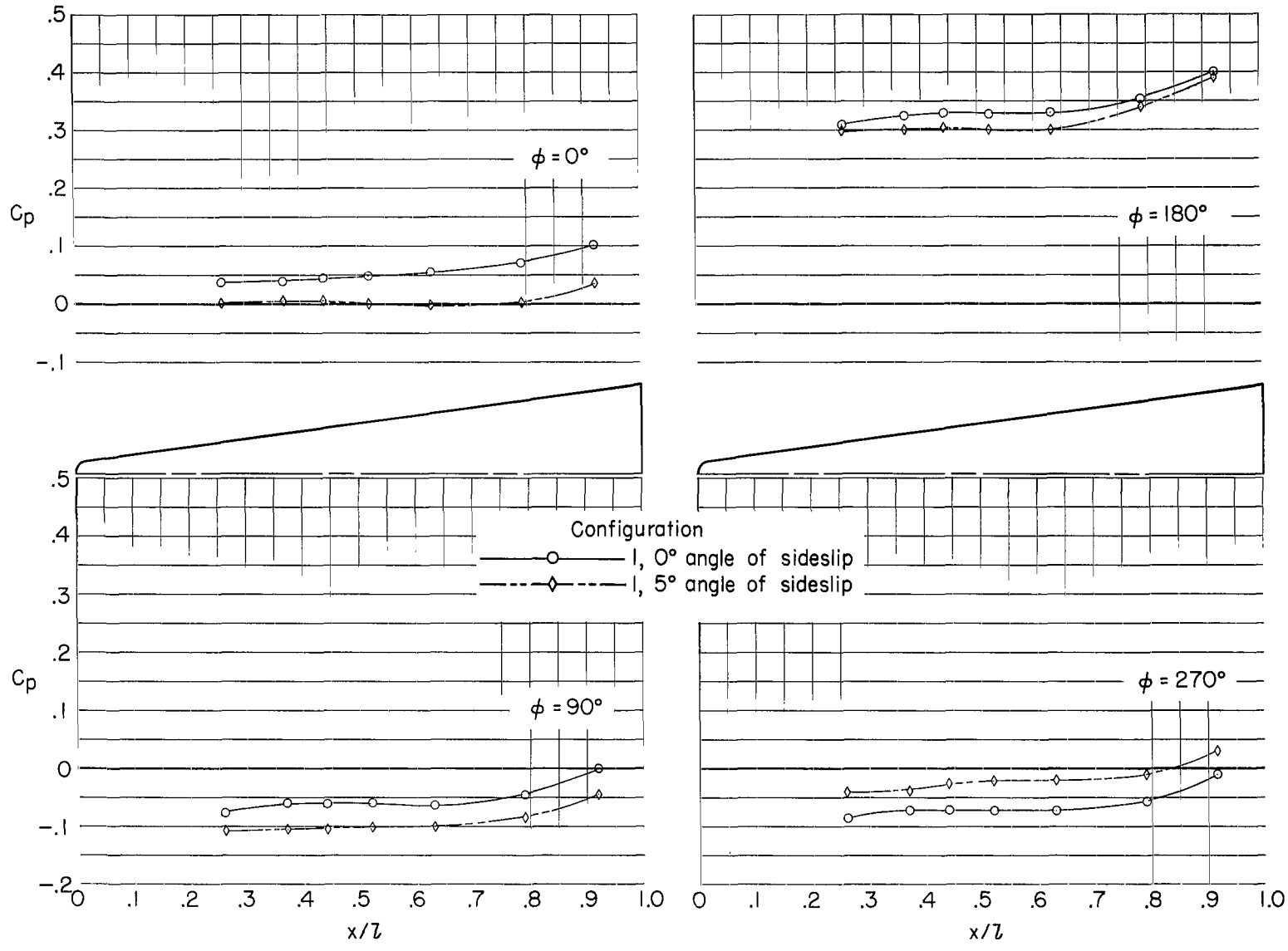

(e) $\alpha = 15.0^0$.

Figure 17.- Concluded.

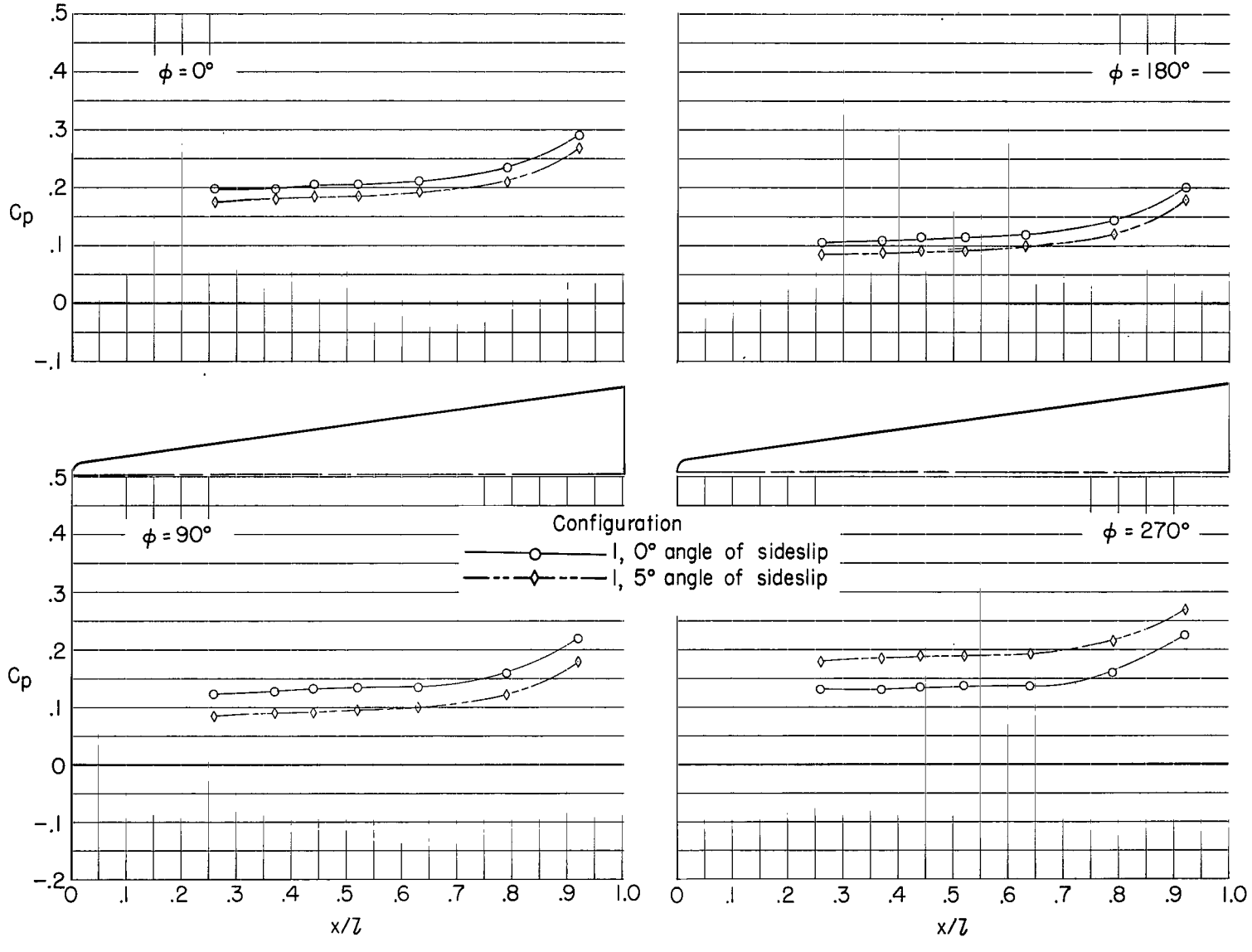

(a) $\alpha = -4.8^0$.

Figure 18.- Longitudinal pressure distributions. M = 0.90.

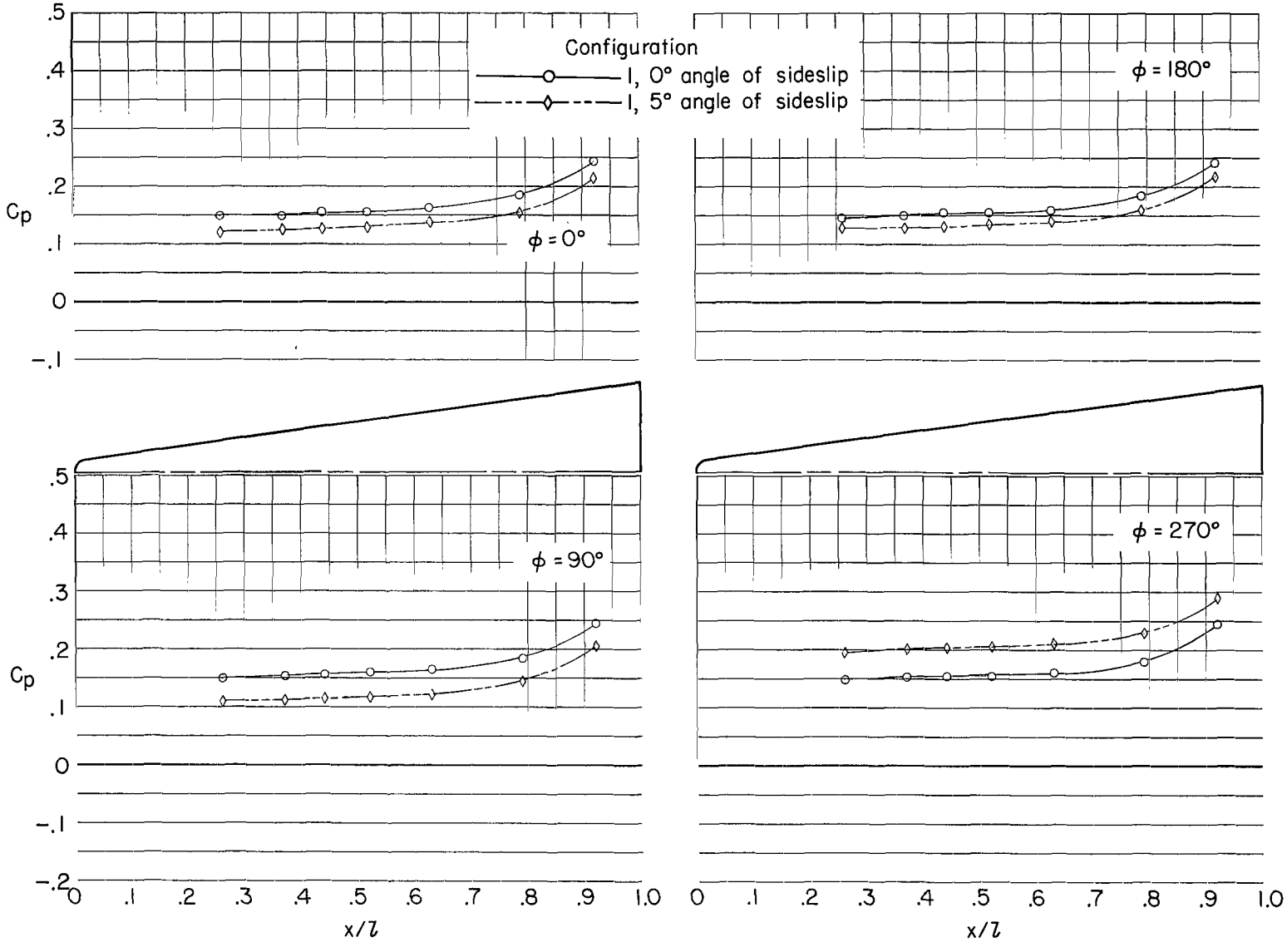

(b) $\alpha = 0.2^0$.

Figure 18.- Continued.

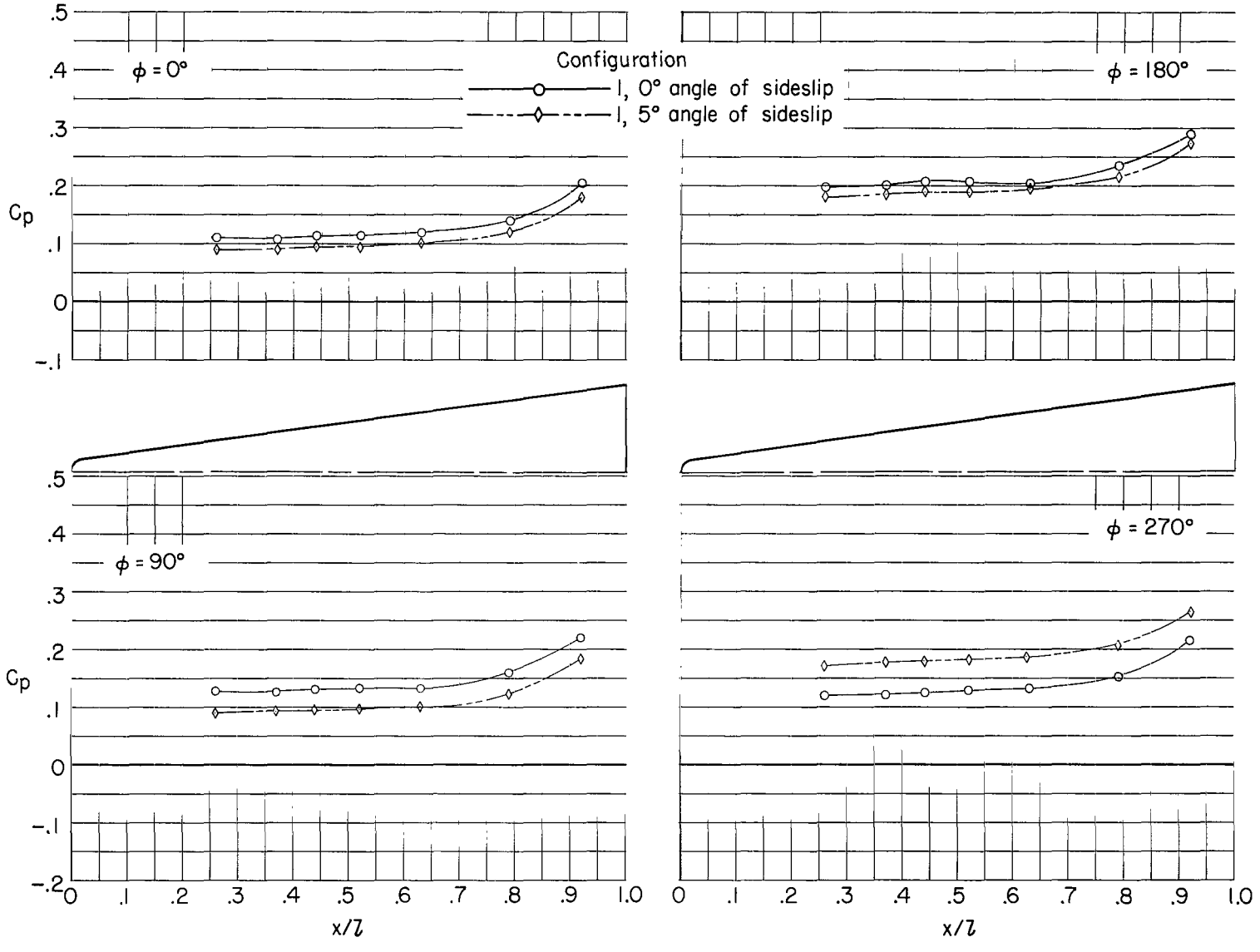

(c) $\alpha = 5.2^{0}$.

Figure 18.- Continued.

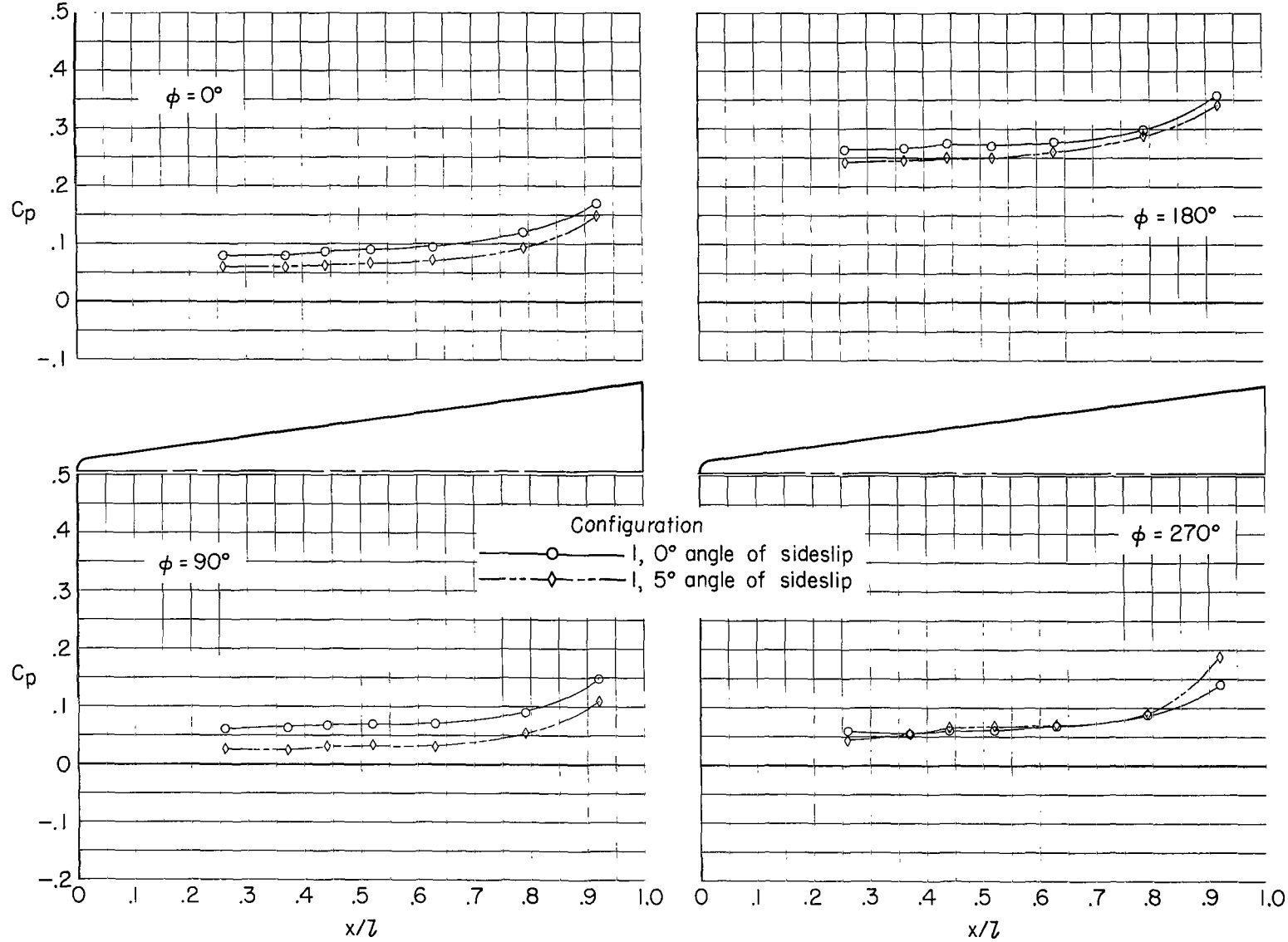

(d) $\alpha = 10.2^0$.

Figure 18.- Continued.

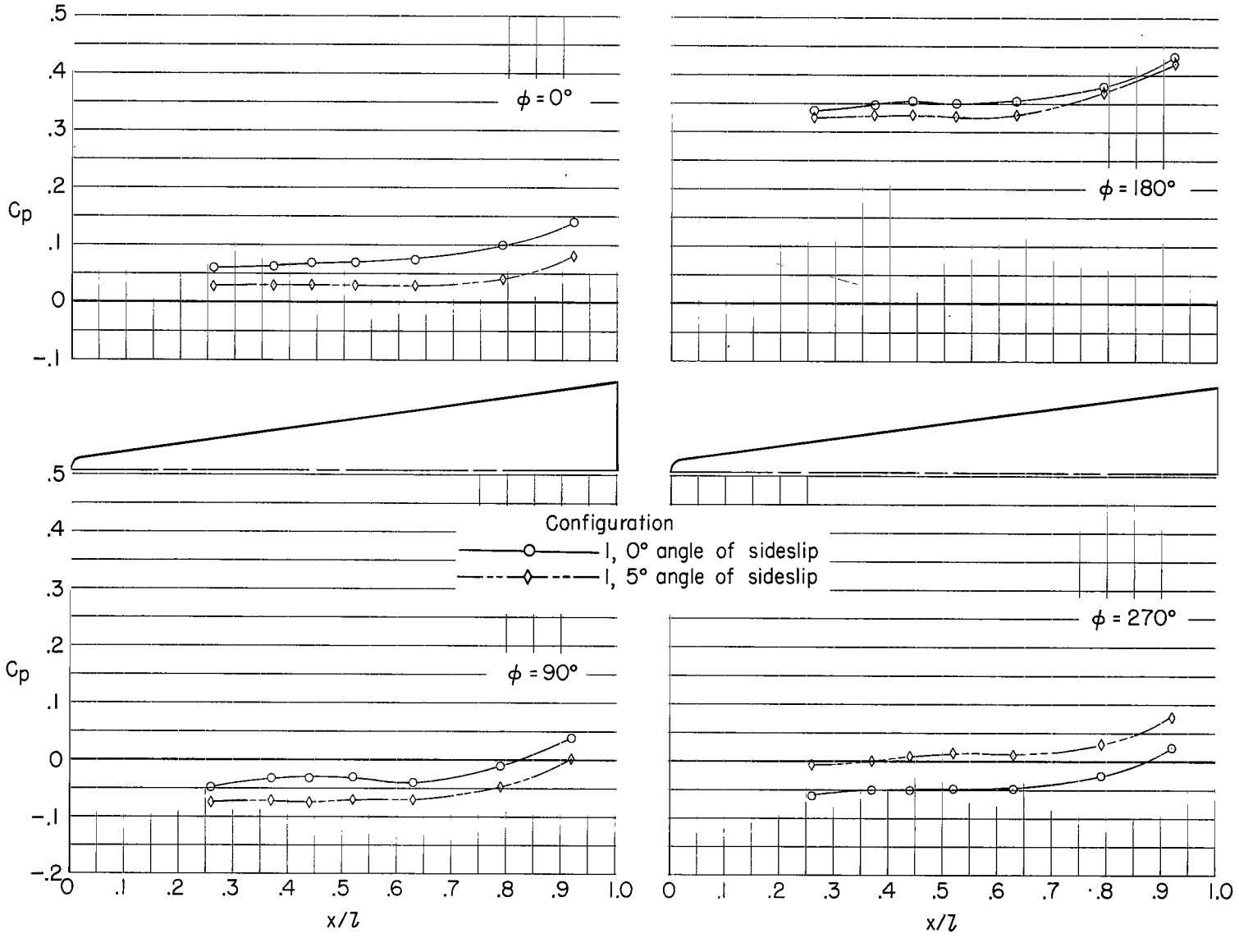

(e) $\alpha = 15.0^0$.

Figure 18.- Concluded.

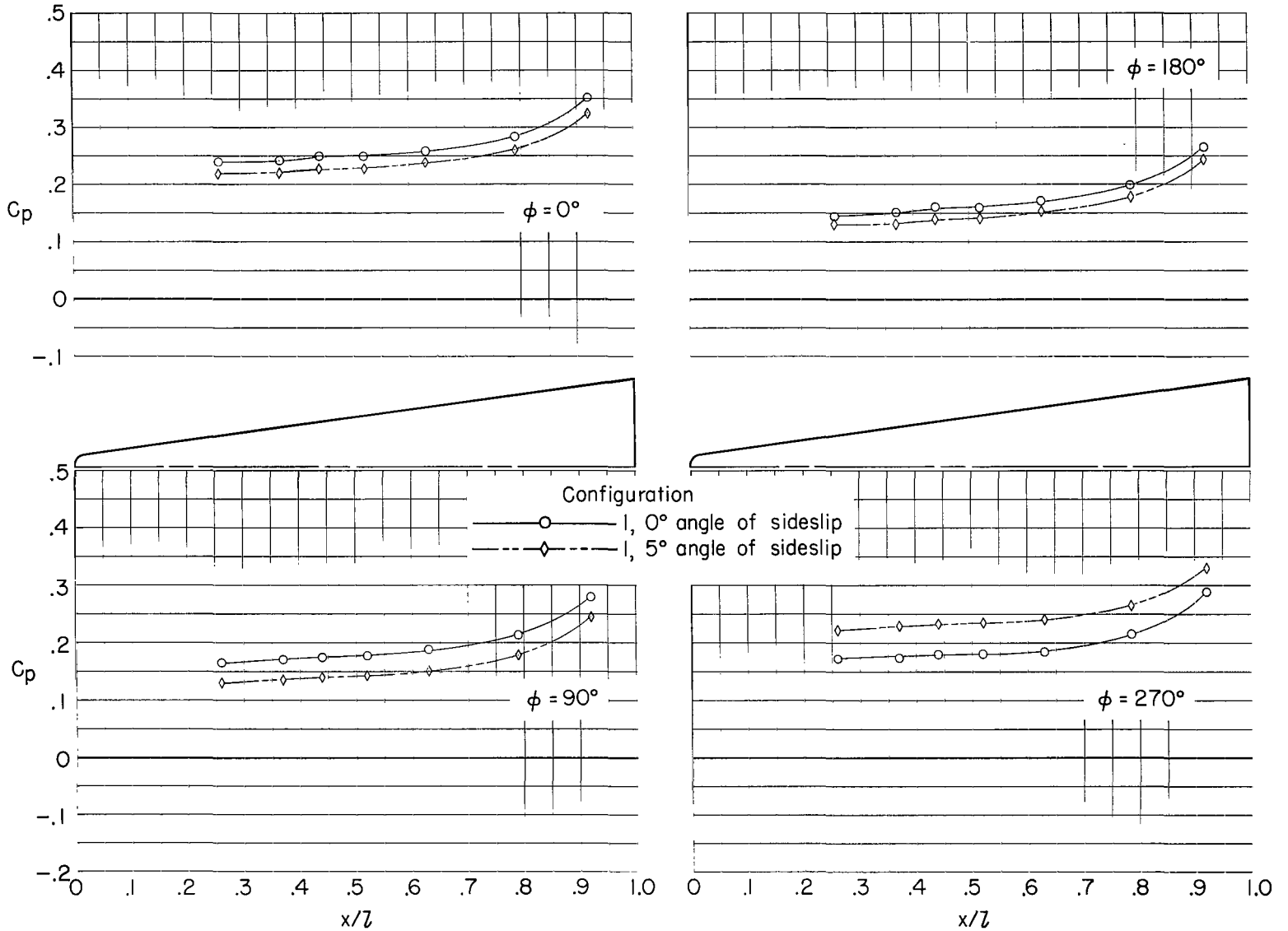

(a) $\alpha = -4.8^{0}$.

Figure 19.- Longitudinal pressure distributions. M = 1.00.

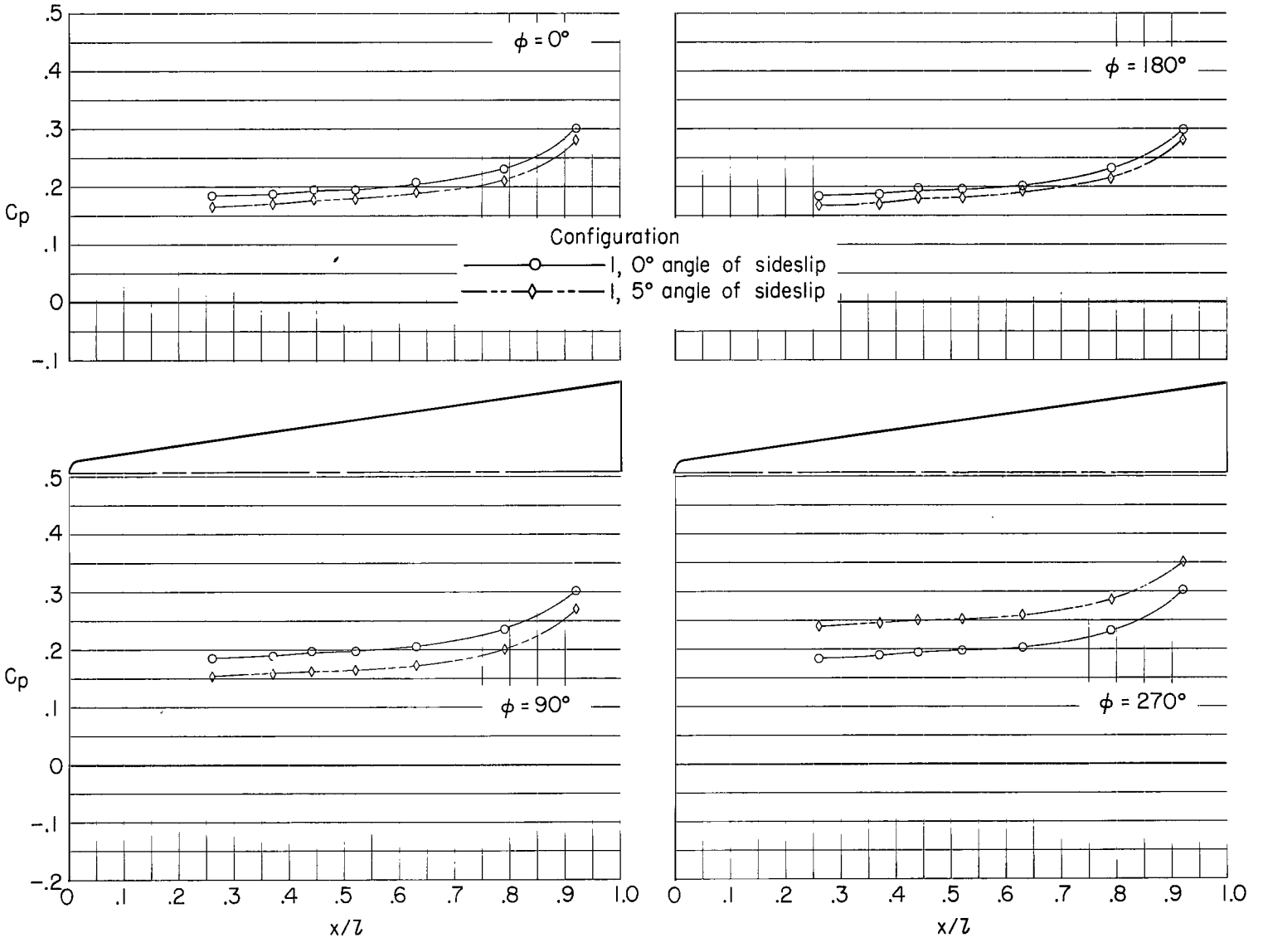

(b) $\alpha = 0.2^0$.

Figure 19.- Continued.

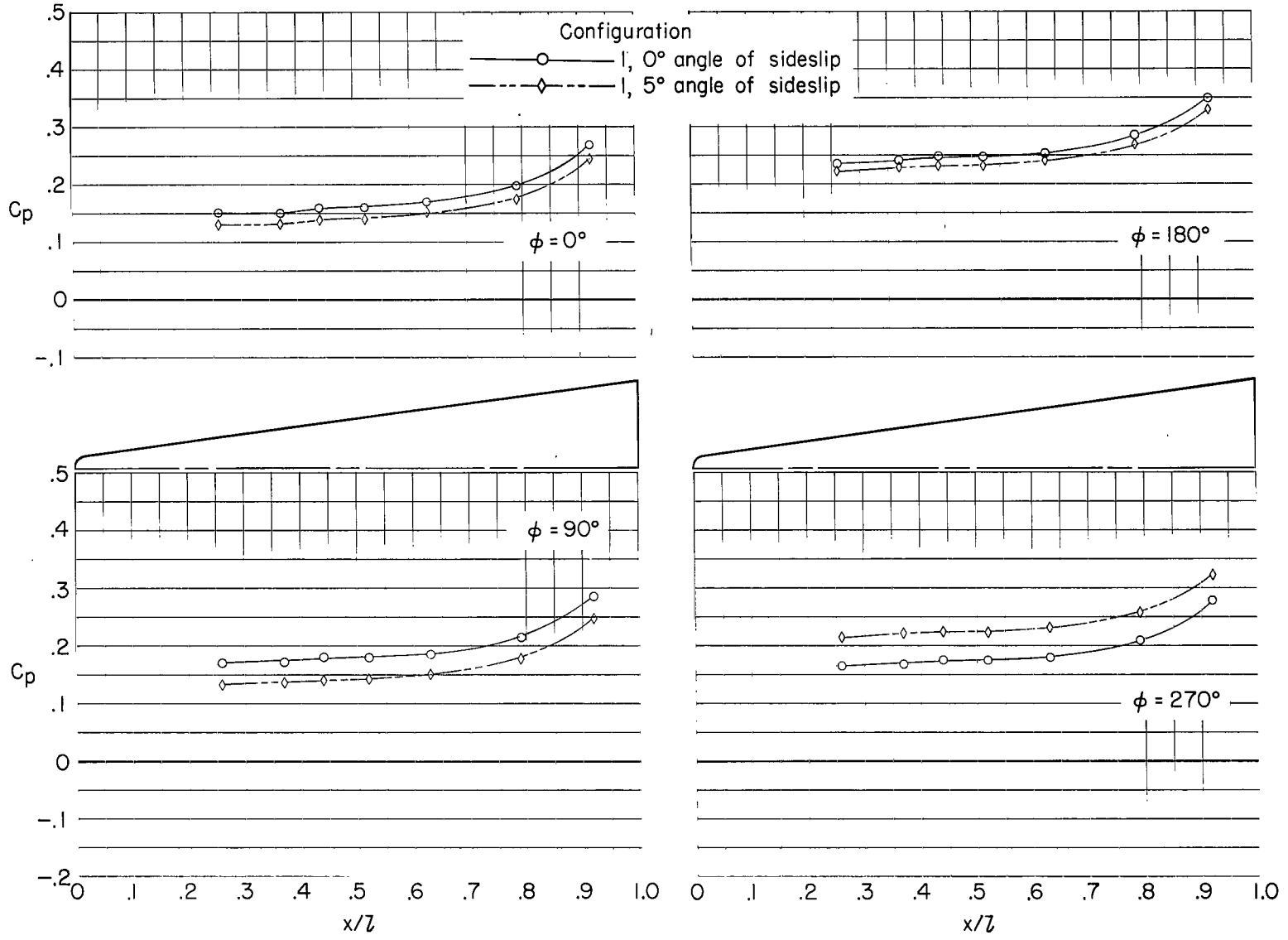

(c) $\alpha = 5.2^0$.

Figure 19.- Continued.

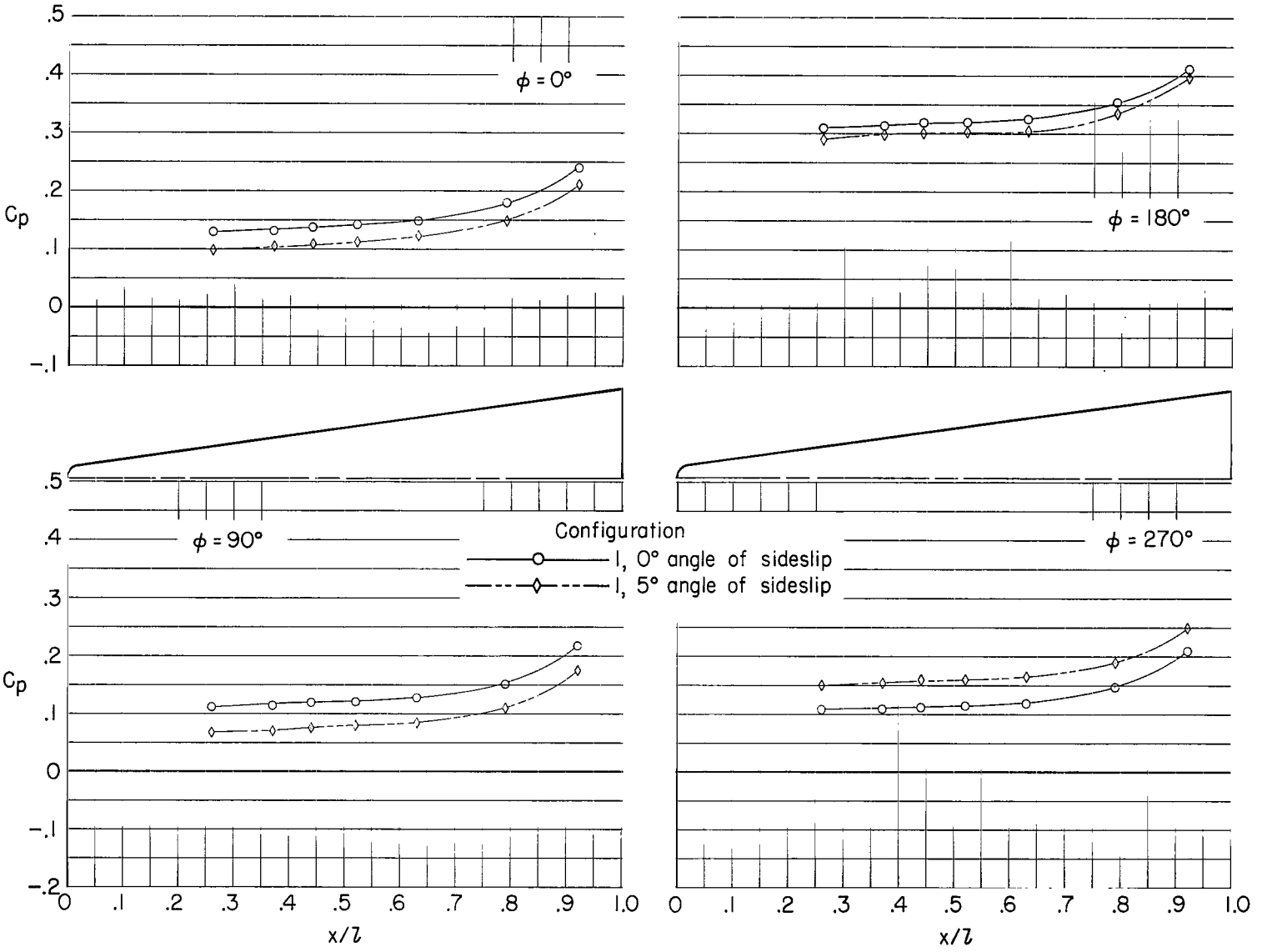

(d) $\alpha = 10.2^0$.

Figure 19.- Continued.

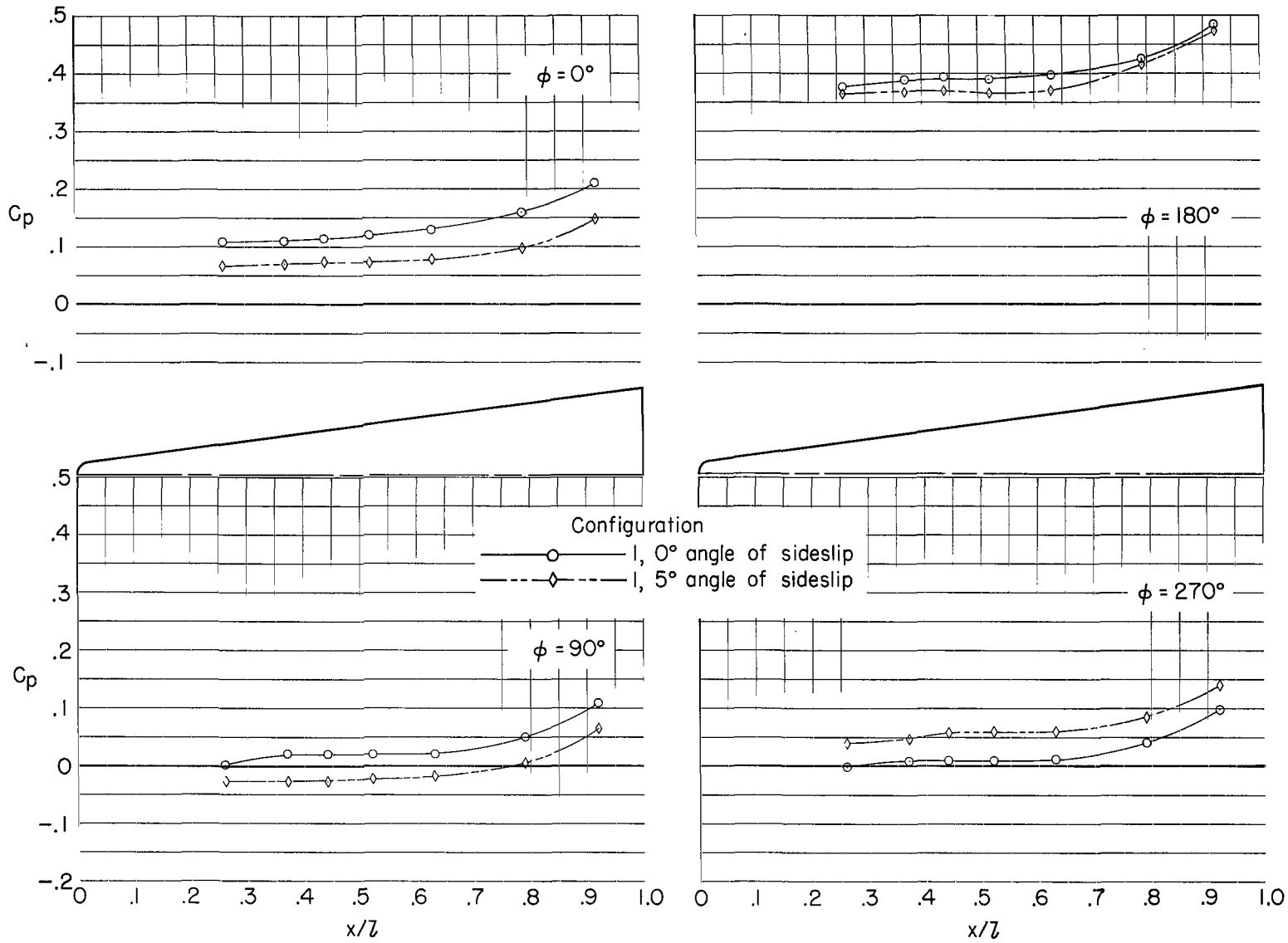

(e) $\alpha = 15.0^{0}$.

Figure 19.- Concluded.

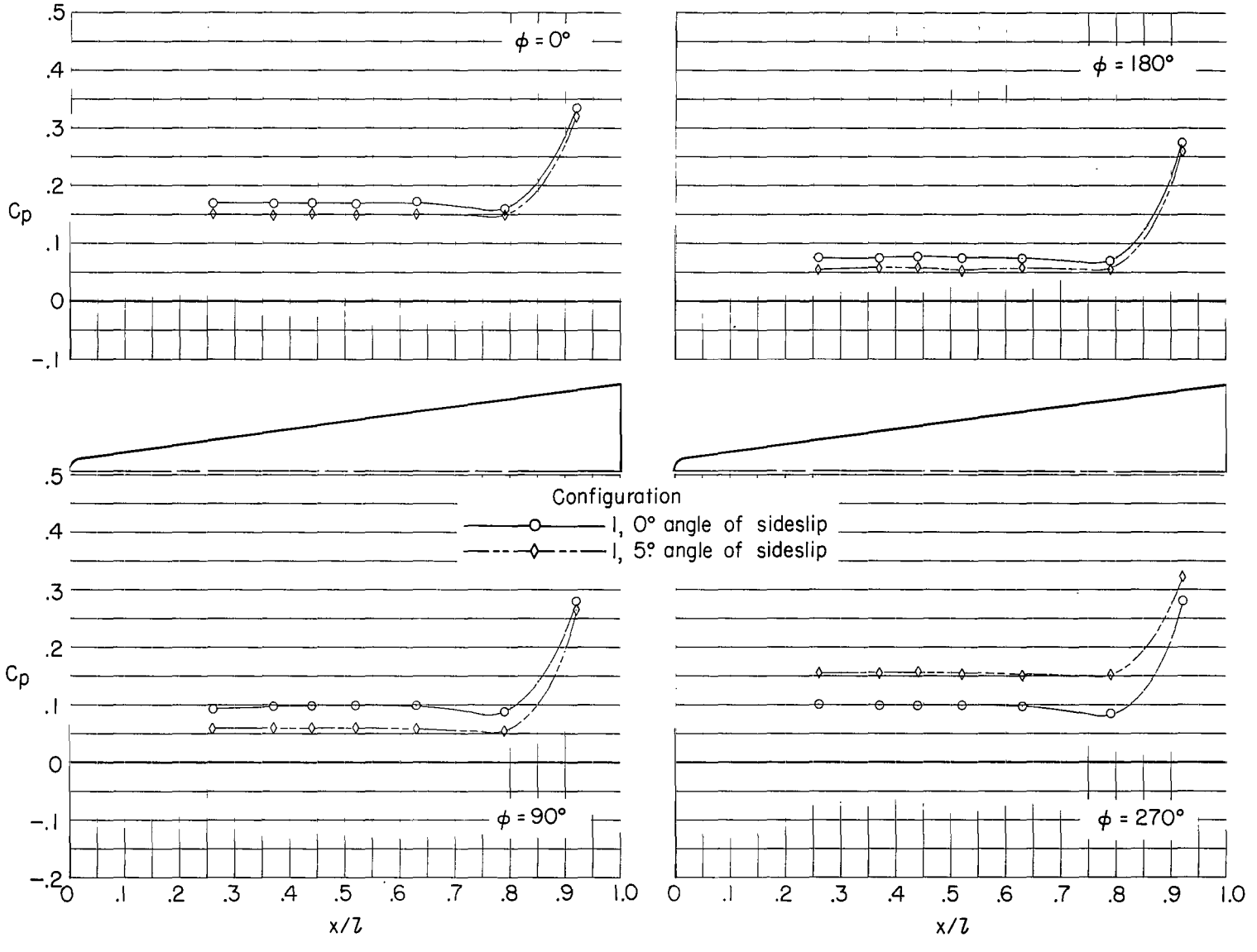

(a) $\alpha = -4.8^0$.

Figure 20.- Longitudinal pressure distributions. M = 1.10.

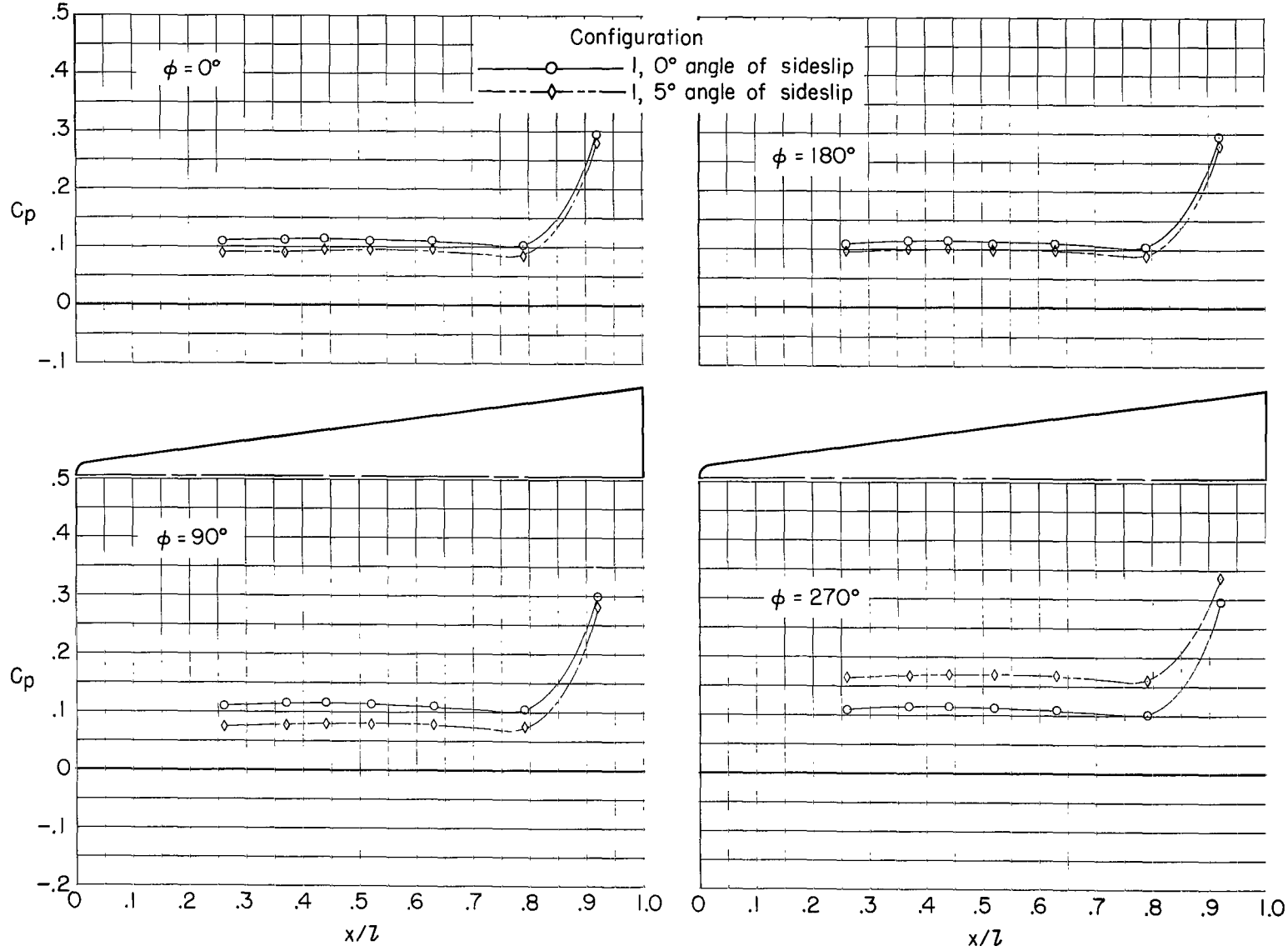

(b) $\alpha = 0.2^0$.

Figure 20.- Continued.

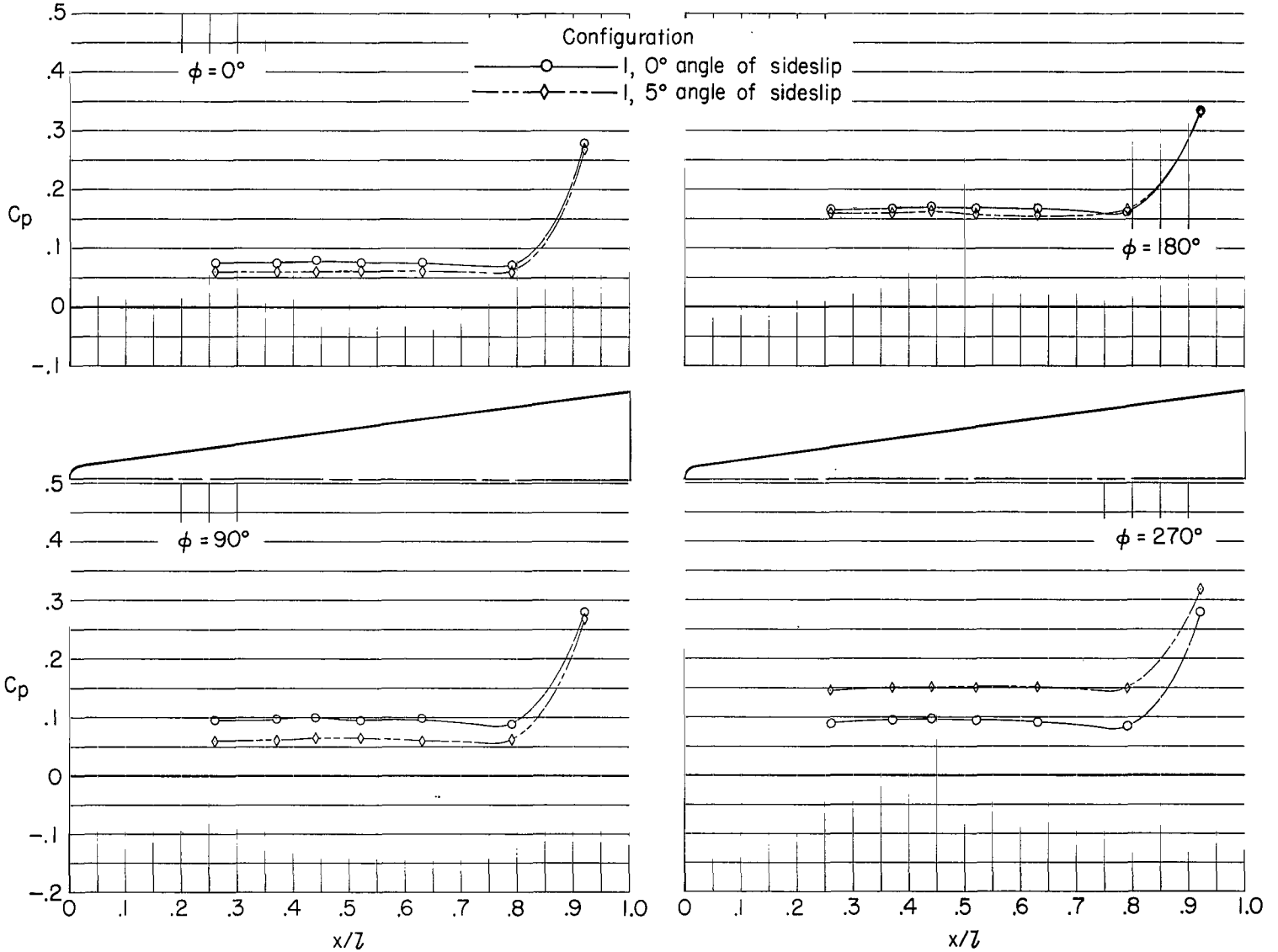

(c) $\alpha = 5.2^0$.

Figure 20.- Continued.

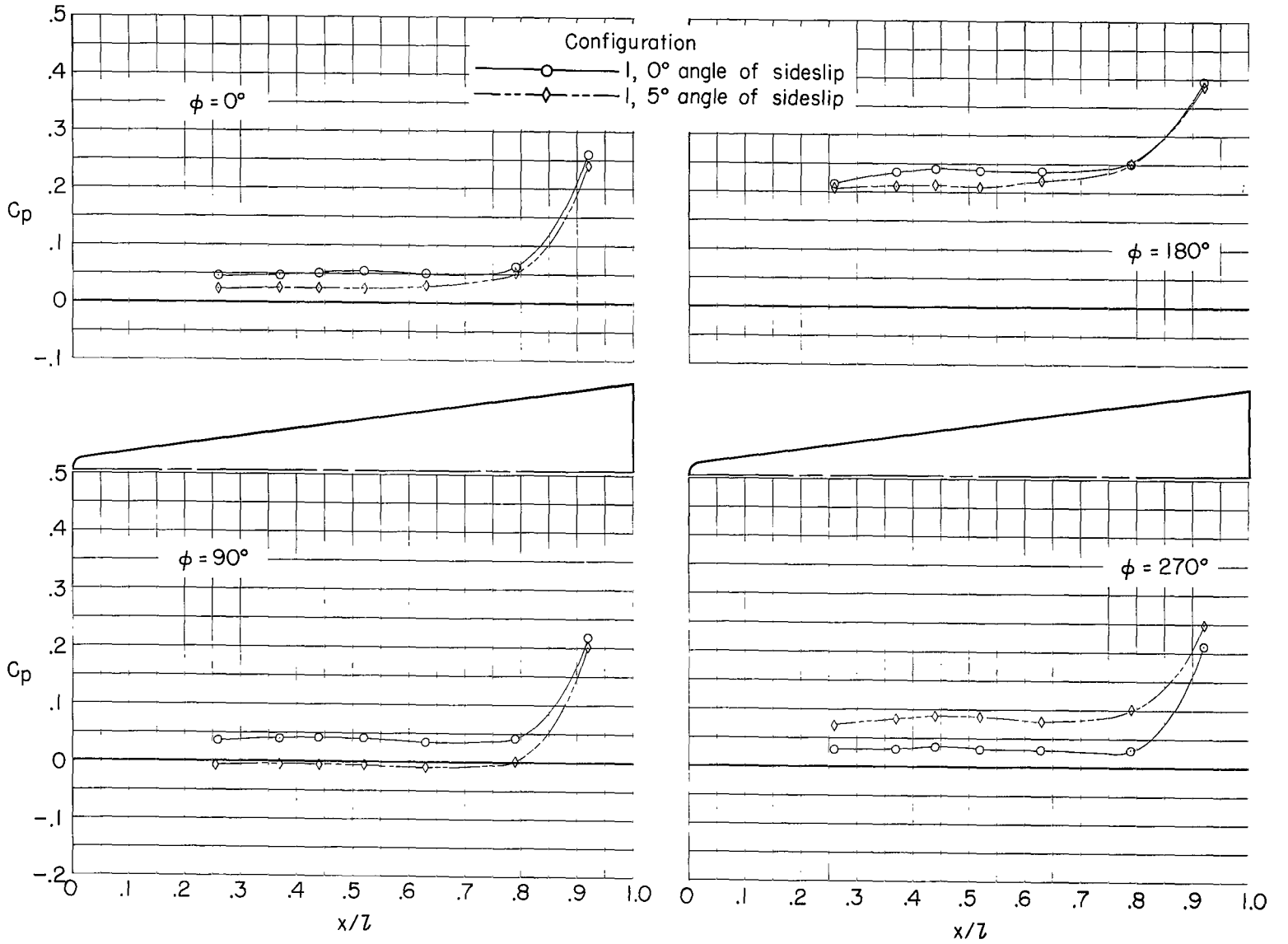

(d) $\alpha = 10.2^0$.

Figure 20.- Continued.

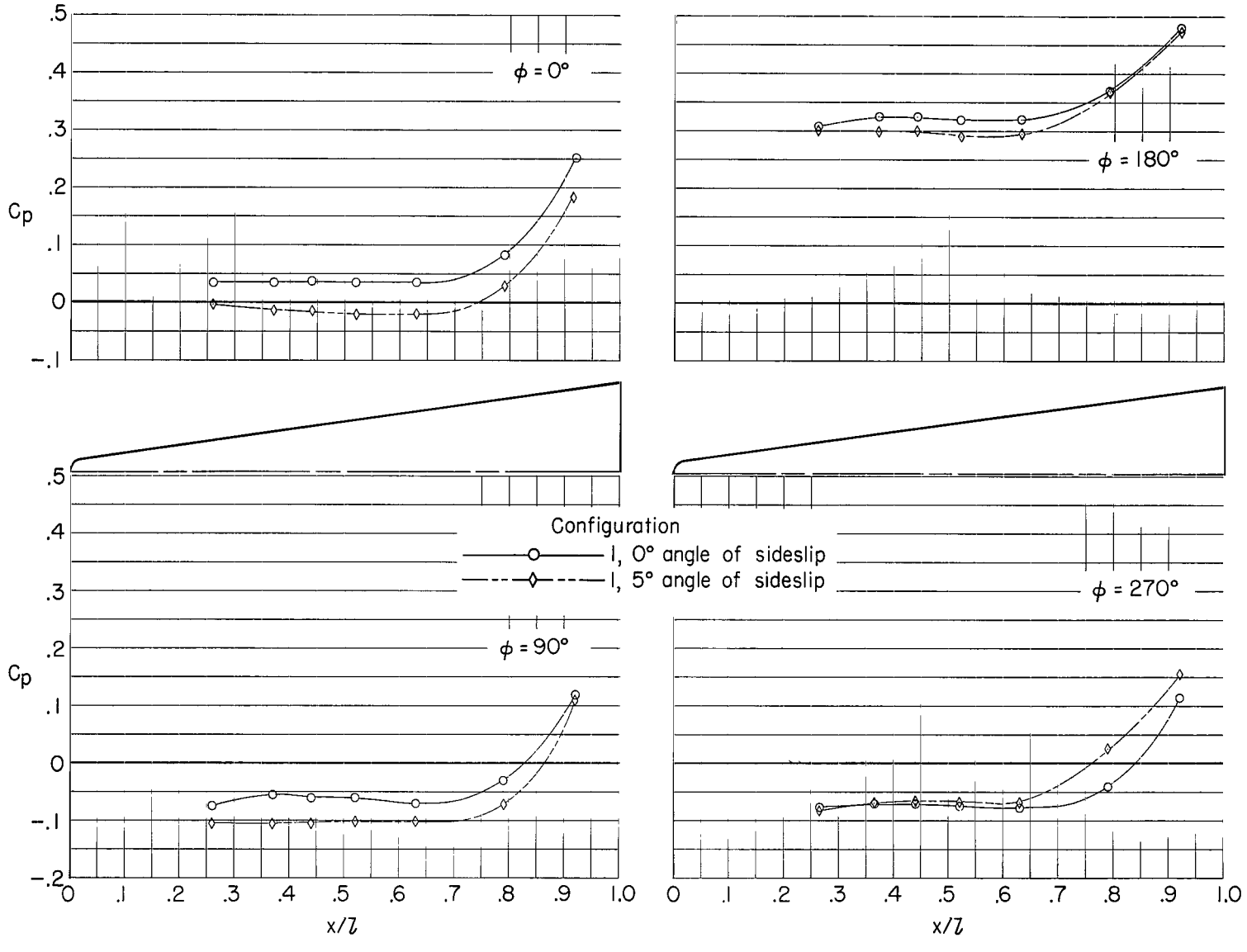

(e) $\alpha = 15.0^0$.

Figure 20.- Concluded.

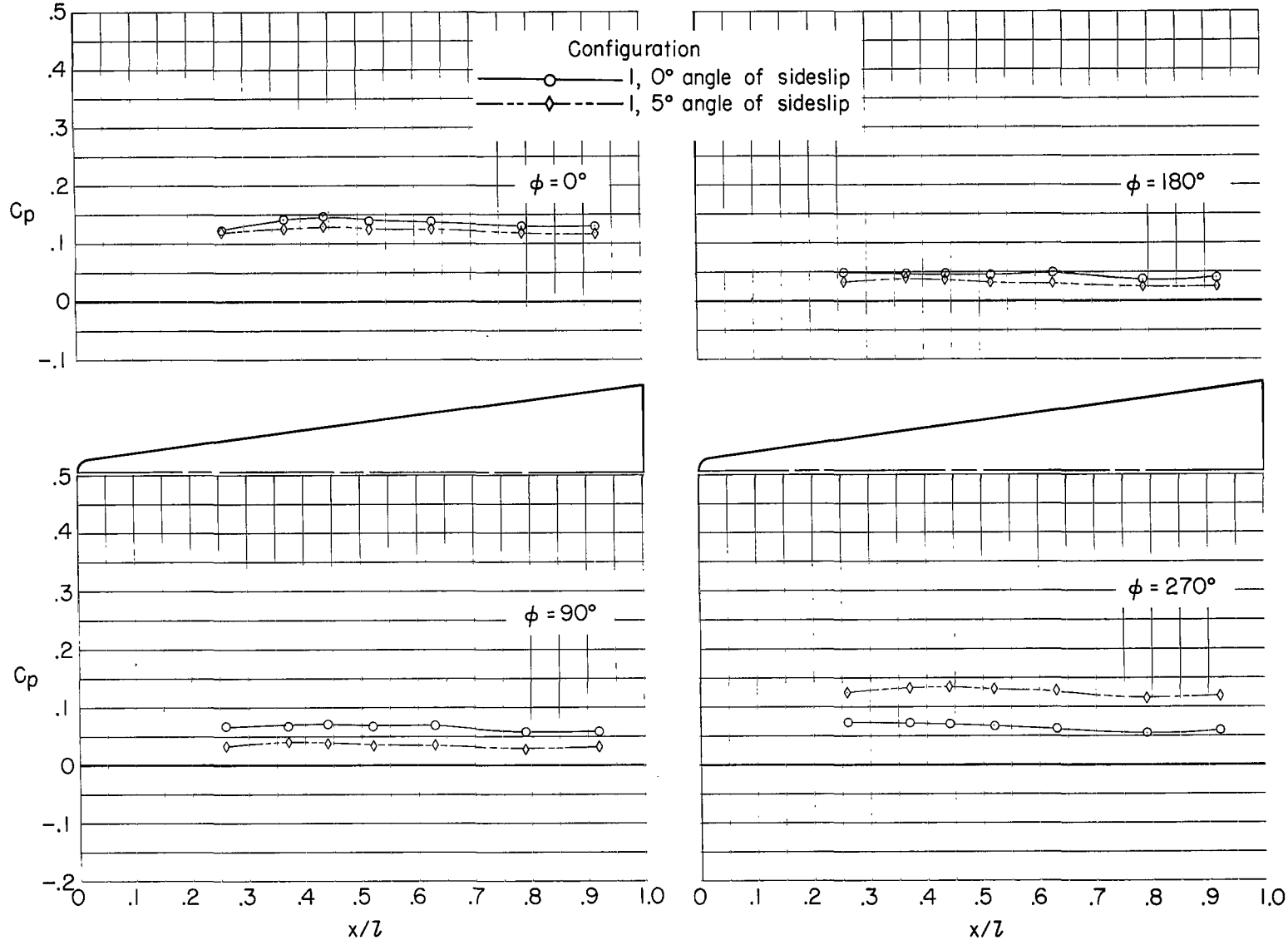

(a) $\alpha = -4.8^0$.

Figure 21.- Longitudinal pressure distributions. M = 1.20.

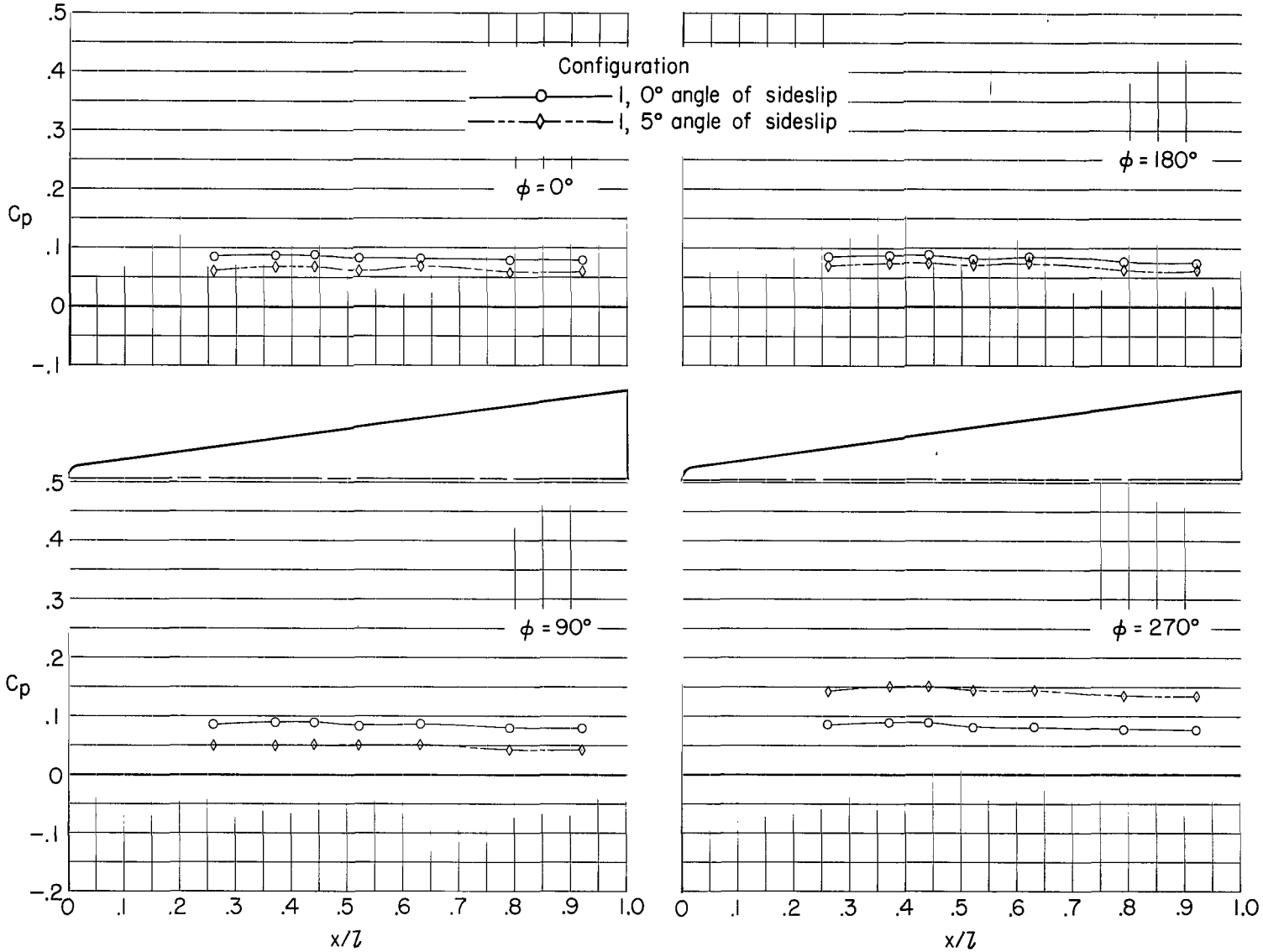

(b) $\alpha = 0.2^0$.

Figure 21.- Continued.

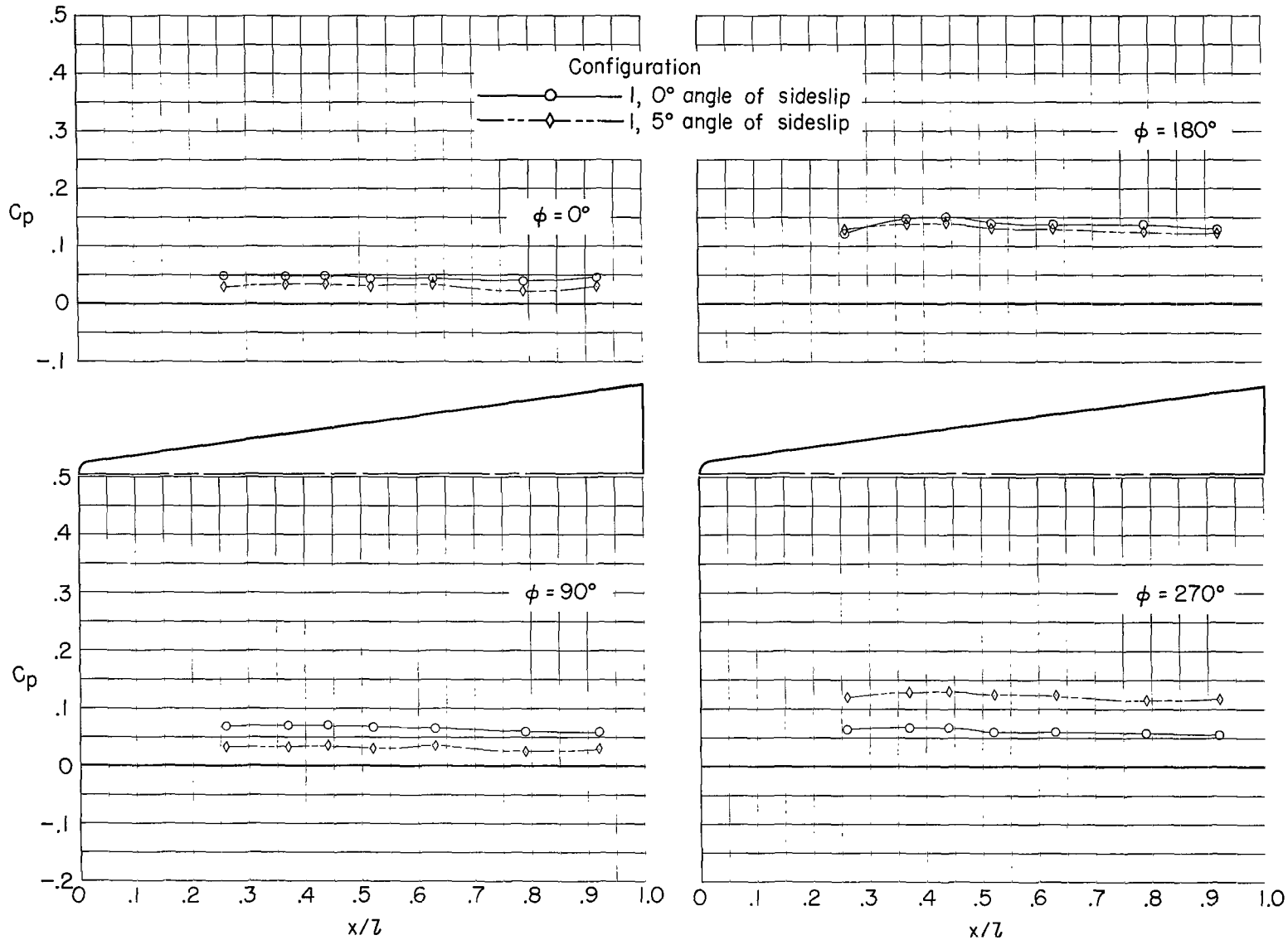

(c) $\alpha = 5.2^0$.

Figure 21.- Continued.

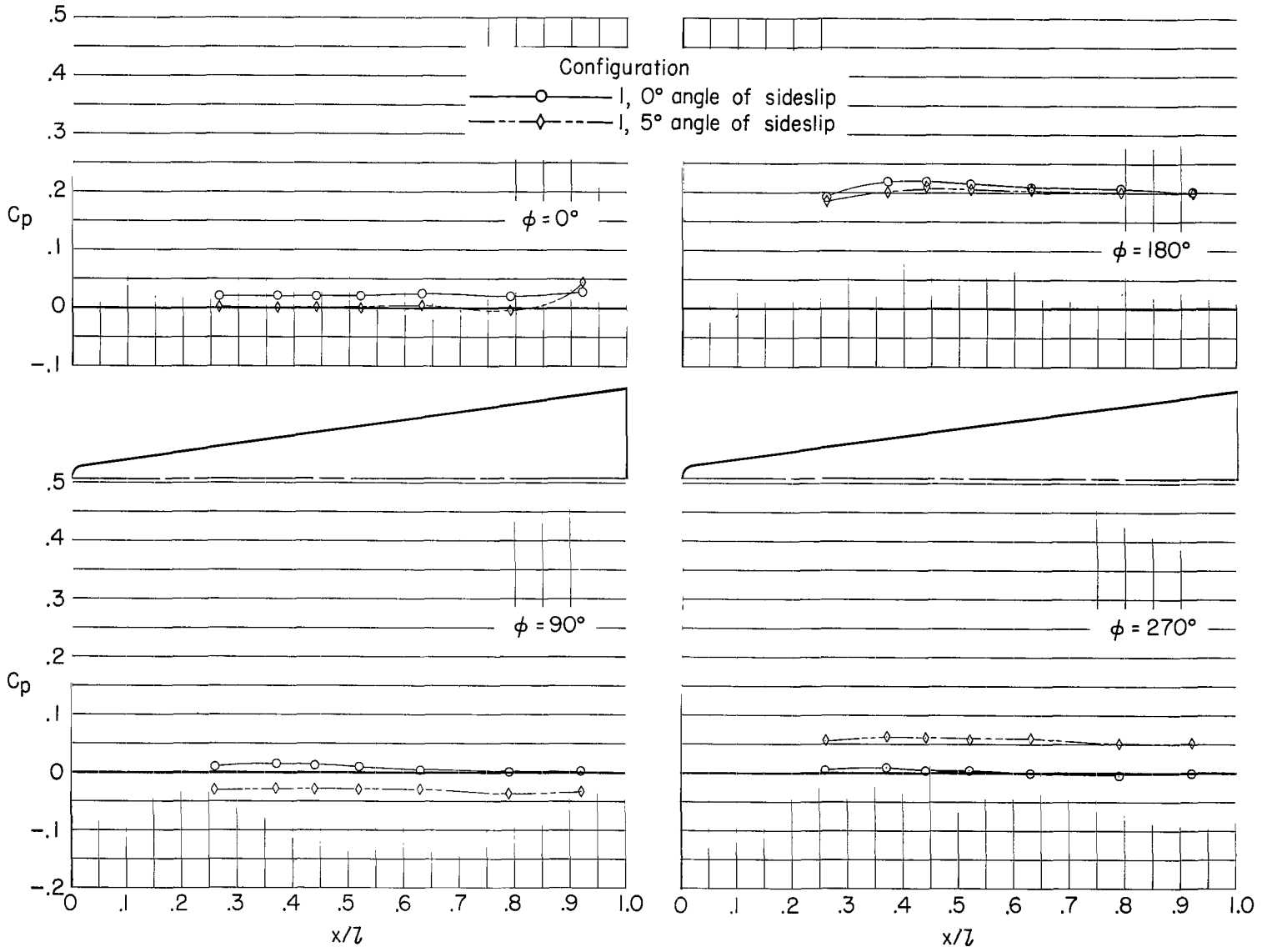

(d) $\alpha = 10.2^0$.

Figure 21.- Continued.

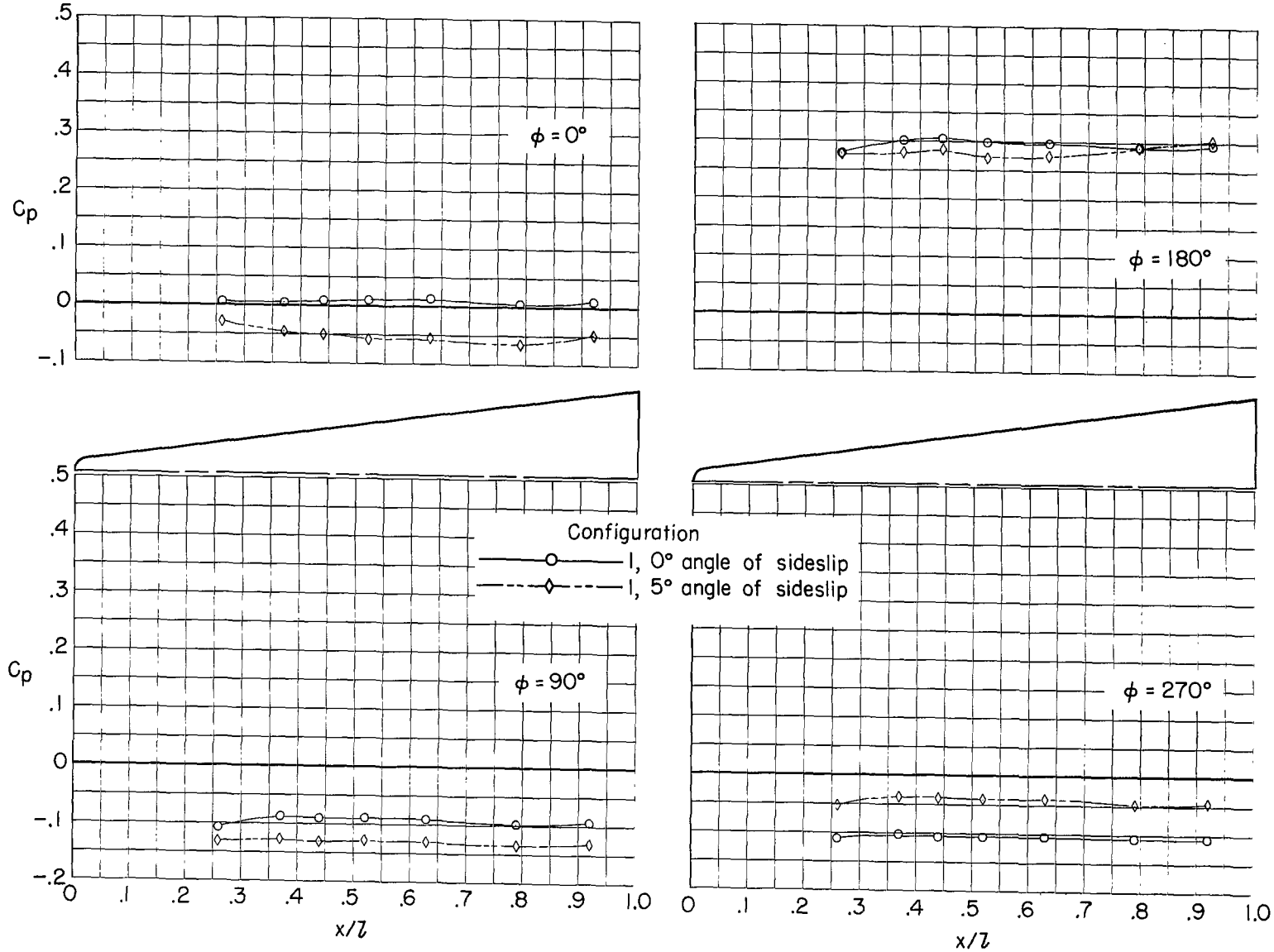

(e) $\alpha = 15.0^0$.

Figure 21.- Concluded.

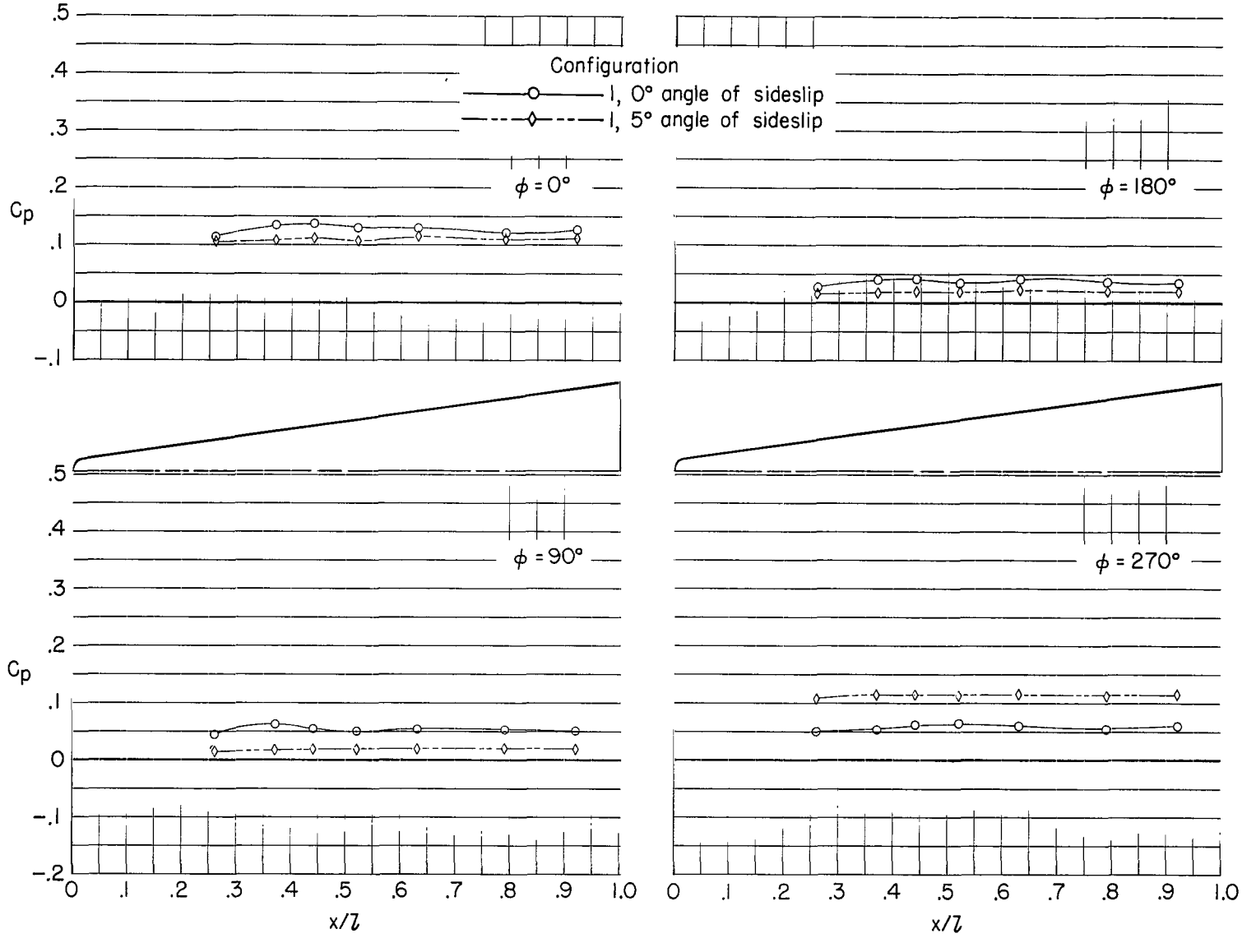

(a) $\alpha = -4.8^0$.

Figure 22.- Longitudinal pressure distributions. M = 1.29.

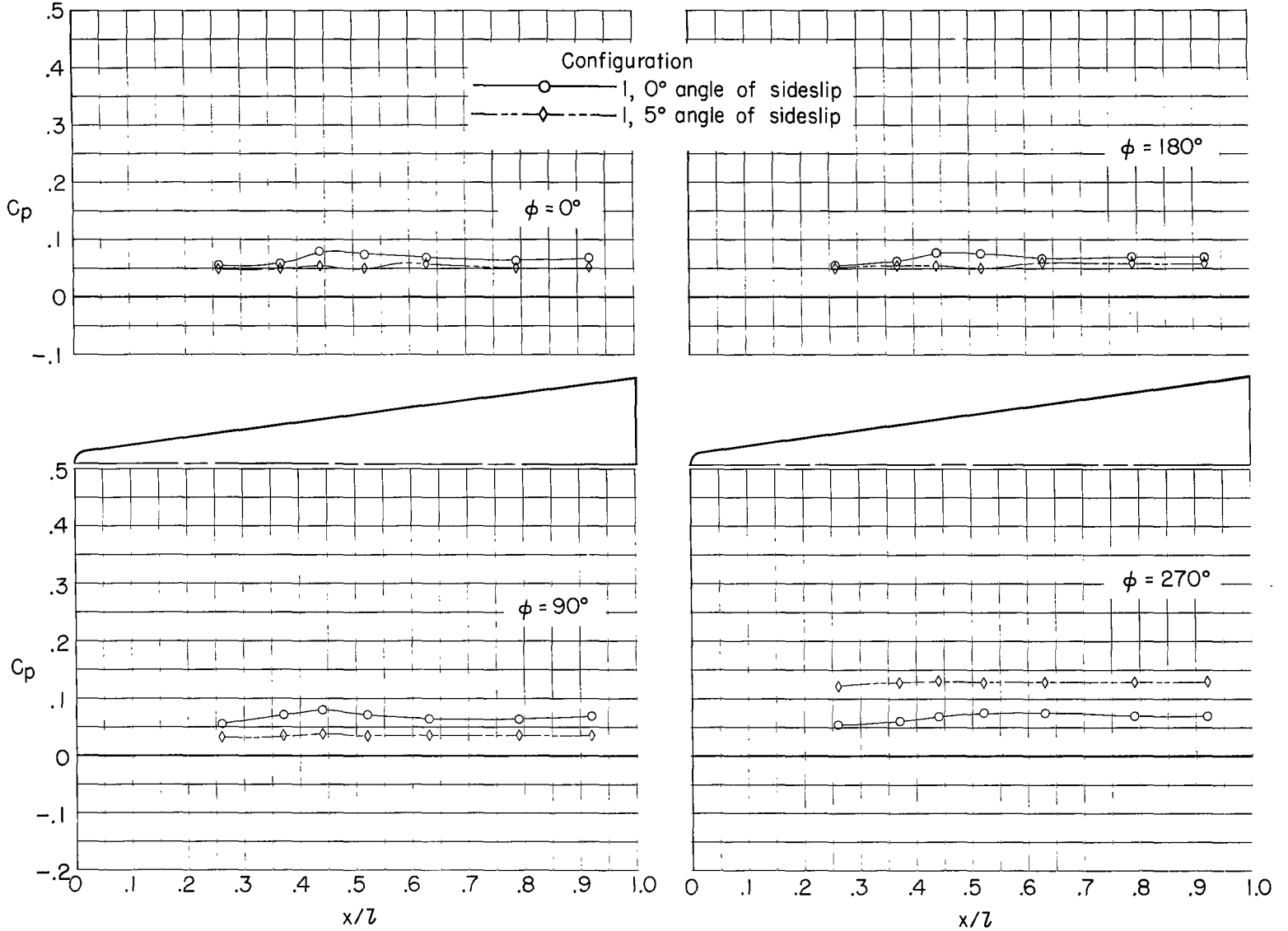

(b) $\alpha = 0.2^0$.

Figure 22.- Continued.

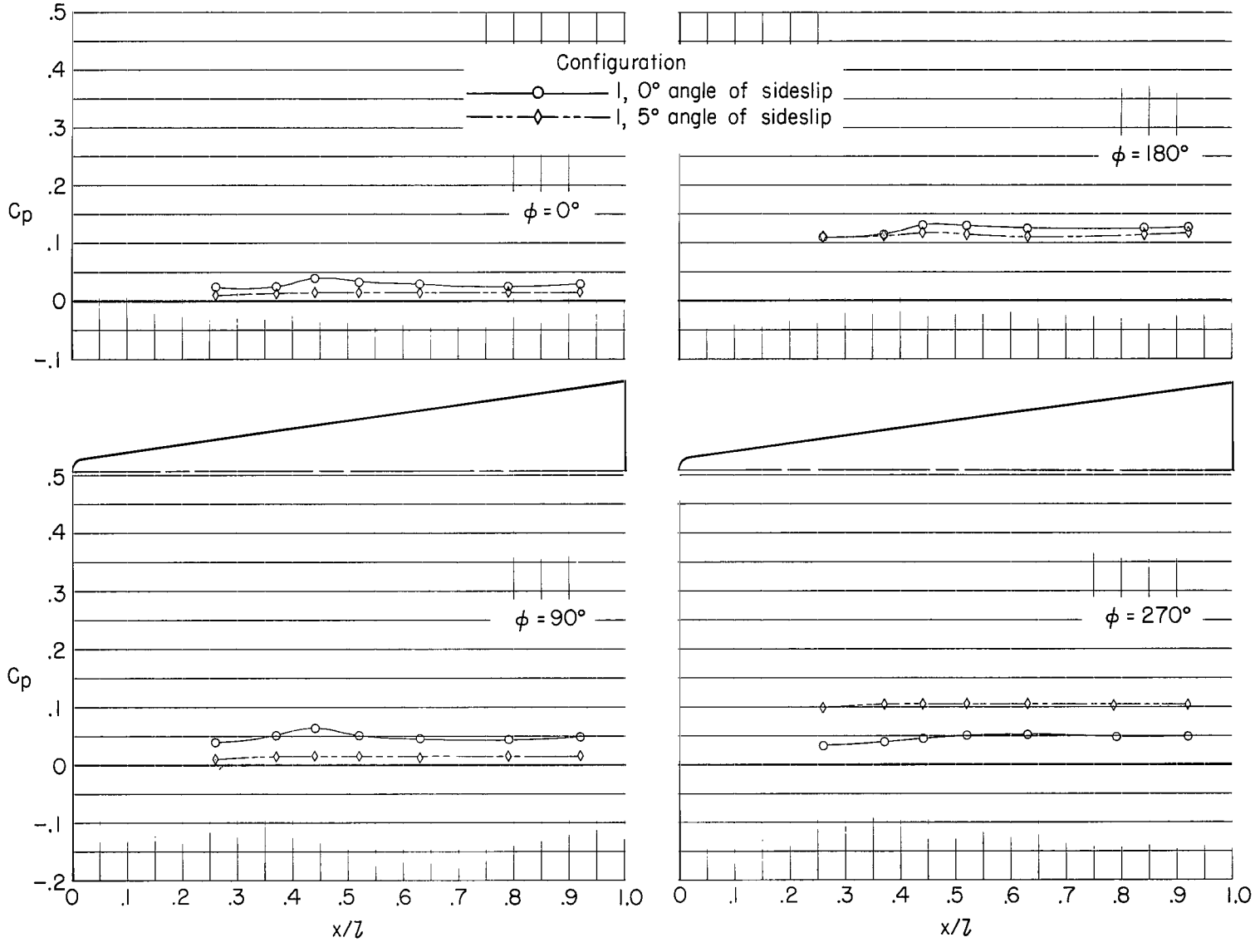

(c) $\alpha = 5.2^0$.

Figure 22.- Continued.

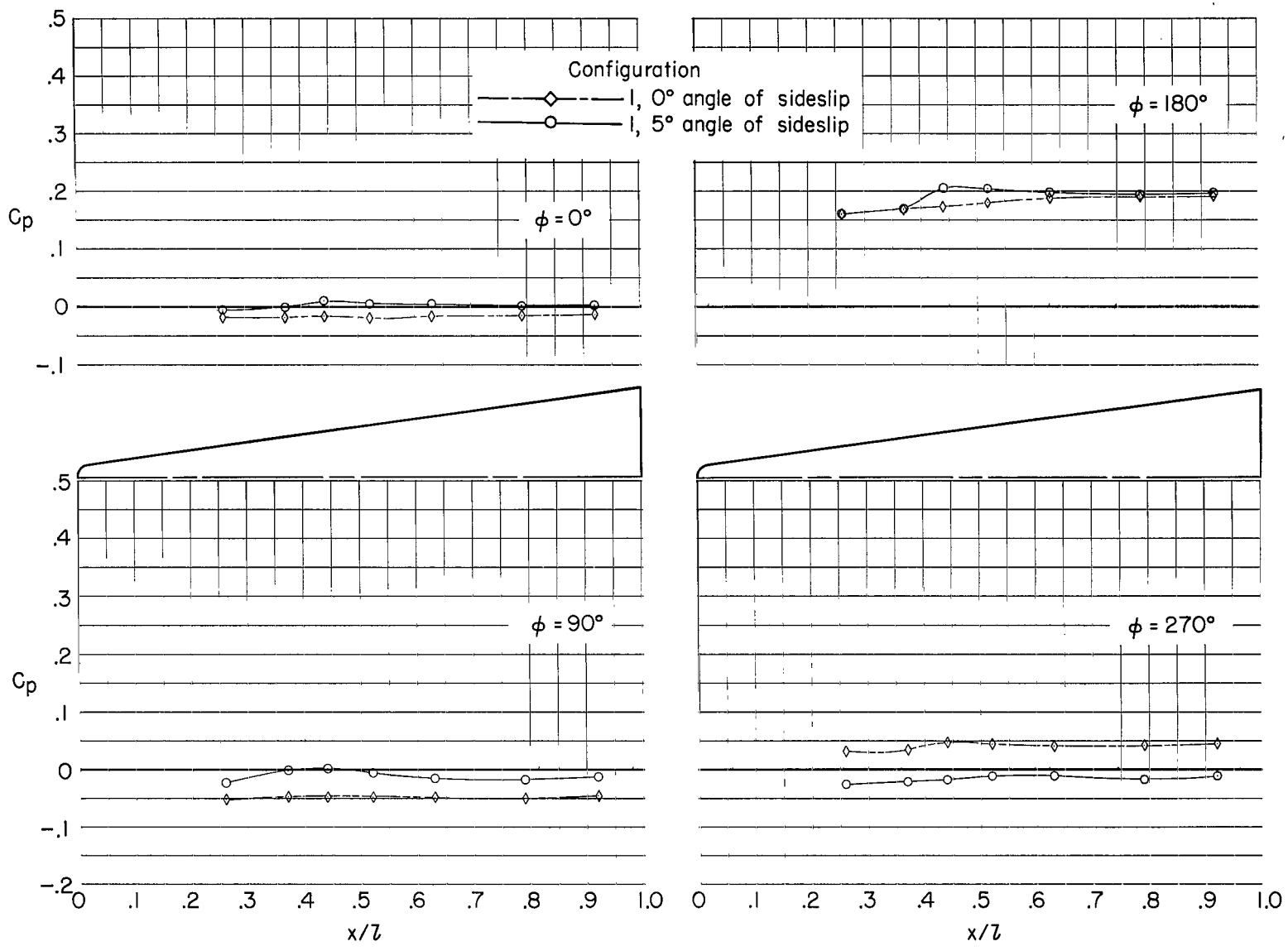

(d) $\alpha = 10.2^0$.

Figure 22.- Continued.

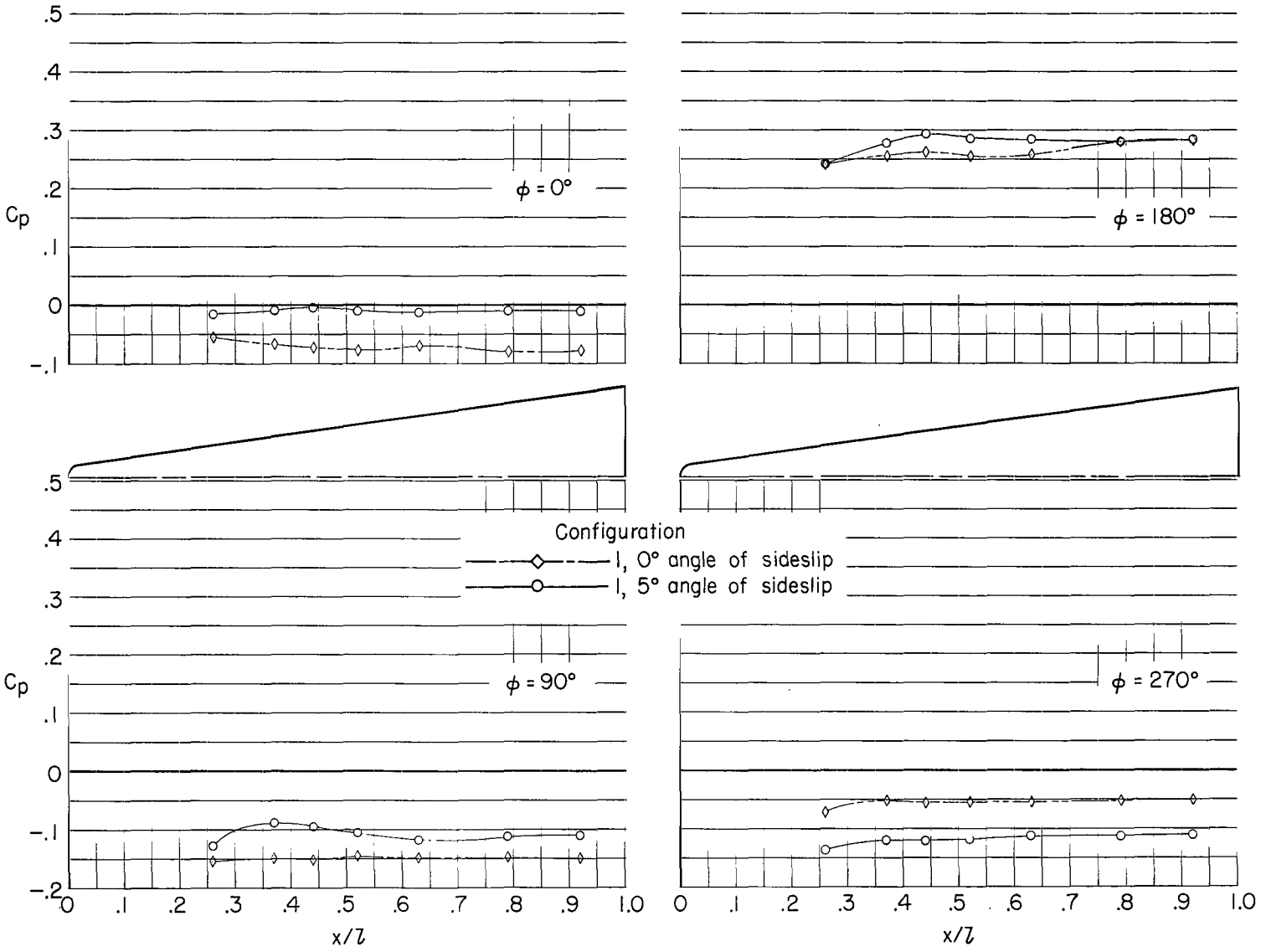

(e) $\alpha = 15.0^0$.

Figure 22.- Concluded.

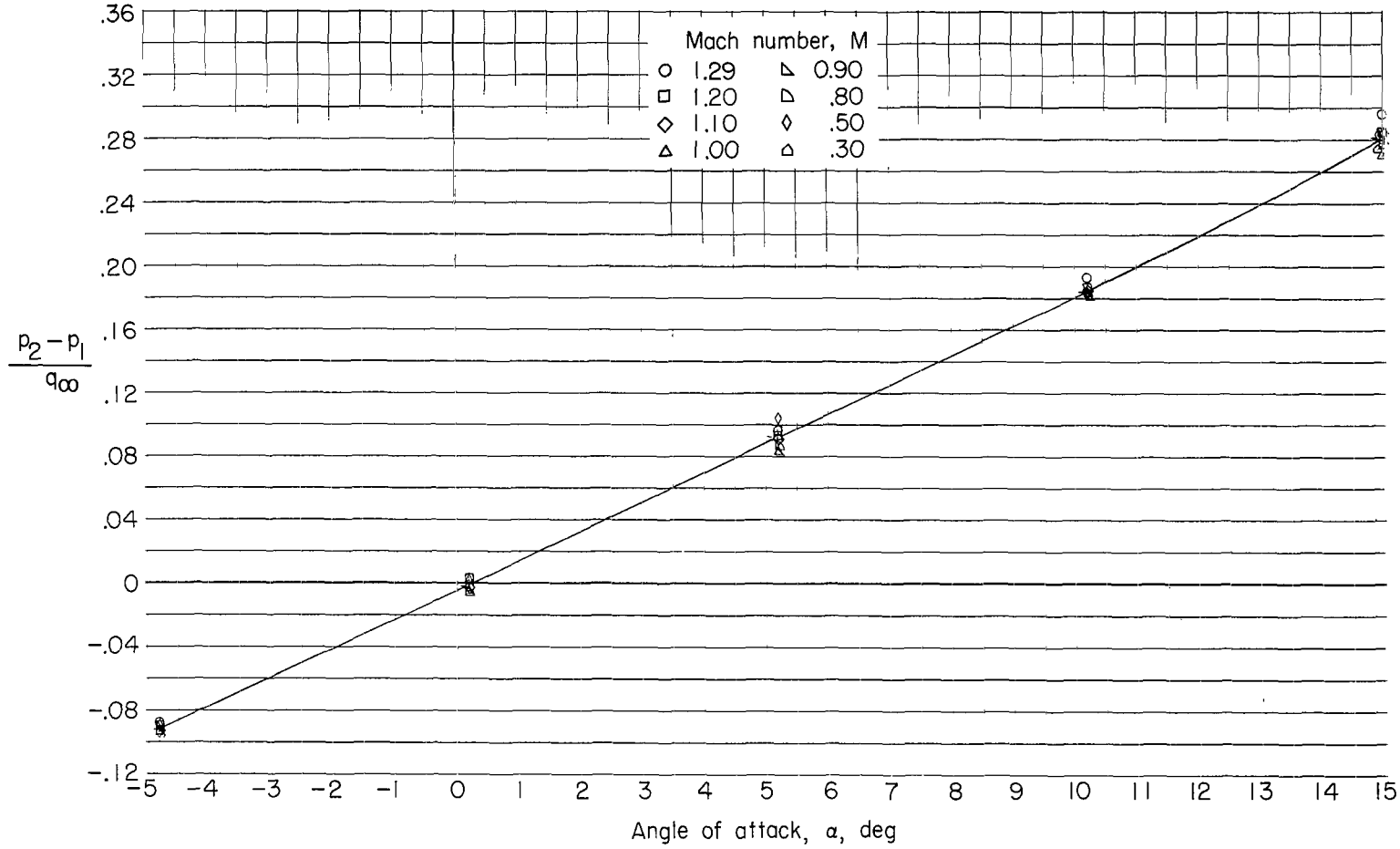

(a) $\beta = 0^0$.

Figure 23.- Sensitivity of pressure ratio to angle of attack at station B for various Mach numbers.

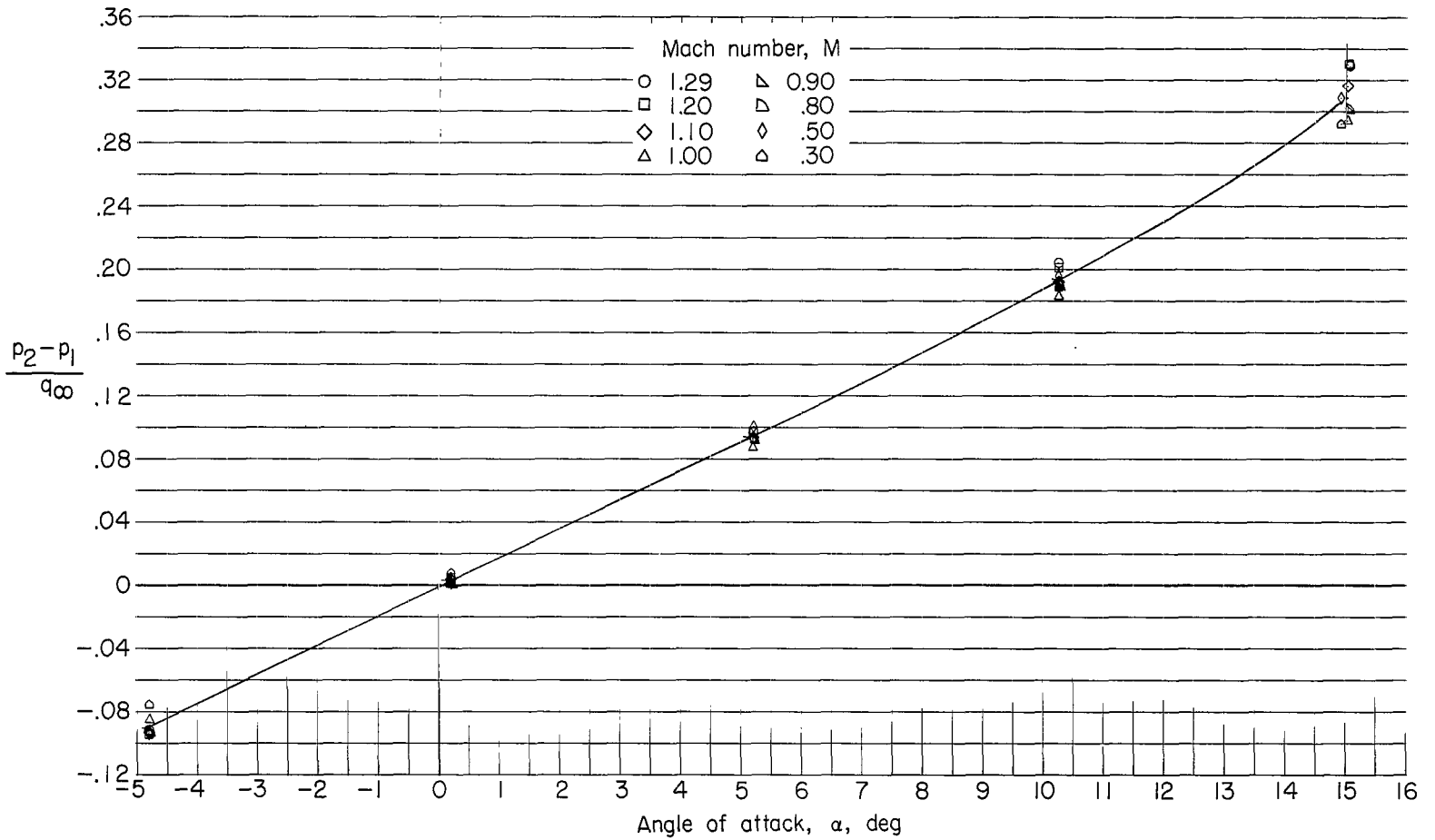

(b) $\beta = 5^0$.

Figure 23.- Concluded.

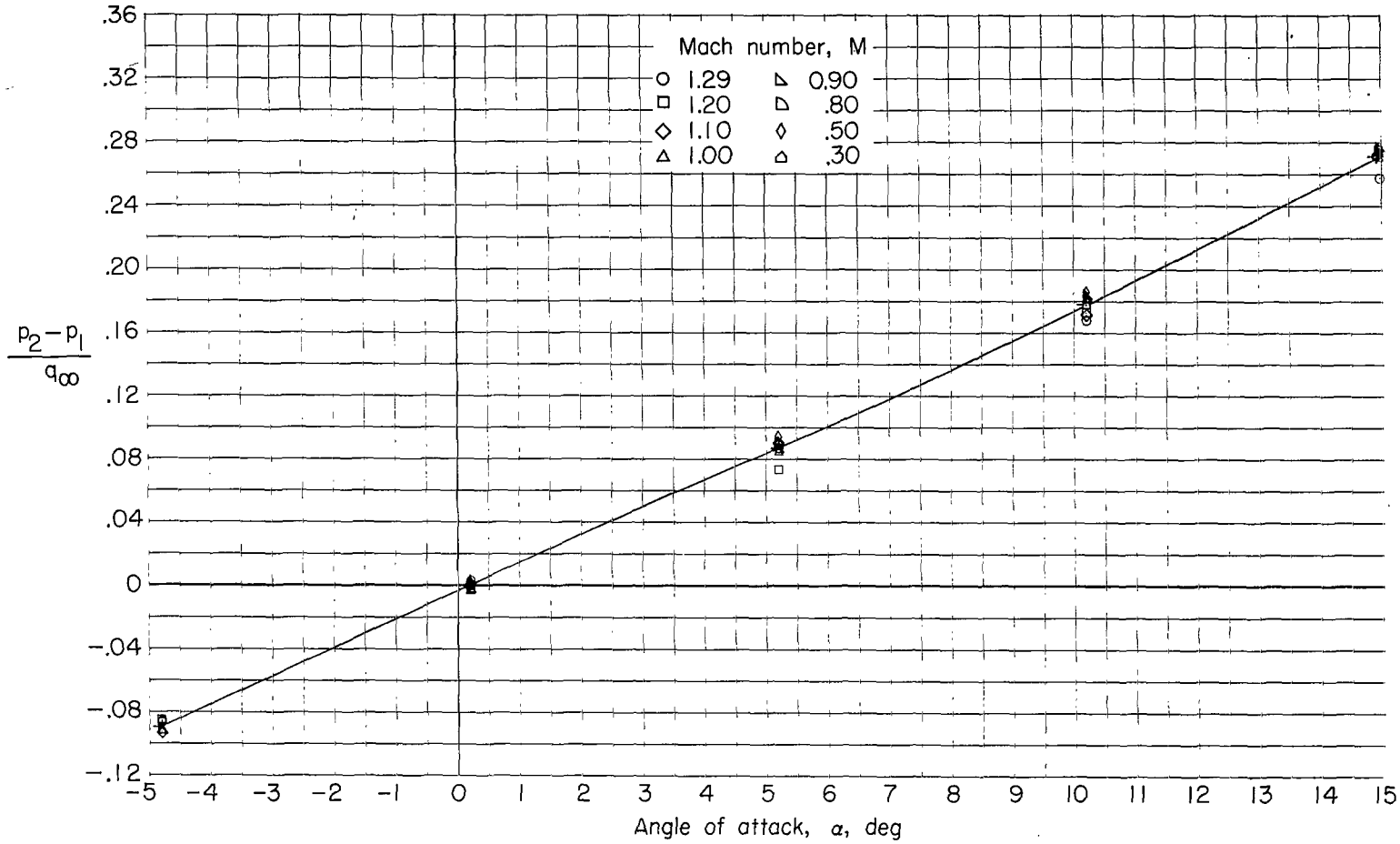

(a) $\beta = 0^0$.

Figure 24.- Sensitivity of pressure ratio to angle of attack at station E for various Mach numbers.

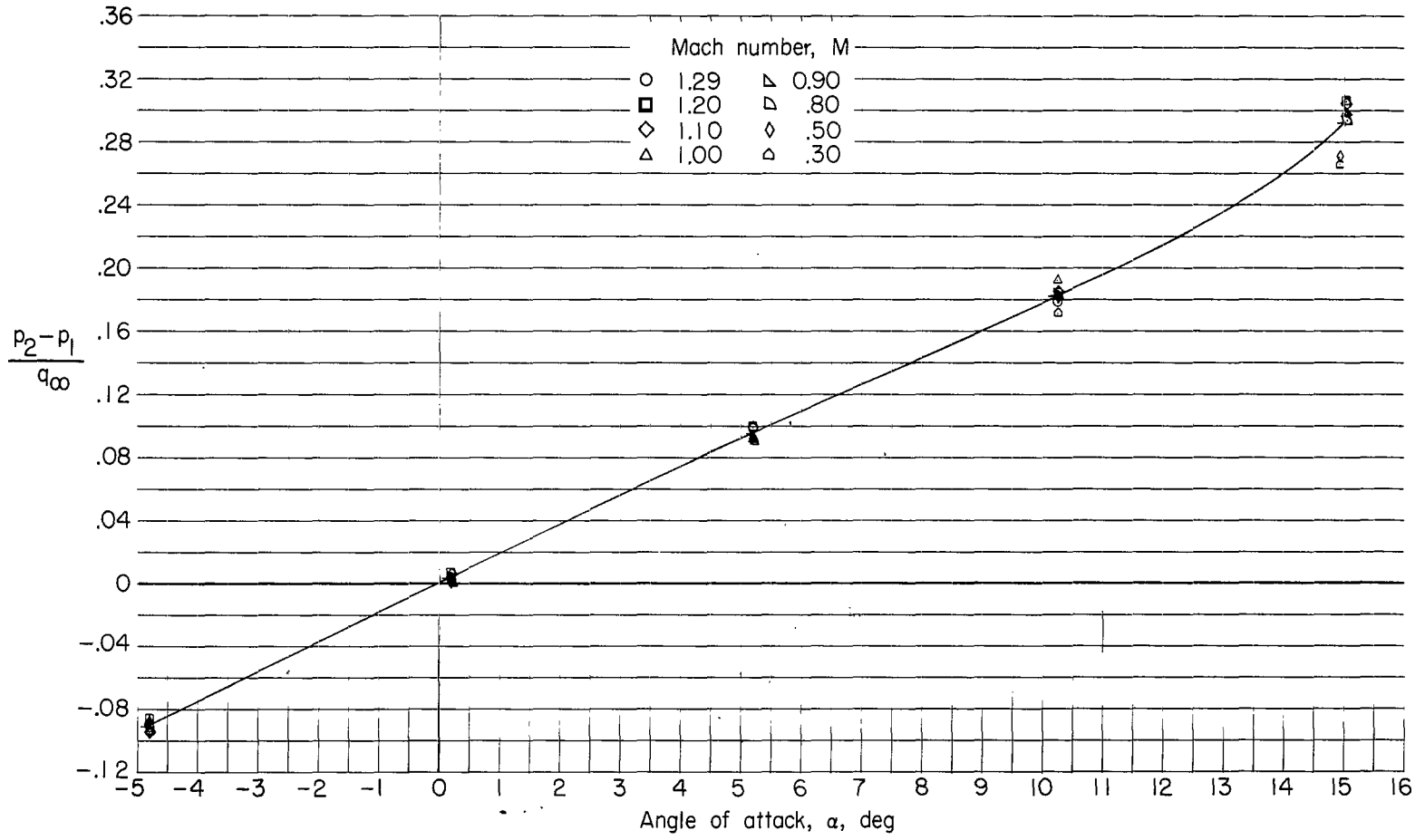

(b) $\beta = 5^0$.

Figure 24.- Concluded.

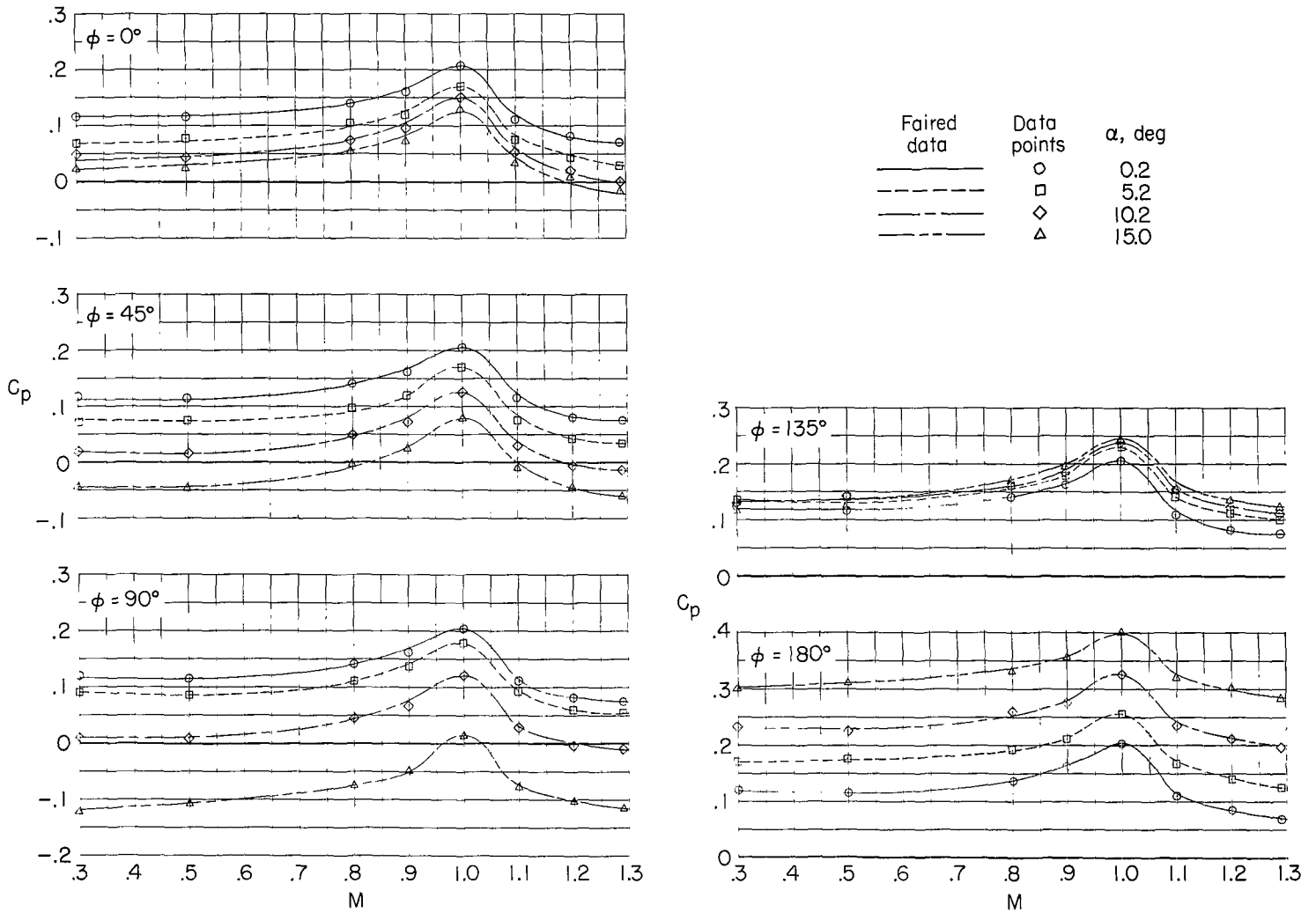

(a) $\beta = 0^0$.

Figure 25.- Variation of C_p with M at station E.

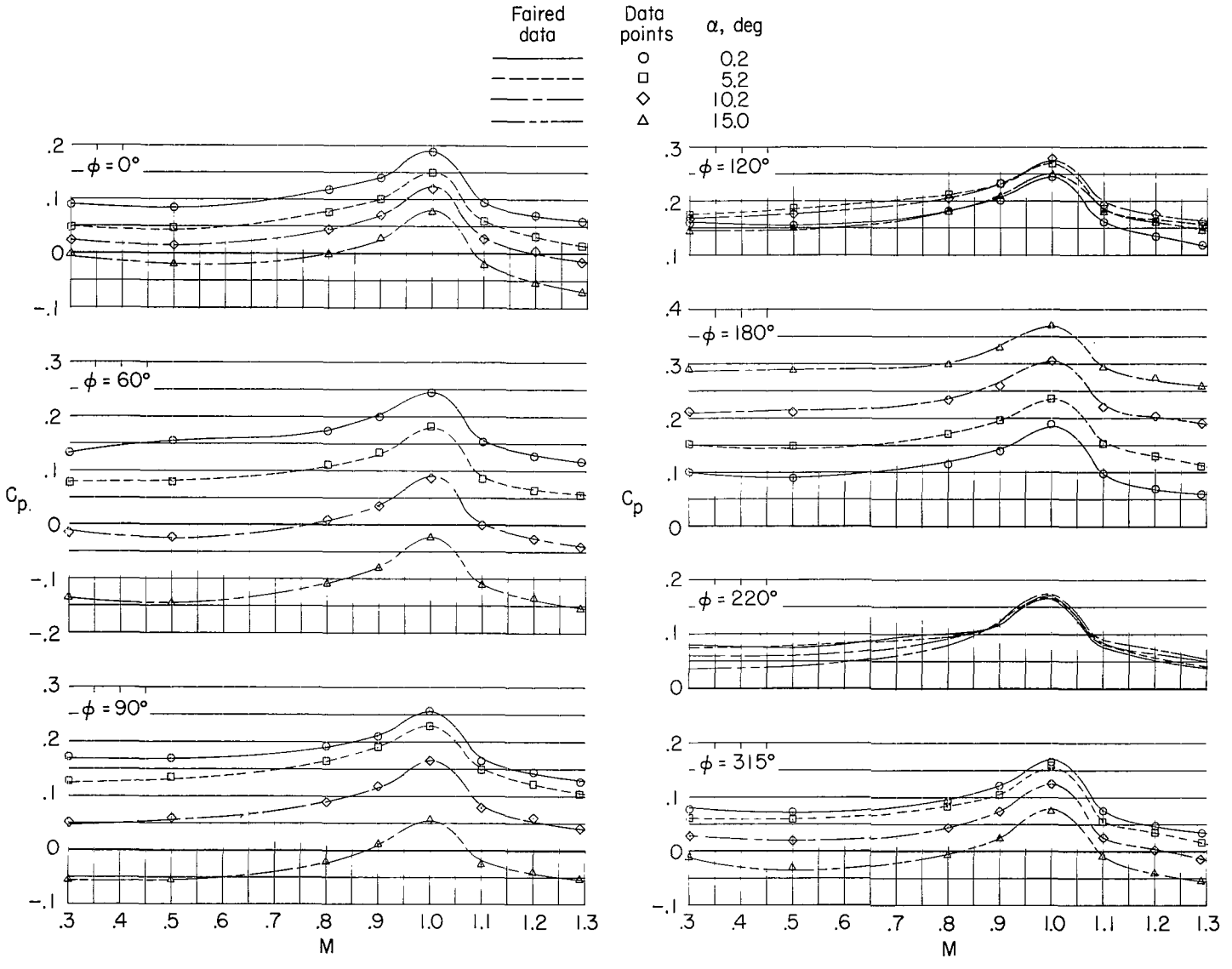

(b) $\beta = 5^0$.

Figure 25.- Concluded.

"The aeronautical and space activities of the United States shall be conducted so as to contribute . . . to the expansion of human knowledge of phenomena in the atmosphere and space. The Administration shall provide for the widest practicable and appropriate dissemination of information concerning its activities and the results thereof."

—NATIONAL AERONAUTICS AND SPACE ACT OF 1958

NASA SCIENTIFIC AND TECHNICAL PUBLICATIONS

TECHNICAL REPORTS: Scientific and technical information considered important, complete, and a lasting contribution to existing knowledge.

TECHNICAL NOTES: Information less broad in scope but nevertheless of importance as a contribution to existing knowledge.

TECHNICAL MEMORANDUMS: Information receiving limited distribution because of preliminary data, security classification, or other reasons.

CONTRACTOR REPORTS: Technical information generated in connection with a NASA contract or grant and released under NASA auspices.

TECHNICAL TRANSLATIONS: Information published in a foreign language considered to merit NASA distribution in English.

TECHNICAL REPRINTS: Information derived from NASA activities and initially published in the form of journal articles.

SPECIAL PUBLICATIONS: Information derived from or of value to NASA activities but not necessarily reporting the results of individual NASA-programmed scientific efforts. Publications include conference proceedings, monographs, data compilations, handbooks, sourcebooks, and special bibliographies.

Details on the availability of these publications may be obtained from:

SCIENTIFIC AND TECHNICAL INFORMATION DIVISION

NATIONAL AERONAUTICS AND SPACE ADMINISTRATION

Washington, D.C. 20546